UC Irvine
UC Irvine Electronic Theses and Dissertations

Title
An Explicit Representation of River Networks in a Continental-Scale Catchment-based Land Surface Model

Permalink
https://escholarship.org/uc/item/1b99f6k5

Author
Liu, Zhao

Publication Date
2014

Peer reviewed|Thesis/dissertation

eScholarship.org Powered by the California Digital Library
University of California

UNIVERSITY OF CALIFORNIA,
IRVINE

An Explicit Representation of River Networks in a Continental-Scale Catchment-based Land Surface Model Framework

DISSERTATION

submitted in partial satisfaction of the requirements
for the degree of

DOCTOR OF PHILOSOPHY

in Earth System Science

by

Zhao Liu

Dissertation Committee:
Professor James S. Famiglietti, Chair
Professor Charles S. Zender
Professor Keith Moore
Professor Brett F. Sanders

2014

© 2014 Zhao Liu

Table of Contents

Page

List of Figures iv
List of Tables vi
Acknowledgements vii
Curriculum Vitae viii
Abstract of the Dissertation x
1. Introduction 1
2. Background 6
2.1 Runoff Simulation by LSM 6
2.2 Flow routing algorithm 8
2.3 Simulating river discharge and floodplain dynamics with a floodplain hydraulic model 10
2.4 Methods of relating flow dynamics with channel geometry and landscape morphology 15
2.4.1 Traditional method 15
2.4.2 Remote sensing estimates 20
3. A National-Scale, Catchment-Based Land Surface Modeling Framework with an Explicit Representation of River Network Dynamics 26
3.1 Introduction 26
3.2 Background 29
3.2.1 Methods of relating flow dynamics with channel geometry and landscape morphology 29
3.2.2 Current state-of-the art for grid-based and catchment-based river routing models 30
3.3 Catchment-based land surface and river modeling with CHARMS 32
3.3.1 The CHARMS template 33
3.3.2 Runoff generation and explicit river dynamics in CHARMS 35
3.3.3 Separation of river flow into channel/floodplain components and estimation of river depth, width and floodplain extent 36
3.4 Data preparation for CHARMS 37
3.4.1 Building a national modeling template for CHARMS by upscaling NHDPlus data 37
3.4.1.1 The NHDPlus Dataset 37
3.4.1.2 Upscaling NHDPlus data 38
3.4.2 Land surface data and atmospheric forcing for CHARMS 42
3.4.3 Extracting river cross-section profiles using empirical relationships 43
3.5 Results 47
3.5.1 Land Surface Model Calibration 47
3.5.2 Model Simulations 49
3.5.2.1 Choice of gauging stations 49
3.5.2.2 Temporal variations of simulated streamflow 52
3.5.2.3 Temporal variations of simulated water depth and inundation extent 56
3.5.2.4 Spatial variation of simulated river depth and inundation extent 60
3.5.2.5 The challenge of validating spatial variations of river widths 64
3.6 Discussion 67
3.7 Conclusions 69
3.8 Appendix A - Runoff generation in CHARMS 70
3.9 Appendix B- Routing from hillslope to river channel in CHARMS 72
3.10 Appendix C - Routing within river channels and floodplains in CHARMS 73

3.11 Acknowledgments 75
4. Further Exploration of Hydraulic Geometry Relationships 76
4.1 Updated Relationship Table 76
4.2 Log-scale transformation and Outlier analysis 78
4.3 Impact of Drainage basin size 83
4.4 Impact of anthropogenic effect 84
5. Future work and Summary 89
5.1 Adding hillslope river transport component 89
5.1.1 Linear and non-linear kinematic wave approximation for water routing 90
5.1.1.1 Linear Solution for Eq. (5.6) 91
5.1.1.2 Non-linear Solution for Eq. (5.6) 91
5.2 Separating natural and regulated gauging stations based on streamflow variability and flow duration curve 93
5.3 Future Global Application Feasibility 96
References 98

List of Figures

Chapter 2

Figure 2.1 Schematic plot of CHARMS modeling unit by *Goteti et al.* [2008]. 14
Figure 2.2 Relationship between (a) bankfull discharge (Q_b), (b)bankfull width (w_b), (c) cross-sectional area (A_b), and (d) bankfull depth (d_b) as a function of upstream drainage area (A_d) *Beighley and Gummadi*, [2011] 22
Figure 2.3 (a) Upper: Distribution of b exponent values for the full spectrum of reach length scales over Lena River (b) Bottom: The first continuous mapping of a classical hydraulic geometry parameter from space. *Smith and Pavelsky*, [2008] 24

Chapter 3

Figure 3.1 Schematic plot of (a) CHARMS representation of river networks; (b) CHARMS representation of the river network in one catchment; (c) cross-section profile and channel dimension; (d) river routing and separation of total stream flow into main channel and floodplain flow from upstream reach (j) to downstream reach (j+1). 34
Figure 3.2 (a)-(d) Schematic plots of the upscaling process for the Klamath River basin with the NHDPlus dataset; (e) Schematic plot of the interpolation process to convert grid-based meteorological forcing and land surface input data into catchment-based input datasets. 40
Figure 3.3 (a) Explicit representation of river networks for the continental-scale CHARMS modeling template with 17 USGS gauge sites for model validation. Blue lines represent the main river reaches in each catchment; (b) 19 HUC2 water resources regions by NHDPlus with the main river reaches and USGS gauge sites. The brown dots denote the major dams/reservoirs across the contiguous U.S. 41
Figure 3.4 (a) Schematic plot of a stage-discharge relationship at a hypothetical gauging station; (b), (c), (d) bankfull depth, bankfull width, and bankfull discharge derived based the empirical relationship summarized in Table 3.1; (e-f) bankfull depth and bankfull width product by *Andreadis et al.*, [2013] for comparison. 46
Figure 3.5 Comparison between CHARMS simulated daily discharge (red dotted line) and USGS observations (black solid line) at gauging stations over natural rivers relatively free of human impact (left) and major rivers (right) across the country. 55
Figure 3.6 Comparison between CHARMS simulated (red dotted line) river depth (left) and inundation extent (right) and USGS gauge field measurements (black dots). The blue lines in the figures on the left are the derived bankfull depth of each corresponding river reach. 58
Figure 3.7 CHARMS simulated monthly (from April to July) river depth for the U.S. in year 2007 (left) and 2008 (right) 61
Figure 3.8 CHARMS simulated monthly (from April to July) inundation extent for the U.S. in 2007 (left) and 2008 (right) 62
Figure 3.9 (a) Simulated inundation extent for the U.S.; (b) Satellite observation of inundation extent by *Prigent et al.*, [2007]. 66

Chapter 4

Figure 4.1 Fitted empirical power law relationships between bankfull discharge (Q_{full}) and drainage area (A), and between bankfull discharge (Q_{full}) and bankfull depth (h_{full}) at log scale for each HUC2 water resource region with USGS field measurements between 01/01/1990 to 03/31/2010 with outlier analysis 83
Figure 4.2 Fitted empirical power law relationships between bankfull discharge (Q_{full}) and drainage area (A), and between bankfull discharge (Q_{full}) and bankfull depth (h_{full}) at log scale for HUC2 water resource region 10U, 10L, 14, 15, and 18, with USGS field measurements between 01/01/1990 to 03/31/2010, over HCDN gauging stations. 87
Figure 4.3 Fitted empirical power law relationships between bankfull discharge (Q_{full}) and drainage area (A), and between bankfull discharge (Q_{full}) and bankfull depth (h_{full}) at log scale for HUC2 water resource region 10U, 10L, 14, 15, and 18, with USGS field measurements between 01/01/1990 to 03/31/2010, over non-HCDN gauging stations. 88

Chapter 5

Figure 5.1 Schematic plot of lumped runoff process with hillslope-to-channel transport missing 90
Figure 5.2 Hydrographs and flow duration curves (both normalized and log-normalized scale) over natural (right) and regulated (left) gauge stations. 94
Figure 5.3 Cluster classification of regulated gauges and natural gauging stations based on slope of flow duration curves using Support Vector Machine (SVM). Green and blue triangles are the training datasets as pre-defined regulated and natural gauges, black and red circle are the classified regulated and natural gauges using SVM with the prior training information. 96

List of Tables

Chapter2

Table 2.1 Empirical power relationships between bankfull width and drainage area by *Faustini et al.,* [2009] for the conterminous United States for each ecoregion and water resources region 19

Chapter 3

Table 3.1 Empirical power law relationships between bankfull discharge (Q_{full}) and drainage area (A), and between bankfull discharge (Q_{full}) and bankfull depth (h_{full}) for each HUC2 water resource region with USGS field measurements between 01/01/1990 to 03/31/2010. 44
Table 3.2 Manual calibration of key parameters. Variation of values described in text. Red underscored values were those selected for model simulation. 48
Table 3.3 Water budget of the Mississippi River basin from CHARMS after initial tuning. Comparisons are to the studies of *Milly et al.,* [2005] and *Kumar and Merwade* [2011]. 49
Table 3.4 List of validation sites of USGS gauging stations and CHARMS performance statistics for daily simulated discharge, compared to gauge observations (10/1/2004-9/30/2009). 51
Table 3.5 Model performance statistics of (a) simulated river depth, and (b) simulated inundation extent compared to USGS field measurements. 57

Chapter 4

Table 4.1 Updated empirical power law relationships between bankfull discharge (Q_{full}) and drainage area (A), and between bankfull discharge (Q_{full}) and bankfull depth (h_{full}) for each HUC2 water resource region with USGS field measurements between 01/01/1990 to 03/31/2010 with new selection criteria 78

Acknowledgements

I would like to thank many people without whom this Ph.D. work cannot be possibly finished. First I would like to thank my dearest Ph.D. advisor Prof. Jay Famiglietti, who kindly accepted me as a graduate student 5 years ago. Thanks Jay for providing generous support and advice throughout my entire Ph.D. Thanks Jay for the great freedom for me both conducting research and looking for different career opportunities outside academia.

Thanks to my committee members, Prof. Charlie Zender, Prof. Keith Moore and Prof. Brett Sanders for all their time providing me suggestions and comments. Also thank Prof. Lawrence Smith for serving as my advancement committee member. Special thanks Dr. Cédric David for being my mentor during the last two years of my Ph.D. offering me numerous research and career advice. I also want to thank Dr. Brian Thomas, Dr. Minhui Lo, Dr. Gopi Goteti, Dr. HyungJun, and Dr. JT Reager who generously offered me valuable suggestions and help throughout my stay at UCI. Thank all the ESS faculty members who taught me 15 classes at the first year of graduate school, providing me a solid comprehensive understanding of Earth System Science as the foundation of my research.

It is truly an honor to spend my past five years to stay in the hydrology and climate research group with a warm atmosphere of friendship and great memories. Special thank to Collin Lawrence and Sasha Richey as my dearest officemates, with whom we share the joy, stress, and sadness through our graduate school life. Thank my ESS classmates of 2009, with whom we survive and thrive our first year. I also thank all the ESS graduate students for such an enjoyable environment. Also thank to Cynthia Dennis, Morgan Sibley, Jennifer Wilkens, Linda Nelson, Callie Brazil and all the other administrative staffs at ESS for all the support and help.

I also want to thank Dr. Yasir Kaheil, Dr. Jeffery McCollum, and Research Area Director Dr. Hosam Ali at FM Global, who kindly offered me a great internship in the Hydro-Sciences group in the Structures and Natural Hazard Research Area, where I am able to apply my graduate school experience into practice to work at insurance business.

Last but not least, I want to express my thanks to my dearest parents, Qing Xu and Zhongsheng Liu. It is their endless love that supports me for all the achievements throughout my life.

Curriculum Vitae

Education

University of California, Irvine

- Ph.D., Earth System Science, GPA 3.97, concentration in Hydrology — Sep 2014
- M.S., Earth System Science, GPA 3.95 — Jun 2011

Nanjing University, China

- B.S., Geographic Information Science, Geography, GPA 3.8 — Jun 2009

Research Experience

- **Ph.D. Candidate** — Jun 2011-Sep 2014

  -Department of Earth System Science, UC Irvine

  - Expanded the Catchment-based Hydrologic And Routing Model System (CHARMS) from basin-scale to continental-scale, to simulate streamflow, water depth, and corresponding floodplain inundation extent over the contiguous U.S. with a model template including 3000 watersheds and 200,000 sub-reaches upscaled from the National Hydrography Dataset (NHDPlus) through intensive spatial analysis with ArcGIS
  - First produced spatially distributed dynamic maps of simulated water depth and floodplain inundation extent of 200,000 river reaches across the contiguous U.S. with Generic Mapping Tools (GMT), providing a first continental-to-global scale catchment-based framework enabling the assimilation of altimetry remote sensing observations
  - First established empirical relationships to describe river hydraulic geometry profiles (bankfull depth, bankfull width, and bankfull discharge) for 19 water resources regions across the U.S with USGS gauging observations for both natural and managed regions through statistical analysis
  - Worked independently and collaboratively with group members on a multi-year project with clear timelines and deliverables; and the manuscript was summited to the journal Water Resources Research

- **Internship** — Jun 2014-Sep 2014

  - Hydro-Sciences Group, Structures and Natural Hazards Research Area, FM Global

  - Created automatic algorithm in R to identify anthropogenic regulation process at different gauging stations with Flow Duration Curve through Support Vector Machine Cluster Classification Analysis
  - Created basin similarity indices through conducting basin characteristic statistical analysis using R and Python for model parameter calibration and parameter cloning across different basin scales
  - Provided fully-detail description of two hydrological model as technical support manual documentations for internal use

- **Internship** — May 2008- Jan 2009

  -International Institution of Earth Science Systems (ESSI), Nanjing, China

- Implemented and significantly enhanced the simulation of soil water content using the boreal ecosystem productivity simulator (BEPS) model by 50% through assimilating remotely sensed observations using the Ensemble Kalman Filter (EnKF)
- Worked independently and collaboratively with group members with clear timelines and deliverables and published the results in the Journal of Applied Ecology in Chinese as first author

Awards

- NASA Earth and Space Science Fellowship 2012-2014
  Proposal Title: An Explicit Representation of River Networks in a Catchment-based Land Surface Model Framework for SWOT Assimilation

Certification

- **Engineer In Training (E.I.T., focus on Civil Engineering)** Jul 2013
  Board for Professional Engineers, Land Surveyors, and Geologist, California, License 150562

Teaching and Mentoring Experience

- Teaching Assistant, The Earth's Atmosphere, UC Irvine Spring 2012
- Teaching Assistant, Physical Environment, UC Irvine Fall 2011

- Led weekly discussion to help undergrad students better understand lecture material
- Led review sessions for 400+ students to prepare for the midterm and final exams
- Presented teaching material on Surface Hydrology as a guest lecturer for 400+ undergraduate students

Publications and Selected Conference Presentations

- Liu, Z., C. H. David, H. J. Kim, G. Goteti, and J. Famiglietti, A Continental-Scale, Catchment-Based Land Surface Modeling Framework with an Explicit Representation of River Network Dynamics, 2014, Submitted to Water Resources Research, Under Review
- Liu, Z., H. Kim and J. Famiglietti, An Explicit Representation of High Resolution River Networks using a Catchment-based Land Surface Model with the NHDPlus dataset for California Region, AGU Chapman Conference on Remote Sensing and Terrestrial Water Cycle, Feb. 19-22, 2012, Kona, Hawaii
- Liu, Z., Y. Zhou, W. Ju and P. Gao (2011), Simulation of cropland soil moisture based on Ensemble Kalman Filter, Journal of Applied Ecology, 22(11): 2943-53 (In Chinese)

Abstract of the Dissertation

An Explicit Representation of River Networks in a Continental-Scale Catchment-based Land Surface Model Framework

by

Zhao Liu

Doctor of Philosophy in Earth System Science

University of California, Irvine, 2014

Professor James S. Famiglietti, Chair

Surface water bodies (rivers, lakes, reservoirs, wetlands, floodplains, and other inland waters) are key components of the terrestrial hydrological cycle with an important role in regulating climate both regionally and globally. As population and the associated demand for water continue to grow, the need for integrated continental- and global-scale surface water dynamics simulation systems is becoming more apparent. Without a comprehensive understanding of both the seasonal and long-term variability and spatial distribution of surface water, decision makers will be challenged to manage water resources or to adapt to the changing global waterscape sustainably.

In this study, we present a continental-scale implementation of the Catchment-based Hydrological And Routing Modeling System (CHARMS) that includes an explicit representation of river networks to estimate river discharge, river depth and the corresponding inundation extent. The river networks and contributing catchment boundaries of the contiguous U. S. are upscaled from the National Hydrography Dataset Plus (NHDPlus) dataset. The average upscaled catchment size is 2773 km^2, and provides the template for Community Land Model (CLM)

version 3.5 implementation. Runoff generated by the land surface model within each catchment enters a unique main river channel, each consisting of several river reaches of average length 1.6 km. Nineteen sets of empirical relationships between channel dimension (bankfull depth and width) and drainage area are derived, based on USGS gauge observations, to describe river geometry for the 19 water resource regions of the NHDPlus representation of the contiguous United States. These channel dimensions are used to separate main river channel and floodplain. Modeled daily streamflow values show reasonable agreement with gauge observations and demonstrate that basins with fewer anthropogenic modifications are more accurately simulated. Modeled daily river depth and floodplain extent associated with each river reach are also explicitly estimated over the contiguous U. S., although such simulations are more challenging to validate.

Following the introduction and objectives described in Chapter 1, Chapter 2 next provides a literature review on the runoff generation by land surface model, flow routing algorithms, the current state of both grid and catchment-based river routing models, and empirical relationships between discharge and river geometry (river depth and width) with both *in situ* and remote sensing observations. Chapter 3 presents the continental-scale, explicit representation of river dynamics within a catchment-based land surface modeling framework. Chapter 4 displays a further exploration of hydraulic geometry relationships that are needed by large-scale river routing models. Summary and proposed future works are presented in Chapter 5.

This study has implications for capturing the seasonal-to-interannual dynamics of surface water in climate models. Such a continental-scale modeling framework development would, by design, facilitate the use of existing *in situ* observations and be suitable for integrating

the upcoming NASA Surface Water and Ocean Topography (SWOT) mission measurements for a range of studies in climate, hydrology and water management. It will also allow for simulation of sediment and nutrient transport and trace gas exchange along rivers. Ultimately, such an assimilation-ready continental-scale model template will enable significant improvement in predictive understanding of surface water dynamics.

1. Introduction

Terrestrial freshwater storage, including surface water bodies, snow and ice, soil moisture and groundwater, has a great impact on climate through its interactions with the Earth System at different spatial and temporal scales [*Famiglietti*, 2004] . Surface water bodies, defined as rivers, lakes, wetlands, inland water bodies, and inundated floodplains, are renewable sources of freshwater and key components of the terrestrial hydrological cycle. Due to the role of surface water bodies in both responding to and predicting extreme events, like floods and droughts, through interaction with biogeochemical and energy cycles, spatial and temporal variations of surface water bodies play a crucial role in regulating climate both regionally and globally [*Alsdorf et al.*, 2007; *Goteti et al.*, 2008].

Rivers are the ultimate integrators of watershed hydrology, representing the imprints of upstream climate variability, land surface processes, and human modifications to the system [*Zaitchik et al.*, 2010]. A 200-year simulation of a fully coupled climate model has shown the effect of continental runoff on ocean processes [*Branstetter*, 2001]. This work demonstrated that adding freshwater input would lead to a decrease in sea surface temperature and salinity, resulting in a reduction of North Atlantic Deep Water formation and a slowdown of meridional heat transport, which would positively feedback to the climate on land. Also, the timing and phase of freshwater input into the oceans is critical for accurate simulation of ocean currents and coastal processes. This river transport, accomplished by routing models, is of equal value for GCM's with the goal of accurately simulating the quantity of discharge using a land surface model. *Syed et al.*, [2010] showed an accelerating trend (540 km^3/y^2) of global discharge from 1994 to 2006, which was mainly due to an

increase of global ocean evaporation (768 km^3/y^2). If this trend continues, it will provide evidence of hydrological cycle intensification. Moreover, the differentiation between the main river channel and corresponding inundated area is also important, since the separate fraction of total flooded area determines the flux of evasion of carbon dioxide and methane to the atmosphere [*Richey et al.*, 2002]. Until now, although the need for better hydrologic observations is widespread, neither global nor regional observational networks can provide sufficient information to characterize variations and the distribution of surface water bodies.

Traditionally, streamflow is estimated as a product of three fundamental hydraulic variables: river flow width (w), flow depth (d), and velocity (v). And each of these has a power law relationship with discharge (Q):

$$Q = wdv \qquad (1.1)$$

$$w = aQ^b, d = cQ^f, v = kQ^m \qquad (1.2)$$

This is referred to as "hydraulic geometry" [*Leopold and Maddock*, 1953]. These power functions show the dependence of the hydraulic properties on discharge both at a cross-section ("at-a-station hydraulic geometry") and at the downstream direction ("downstream hydraulic geometry") [*Faustini et al.*, 2009]. River geomorphology is also valuable for studying sediment transport, erosion processes, and river ecology [*Smith and Pavelsky*, 2008]. With instantaneous measurements of discharge and these hydraulic variables, a rating curve describing the relationship can be developed, which can then be applied to estimate discharge continuously [*Durand et al.*, 2010]. Obviously this traditional method is largely limited by the availability of gauging stations, which are relatively sparse in both developing countries and high latitude areas; and in fact, the number of stream gauges is in decline globally [*Alsdorf and Lettenmaier*, 2003].

Throughout the past decade, numerous studies have demonstrated the potential to estimate streamflow from space, by measuring hydrological variables that cannot be easily obtained from *in situ* observations [*Alsdorf and Lettenmaier*, 2003; *Alsdorf et al.*, 2007]. Various approaches have attempted to simulate river discharge and velocity by correlating remotely sensed morphology information to discharge, and to estimate river width, depth, and water slope from satellite images [*LeFavour and Alsdorf*, 2005; *Bjerklie*, 2007; *Pavelsky and Smith*, 2008; *Smith and Pavelsky*, 2008].

The Surface Water and Ocean Topography (SWOT) mission, recommended by the National Research Council (NRC) Decadal Survey [National Research *Council*, 2007] to measure ocean topography and water surface elevation (WSE) over land, is a Ka-band SAR interferometric system. This swath mapping radar altimeter will provide direct measurements of WSE, slope (spatial variability in height), inundation area, and storage change for rivers, lakes, and wetlands. The spatial and temporal resolution of the measurements from SWOT is expected to be 50-100m and weekly, respectively, with an accuracy of 1cm/1km. NASA has announced that SWOT will be launched in 2020. Although SWOT is promising and can shed some light on space-based river studies, it still cannot produce spatially or temporally continuous measurements due to the limitation of the satellite design (e.g., inclined orbits of the platform). Moreover, streamflow cannot be obtained directly from SWOT, since first-order hydraulic parameters, as mentioned above, are needed [*Durand et al.*, 2008]. A comprehensive, SWOT-ready global modeling framework is required in order to fully utilize mission information to enable significant improvement in predictive understanding of surface water dynamics.

Land Surface Models (LSMs) are powerful tools for continuous simulation of the terrestrial hydrologic cycle at both regional and global scales. With an explicit representation of river networks, including of flow depth and floodplain extent, hydraulic measurements from SWOT can be assimilated into an LSM. The combination of these two will provide a more accurate estimation of streamflow by taking the advantage of both the continuous, physically based simulation of surface water dynamics, and the accuracy and global nature of SWOT measurements. The main motivation of this project is to characterize how accurately we can estimate river discharge, river depth and inundation extent using an explicit representation of the river network and river width at the national scale using a Catchment-based Hydrological And Routing Model System (CHARMS, [*Goteti et al.*, 2008]) framework. This template will serve as a framework towards building a global catchment-based land surface model system for hydrological, climate and SWOT applications. With an explicit representation of river networks, including of flow depth and floodplain extent, hydraulic measurements from SWOT can be assimilated into an LSM. The combination of these two will provide a more accurate estimation of streamflow by taking the advantage of both the continuous, physically based simulation of surface water dynamics, and the accuracy and global nature of SWOT measurements.

In this study, we proposed to build a continental-scale, catchment-based land surface hydrologic modeling framework based on CHARMS. The eventual aim is to facilitate the incorporation of the measurements from SWOT for hydrological and climate applications. Ultimately, the following scientific and technical questions will thus be addressed:

• How do the dynamics of surface water bodies, including their heights, areal extents, and storage volumes, vary on daily, seasonal-to-interannual, and longer timescales? How do these respond to variations in precipitation and climate oscillations like ENSO?

• How are these surface water bodies responding to climate change, and to changes in extreme flooding and drought events?

• Can missions like SWOT contribute to the grand challenge of seamless space-time prediction of surface water dynamics?

The remainder of this dissertation is organized as follows: Chapter 2 provides further background review on the runoff generation by land surface model, flow routing algorithms, the current state of both grid and catchment-based river routing models, and relating discharge with river geometry (river depth and width) through empirical relationships with both *in situ* and remote sensing observations. Chapter 3 presents the continental-scale, explicit representation of river dynamics within a catchment-based land surface modeling framework. Chapter 4 displays a further exploration of hydraulic geometry relationships that are needed by large-scale river routing models. Summary and proposed future work are presented in Chapter 5.

2. Background

2.1 Runoff Simulation by LSM

In a river routing system, runoff is transported from continental interiors through river channels to lakes or oceans [*Goteti et al.*, 2008]. Considering the meteorology, land cover, soil characteristics and other conditions, LSMs can estimate surface and subsurface runoff within each LSM modeling unit required by the routing system [*Goteti et al.*, 2008]. Runoff can be generated in a uniform basin through at least four mechanisms: rainfall intensity exceeds infiltration or storage capacity leading to overland flow; rainfall intensity exceeds infiltration or storage capacity on near-saturated soils; rain falls on stream channels and completely saturated soils; subsurface flow/downslope lateral flow of saturated or unsaturated soil water [*Beven and Kirkby*, 1979]. Following the conceptual rainfall-runoff model, TOPMODEL [*Beven and Kirkby*, 1979; *Sivapalan et al.*, 1987] used the "topographic index" or "wetness index" $\lambda = \ln(\alpha / \tan\beta)$ to incorporate the topographic effect, in which α is the specific catchment area, and $\tan\beta$ is the local surface topographic slope. *Famiglietti and Wood*, [1994] parameterized the subgrid variability of soil moisture and runoff in the discretized framework by disaggregating the distribution of the topographic index into different increments to represent a fraction of a watershed with similar water table depth and soil moisture. Later studies [*Stieglitz et al.*, 1997; *Niu and Yang*, 2003] used a three-parameter gamma distribution function to represent the distribution of the topographic index, which is more computationally efficient and consistent with climate models, but less accurate for mountainous regions [*Niu et al.*, 2005]. TOPMODEL assumes that soil saturated hydraulic conductivity, K_{sat}, decreases with soil depth to create water table depth and is only used to generate runoff, while they defined K_{sat} as a function of soil texture, affecting evaporation and transpiration [*Niu et al.*, 2005]. Using the topographic index

to explicitly describe the subgrid soil moisture variability can capture the difference between upslope and downslope hydrological behavior [*Koster et al.*, 2000].

Niu et al., [2005] developed a simple TOPMODEL-based runoff parameterization (SIMTOP), mitigating several problems with the TOPMODEL-based runoff scheme. There are two major features that SIMTOP simplifies for the TOPMODEL based runoff scheme. Firstly, subsurface runoff is a product of an exponential function of water table depth and a single coefficient for maximum subsurface runoff, making the parameterized subsurface runoff independent of soil surface K_{sat}. This simplification reduces the uncertainties from computing the topographic index using a coarse-resolution DEM. Secondly, they use an exponential function to represent the discrete distribution of the topographic index. In other words, SIMTOP uses a single topographic parameter, the maximum fractional saturated area, to accommodate the topographic data, which showed a better performance in mountain regions and preserved the accuracy in relatively flat areas. Instead of using a catchment as the fundamental land unit, they applied the SIMTOP scheme to rectangular grid cells to avoid uncertainties in converting between GCM grid cells and catchments. This scheme was incorporated into the National Center for Atmospheric Research Community Land Model version 2.0 (CLM 2.0). Compared with baseline CLM 2.0 runoff simulations at global scale, the root mean square error of simulated runoff is largely reduced, and the timing of runoff production better matches the timing of observational runoff data. Furthermore, the SIMTOP scheme produces much less surface runoff relative to subsurface runoff compared to CLM baseline run. Either with K_{sat} determined by soil texture or with exponentially decaying K_{sat}, SIMTOP has improved runoff simulation globally. With this SIMTOP scheme incorporated in the CLM 3.5, both phase and amplitude of runoff annually cycle are also improved [*Oleson et al.*, 2008].

2.2 Flow routing algorithm

The purpose of large scale river routing is to simulate the transport of runoff generated within each model unit (grids, watersheds, or other spatially defined units) through a river network to its delivery point on the continental margin, and to provide information on streamflow at any location along the channel [*Olivera et al.*, 2000]. Although various flow routing schemes exist with different levels of complexity, two main groups include cell-to-cell (CTC) and source-to-sink (STS). Most of the early large-scale flow routing models used the CTC method, in which the runoff flux from each cell was routed to its downstream neighbor and was tracked over the river network [*Vörösmarty et al.*, 1989; *Liston et al.*, 1994; *Miller et al.*, 1994; *Coe*, 1998; *Branstetter and Famiglietti*, 1999; *Oki et al.*, 1999]. The CTC algorithm uses the principle of continuity, deriving a mass balance of water stored in each land model cell, shown as the following:

$$\frac{dS_i(t)}{dt} = \sum I_{j-i}(t) - O_i(t) + R_i(t) - E_i(t) \qquad (2.1)$$

where S_i is the water volume stored in cell i, t is time, I_{j-i} is the inflow to cell i from each of the immediately upstream neighbor cells j, O_i is the outflow from cell i, R_i is the runoff generated within cell i, and E_i is the losses due to evaporation and infiltration from the river network within cell i, which accounts for loss during the routing process after the runoff has been generated. $S_i=K_i*O_i$, with K_i representing the residence time in cell i. A primary disadvantage of the CTC schemes is that they do not take the routing process of water from different areas of the cell to the cell outlet into account, which obviously can lead to inaccuracy with coarser resolution due to hydraulic heterogeneity [*Naden*, 1993; *Zaitchik et al.*, 2010]. Although high resolution DEM's may help to capture these variations, the intensive computation burden also limits the feasibility of CTC to be implemented at continental and global scales.

The Source-to-Sink (STS) routing scheme was developed as an alternative to the CTC algorithm [*Naden*, 1993; *Kite et al.*, 1994; *Lohmann et al.*, 1996; *Olivera et al.*, 2000]. Sources refer to runoff-producing areas where water enters the surface water system as runoff; sinks refer to runoff-receiving units, defined as areas where water needs no further routing, and are located along continental margin or the lowest elevation of inland catchments [*Olivera et al.*, 2000]. In such a routing scheme, all runoff is routed explicitly between sources and sinks, and only the discharge at points of interest will be solved via applying a watershed response function to all sources of runoff within the drainage basin [*Zaitchik et al.*, 2010]:

$$Q_i(t) = \sum_j Q_j(t) \qquad (2.2)$$

where $Q_i(t)$ is the streamflow of sink i, and $Q_j(t)$ is the contribution of source j:

$$Q_j(t) = A_j R_j(t) * u_j(t) \qquad (2.3)$$

where A_j is the area of source j, R_j is the time series of runoff generated at source j, which is simulated by LSM, $u_j(t)$ is the response function of source j at sink i.

There are several advantages of STS: through Geographic Information System (GIS) tools, it uses river network topology generated from high resolution DEM data to estimate the response function parameters that could be used in lower resolution global climate models; high resolution STS schemes accommodate spatially variable streamflow parameters (i.e., flow velocity, attenutation coefficient, and loss parameter), and only those parameters relevant to routing need to be defined at high resolution during pre-processing. Instead of routing within all the cells, only the streamflow transported directly from points of runoff generation to the watershed outlet is needed, which leads to a much higher computational efficiency compared to the CTC approach [*Olivera et al.*, 2000; *Zaitchik et al.*, 2010]. *Zaitchik et al.*, [2010] applied the STS routing scheme to the Global Land Data Assimilation System (GLDAS) [*Rodell et al.*, 2004]. Compared with gauge data from GRDC

(http://grdc.bafg.de), the simulated discharge was smoothed and had a delayed peak relative to the simulated runoff for the watershed, consistent with results from *Olivera et al.*, [2000] The smoothing and delay were most pronounced for large watersheds with more lake coverage. Their results further showed that routed discharge had substantially larger correlation with daily gauge data for most basins compared with un-routed summed runoff, reflecting the ability of the STS scheme to translate and attenuate distributed runoff across the basin.

2.3 Simulating river discharge and floodplain dynamics with a floodplain hydraulic model

Many grid-based models have been developed to either simulate river discharge through different routing schemes as mentioned above and to estimate floodplain inundation, water depth, velocity and other hydraulic elements. LISFLOOD-FP [*Bates and De Roo*, 2000] is a simple raster-based, coupled 1D/2D model floodplain hydraulic model. Channel flow is treated through the kinematic approximation of the one-dimensional St. Venant equation with an explicit finite difference procedure:

$$Continuity: \frac{\partial Q}{\partial x} + \frac{\partial A}{\partial t} + q = 0 \quad (2.4)$$

$$Momentum: S_0 = S_f \quad (2.5)$$

Floodplain flow is represented with a two-dimensional diffusion wave to simulate floodplain water depths and associated inundation extent. Water is routed to adjacent cells of the DEM if the bankfull depth is exceeded. For each cell, the storage change is defined as the sum of fluxes in and out of the cell:

$$\frac{dV}{dt} = Q_{up} + Q_{down} + Q_{left} + Q_{right} \quad (2.6)$$

The input boundary condition for the model is the upstream inflow hydrograph, which can be obtained from either gauge records or other model outputs. The output from LISFLOOD is a raster file of flow depth at each time step and discharge at the downstream boundary. This approach is similar with several others that have been summarized in *Bates and De Roo*, [2000]. *Wilson et al.*, [2007] first applied this model to a large spatial scale of about 13,000 km^2. They estimated the inundation area and river discharge of the Central Amazon region in Brazil with the 90m resolution DEM from the Shuttle Radar Topography Mission (SRTM) for a 22-month period. Flow between cells was calculated as below:

$$Q_{i,j} = \frac{h_{flow}^{5/3}}{n}\left(\frac{h^{i-1,j} - h^{i,j}}{\Delta x}\right)^{1/2} \Delta x \qquad (2.7)$$

Compared with JERS-1 images and ground observations, the model results showed that it did well in simulating inundation extent for high water, but it led to over-prediction at low water due to the lack of full drainage of the floodplain. It also showed a reasonable result for modeled water stage data. This was the first time that full drainage of a topographically complex inundation extent had been represented from a hydrodynamic model. *Yamazaki et al.*, [2011] proposed a global river routing model, CaMa-Flood. It is able to explicitly represent floodplain inundation dynamics with backwater effects taken into account through a diffusive wave equation. For each grid point, river and floodplain water storage, river discharge, water depth and inundation extent are estimated with subgrid-scale topographic parameters. Their results showed that estimations of river discharge had been improved after incorporating the subgrid floodplain topography. The water surface elevation was smoothed using a diffusive wave equation. The simulation of inundation extent also compared well with observations.

Nonetheless, grid-based LSMs consider the heterogeneity of land cover and topography within each grid cell when simulating runoff, whereas routing models incorporating runoff from these LSMs assume each grid to be homogenous. The spatial variation in rivers and inundation extent could hardly be simulated realistically by grid-based LSMs with a typical resolution of 0.5°, since those variations are controlled by features with much finer resolution [*Goteti et al.*, 2008]. Therefore, there is a high computational demand for grid-based LSMs to realistically represent river channels and other surface water bodies, which is a particular drawback when routing schemes are implemented at continental or global scale.

An alternative is a catchment-based LSM coupled to a routing model that uses an explicit representation of the river network. In this approach, the land surface is represented as a mosaic of catchments, and horizontal heterogeneity within catchments (e.g., in soil moisture and runoff generation) is parameterized using a numerical topographic index [*Famiglietti and Wood*, 1994; *Stieglitz et al.*, 1997; *Koster et al.*, 2000]. The routing model can capture the movement of streamflow occurring across the actual river channel, and therefore floodplain storage can be estimated through river geometry [*Goteti et al.*, 2008]. Taking into account sub-grid heterogeneity, the catchment-based approach is able to simulate discharge and surface water storage more realistically using less computational resources compared to grid-based LSMs. *Goteti et al.*, [2008] presented a Catchment-based Hydrologic and Routing Model System (CHARMS) coupled with the Community Land Model (CLM) 3.0, with an application to the Wabash River basin from 1949 to 1960 (Figure 2.1). The CLM operated on a catchment template, while the river network was represented explicitly, using discretized linear reaches. For each catchment, the total discharge of the downstream end of the corresponding river reach consists of the contribution from hillslope

surface runoff, subsurface runoff and discharge from the main river channel and floodplain, shown as below:

$$Q(t) = Q_{h.surf}(t) + Q_{h,base}(t) + Q_{chnl}(t) + Q_{fldp}(t) \qquad (2.8)$$

The river cross-section profile was extracted from the 3 arc sec SRTM (~90m), such that river depth and inundation extent were also estimated. It showed that daily streamflow from CHARMS captured the seasonal variability fairly well, and the simulation of river depth and inundation extent also followed the seasonal pattern of discharge. This work is a significant step towards incorporating river channel cross-sectional geometry to explicitly simulate both river depth and inundation extent associated with discharge.

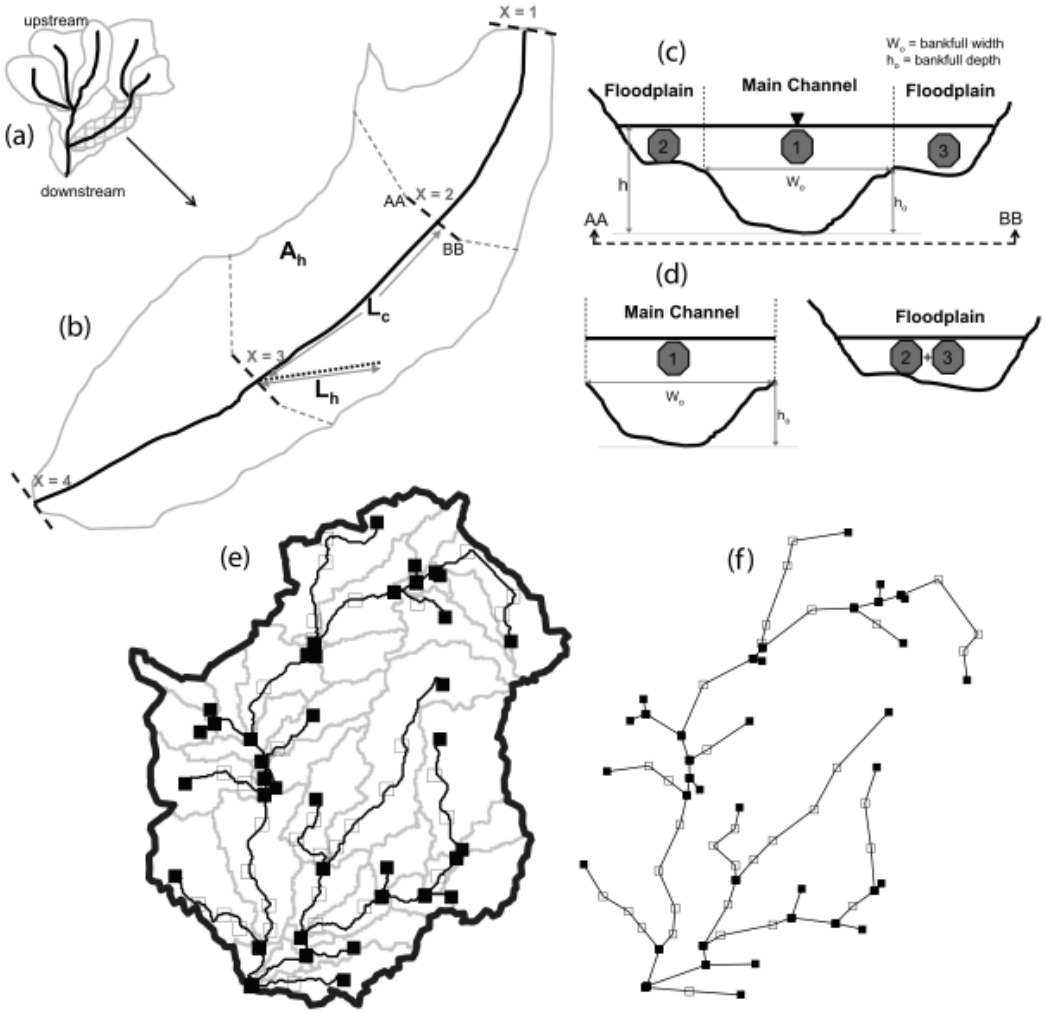


Figure 2.1 Schematic plot of CHARMS modeling unit by *Goteti et al.* [2008]. (a) Schematic of a river network (solid black lines) and associated catchment areas (light grey lines). (b) Enlarged view of the shaded catchment. Channel cross sections ($X = 1$, $X = 2$, etc.) are indicated by broken black lines, and broken grey lines indicate contributing drainage area (A_h) corresponding to each routing reach. (c) Routing model representation of a channel cross section (e.g., AA-BB in Figure 1b). (d) Total discharge with flow depth h separated into within-channel and floodplain components by the routing model. (e) River channels and associated routing reaches within the Wabash River basin. Shaded squares indicate the beginning and ending of a river channel, and routing reaches are separated by open squares. (f) Routing model representation of the river network.

Beighley et al., [2009] developed the sub-basin scale Hillslope River Routing (HRR) model to simulate vertical water-balance, lateral hydraulic transport and water storage for rivers and floodplains over the Amazon and Congo Basins using SRTM. This model framework includes a vertical water balance model (WBM) for vertical fluxes and a routing model for horizontal routing processes. The sub-basin scale is determined by dividing the landscape using Pfafstetter (PFAF) levels. Each PFAF sub-basins were separated into two plains and a channel/floodplain segment, as an "open-book" watershed approximation. The kinematic approximation was used to estimate the surface and subsurface runoff from plains to channel, and the Muskingham-Cunge (MC) method was used for interbasin channel/floodplain reaches. The HRR model was able to capture the annual peaks, seasonal patterns and daily fluctuations reasonably well.

2.4 Methods of relating flow dynamics with channel geometry and landscape morphology

2.4.1 Traditional method

The development of empirical relationships linking flow dynamics with channel geometry and landscape morphology has been ongoing since the nineteenth century. The most notable early relationship is commonly known as Manning's equation [*Gauckler*, 1867; *Manning*, 1891] and expresses flow velocity (v) as a function of hydraulic radius (R), energy slope (S) and friction coefficient (n), shown as:

$$v = (1/n)S^{\frac{1}{2}}R^{\frac{2}{3}} \qquad (2.9)$$

Another significant early effort is the concept of "hydraulic geometry" initially presented by *Leopold and Maddock* [1953] in which flow width (w), flow depth (d), and flow velocity (v) are all related to flow rate (Q) using a similar power law:

$$w = aQ^b; d = cQ^f; v = kQ^m \qquad (2.10)$$

where a, b, c, f, k, m are constant empirical parameters. Due to the continuity equation ($Q=wdv$) these empirical parameters also depend on each other [*Leopold and Maddock*, 1953]:

$$b + f + m = 1; a \cdot c \cdot k = 1 \qquad (2.11)$$

These relationships exist for both "at-a-station hydraulic geometry" (refers to how instantaneous Q, w, d, v change with time at single location) and "downstream hydraulic geometry" (refers to how Q, w, d, v change longitudinally along a river for a given frequency of discharge). One should note, however, that the numerical value of the coefficients $a,b,c,f,k,$ and m differ between the "at-a station" and the "downstream" approaches. Given access to flow measurements, these parameters can be determined and the power law relationships can be used to continuously estimate hydraulic geometry as a function of flow rate, and *vice versa*. Of all the above relationships (Equations (2.9)-(2.11)), the parameters from the manning's Equation (2.9) do not need to be calibrated, while the parameters in Equations (2.19)-(2.11) are derived based on observations of flow quantities and landscape morphology.

Traditionally with *in situ* measurements, hydraulic geometries can be described by drainage characteristics, with spatial and temporal variations constrained by varying coefficients [*Beighley and Gummadi*, 2011]. Thus, discharge Q can be derived from any of the forms in equation (2.9) with known coefficients. Though the coefficients vary in different regions and depend on the scale of the drainage area, *Rhodes*, [1977] pointed out that for the majority of sites, the rate of increase in

width is less than depth with discharge ($b<f$). This implies that the width/depth ratio will decrease as discharge increases; and that the increase in velocity is more rapid than depth with discharge ($m>f$). Early studies [*Leopold et al.*, 1964] has also demonstrated some of the geographic distributions of these coefficients over the United States. Generally, the increase rate of width with discharge over the semiarid area in the western U.S and parts of the High Plains is higher than those in more humid mountainous regions in the east [*Leopold et al.*, 1964].

With increasing river size from upstream to downstream, early studies have also detected the close correlation between river bankfull discharge (Q_{full}) and drainage area (A) [*Leopold et al.*, 1964; *Dunne and Leopold*, 1978]:

$$Q_{full} = \mu A_d^{\gamma} \qquad (2.12)$$

Thus, bankfull flow can easily be determined based on drainage area, which can be useful for regions where discharge estimates are not easily available (i.e. gauge uncertainty or ungauged areas). Similarly, relationships between bankfull channel dimensions (bankfull width, $w_{full,}$ and bankfull depth, h_{full}) and drainage area A_d also exist.

$$w_{full} = \alpha \cdot A_d^{\beta} \quad and \quad h_{full} = p \cdot A_d^{q} \qquad (2.13)$$

Therefore, drainage area can be the dominant control factor in discharge within a certain spatial area with relatively uniform climate [*Faustini et al.*, 2009].

Despite the expected variations in both time and space [*Leopold and Maddock*, 1953; *Knighton*, 1974, 1975; *Richards*, 1976; *Park*, 1977; *Rhodes*, 1977], many studies have demonstrated the transferability of these relationships to increasingly large areas such as New Zealand [*Jowett*, 1998], the US great plains [*Dodov and Foufoula-Georgiou*, 2004], South Australia [*Stewardson*, 2005], 18

water resources regions over the continental US [*Faustini et al.*, 2009], and the Amazon Basin [*Beighley and Gummadi*, 2011]. For example, Using 1588 gauging station data from the Environmental Protection Agency's National Wadeable Streams Assessment (WSA), *Faustini et al.*, [2009] detected the downstream variations in bankfull width of the wadable streams across the U.S. They developed the w_{full}-A_d relationships for the conterminous U.S., nine WSA aggregate ecoregions and 18 water resources regions (Table 2.1). Table 2.1 shows that their results can provide a useful first-order estimate of bankfull river width (especially in eastern United States) using only drainage areas that can be easily obtained from a DEM. They further demonstrated that the enhanced equations incorporating mean annual precipitation, elevation and mean reach slope were able to significantly improve the equation fit.

Region[b]	α	SE_α^*	β	SE_β	RMSE	r^2	n	Fit
Conterminous U.S.	2.81	1.03	0.24	0.007	0.241	0.42	1588	P
WSA Major Regions								
Eastern highlands	2.68	1.05	0.38	0.013	**0.141**	**0.75**	275	G
Plains and lowlands	3.06	1.06	0.21	0.011	0.228	0.39	537	P
West	2.27	1.05	0.28	0.011	0.243	0.44	776	P
WSA Aggregate Ecoregions								
N. Appalachians (NAP)	2.55	1.11	0.39	0.027	**0.145**	**0.72**	87	G
S. Appalachians (SAP)	2.72	1.05	0.37	0.015	**0.139**	**0.77**	188	G
Coastal plain (CPL)	2.63	1.09	0.29	0.025	**0.161**	**0.60**	88	G
Upper midwest (UMW)	1.74	1.14	0.39	0.033	**0.168**	**0.68**	70	G
Temperate plains (TPL)	3.26	1.11	0.22	0.020	0.214	0.40	181	P
Northern plains (NPL)	1.45	1.21	0.28	0.029	0.237	0.41	137	P
Southern plains (SPL)	2.31	1.25	0.23	0.039	0.233	0.36	61	P
Western mountains (WMT)	2.26	1.05	0.31	0.014	0.236	0.45	566	P
Xeric (XER)	1.77	1.09	0.29	0.019	**0.235**	**0.54**	210	M
Water Resources Regions								
New England (01)	2.79	1.20	0.37	0.046	**0.146**	**0.60**	45	G
Mid-Atlantic (02)	2.57	1.09	0.38	0.025	**0.141**	**0.75**	77	G
South Atlantic-Gulf (03)	2.40	1.11	0.36	0.032	**0.153**	**0.68**	60	G
Great Lakes (04)	2.45	1.16	0.33	0.037	**0.177**	**0.62**	53	G
Ohio (05)	3.02	1.08	0.33	0.021	**0.133**	**0.77**	80	G
Tennessee (06)	1.97	1.17	0.44	0.060	**0.154**	**0.68**	27	G
Upper Mississippi (07)	1.92	1.13	0.37	0.030	**0.191**	**0.62**	93	M
Lower Mississippi (08)	2.95	1.14	0.27	0.035	**0.128**	**0.67**	30	G
Souris-Red-rainy (09)	2.27	1.37	0.23	0.046	0.138	0.43	36	P
Missouri (10)	2.33	1.10	0.23	0.017	0.262	0.37	317	P
Arkansas-white-red (11)	3.43	1.19	0.23	0.035	0.257	0.38	72	P
Texas-Gulf (12)	3.21	1.21	0.24	0.044	**0.165**	**0.57**	25	G
Rio Grande (13)	2.17	1.56	0.14	0.116	0.292	0.10	15	P
Upper Colorado (14)	2.99	1.19	0.22	0.036	0.246	0.34	72	P
Lower Colorado (15)	2.81	1.23	0.26	0.039	0.245	0.42	61	P
Great Basin (16)	2.11	1.12	0.28	0.027	**0.234**	**0.57**	84	M
Pacific Northwest (17)	2.00	1.08	0.34	0.023	0.252	0.43	270	P
California (18)	2.49	1.08	0.27	0.022	0.188	0.48	171	P

Table 2.1 Empirical power relationships between bankfull width and drainage area by *Faustini et al.,* [2009] for the conterminous United States for each ecoregion and water resources region

2.4.2 Remote sensing estimates

Although those hydraulic coefficients can be easily retrieved through regression, it is largely limited by the availability of *in situ* measurements from gauging stations. Moreover, in spite of the fact that the relationships of Equations (2.9) – (2.11) were initially derived based on gauge measurements, they have also recently proven useful for estimates mainly based on remotely-sensed observations including water height and inundation area [*Smith et al.*, 1996; *Birkett et al.*, 2002; *Bjerklie et al.*, 2003, 2005b; *Frappart et al.*, 2005; *Ashmore and Sauks*, 2006; *Leon et al.*, 2006; *Bjerklie*, 2007; *Smith and Pavelsky*, 2008; *Durand et al.*, 2010; *Mersel et al.*, 2013]. Estimating discharge and channel dimensions via remote sensing is a relatively new approach starting from the mid 1990s. *Smith and Pavelsky*, [2008] summarize that there are mainly three types of methods of remote sensing discharge: correlating remotely sensed observations (e.g., water level and inundation extent) with ground data at or near a gauge site [*Smith et al.*, 1996; *Bjerklie et al.*, 2003; *Beighley and Gummadi*, 2011], which is quite similar to the traditional way mentioned above; merging satellite observations with prior informed estimates of channel dimensions and characteristics [*LeFavour and Alsdorf*, 2005], simulation output from hydraulic models [*Bates and De Roo*, 2000]), and topographic information [*Bjerklie et al.*, 2005a; *Bjerklie*, 2007] and finally to directly measure three-dimensional water volume storage over predefined regions [*Frappart et al.*, 2005]. For further review of existing studies relating river flow, height and width using satellite observations, the reader is referred to *Smith and Pavelsky*, [2008].

With limited stage-discharge data from the year 1991 to 2005 and Landsat Imagery, *Beighley and Gummadi*, [2011] developed a method to estimate bankfull discharge and the hydraulic geometry coefficient and exponents over the Amazon Basin. Bankfull discharge (Q_b) was found at the

corresponding point of inflection in the stage-discharge relationship. The assumption behind this is that once water begins to flow over the bank into the floodplain, the rate of increase of stage with discharge will decrease. By further relating the data to drainage area derived from the SRTM 90m DEM, the relationship for estimating bankfull discharge (Q_b), bankfull depth (d_b), bankfull width (w_b), and cross-sectional area (A_b) as a function of upstream drainage area A_d were developed (Figure 2.2). This method was able to provide reasonable results for estimating channel and floodplain dimensions based on drainage area. And this is valuable for many large-scale river routing models that need numerous channel cross-section profiles. Moreover, they further built the relationship for estimating cumulative network channel length (L_c) and surface area ($A_{s,c}$) as a function of the threshold channel width (w_m) that is used to define the drainage network. The purpose of this step is to differentiate between the main channel and floodplain fraction to the total inundated area, which is important to quantify the CO_2 and methane flux from the surface area. They show that for the channels greater than 2 meters, the Amazon Basin contains 4.4 million km of channel with a corresponding surface area of 59,700 km^2.

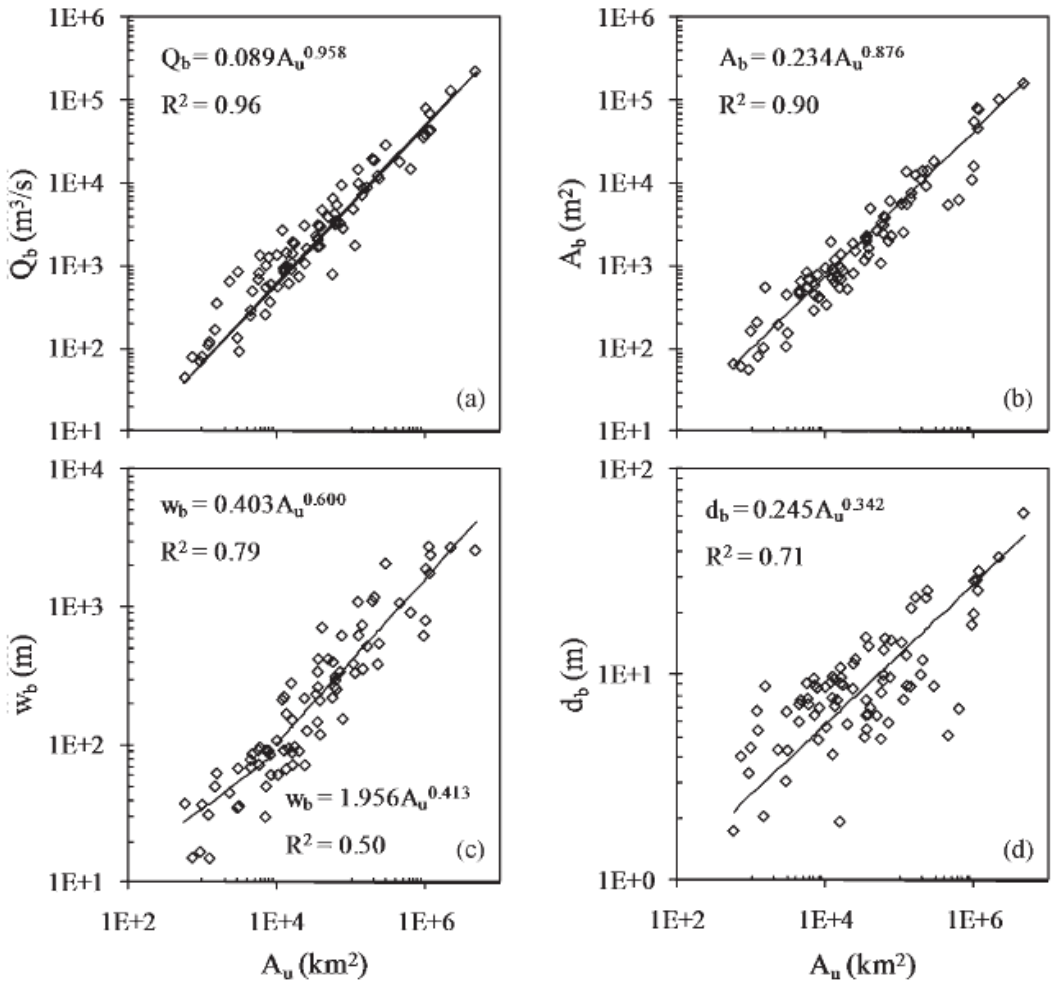
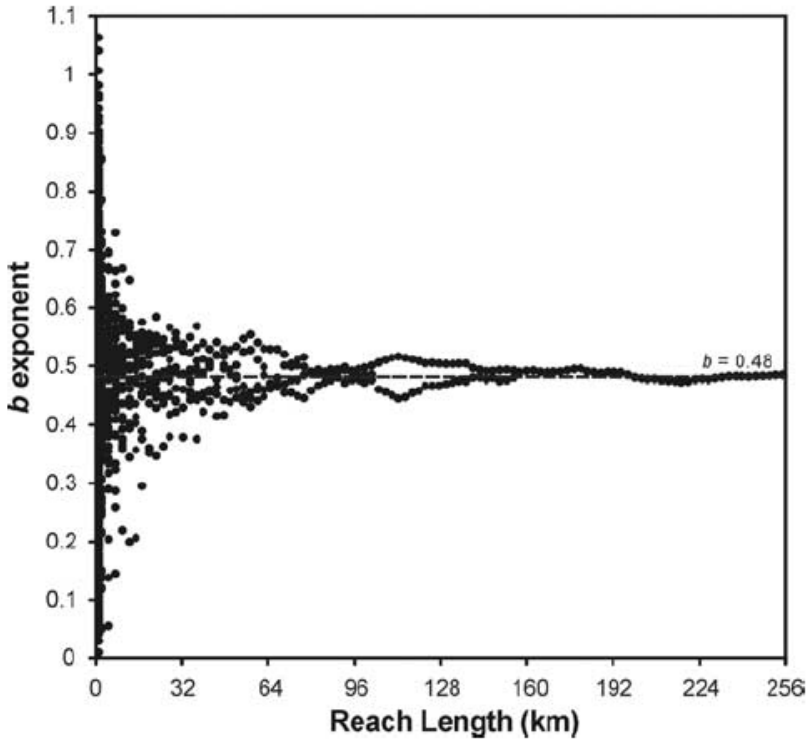


Figure 2.2 Relationship between (a) bankfull discharge (Q_b), (b)bankfull width (w_b), (c) cross-sectional area (A_b), and (d) bankfull depth (d_b) as a function of upstream drainage area (A_d) *Beighley and Gummadi*, [2011]

No matter whether traditional gauge stations or remote sensing observations are used, estimating discharge based on rating curves that describe the empirical relationship is largely limited by the site specificity. In other words, those relationships vary with time and space, which may not be appropriate to be applied to other sites in a similar area. [*Smith and Pavelsky*, 2008] used a satellite derived W_e-Q relationship to estimate river discharge and flow propagation speed in the Lena River. Furthermore, by disaggregating the reach into smaller subreaches, they explored the variability of

the b exponent in the *We-Q* relationship. It showed that at length scales exceeding ~60-90 km, the b exponents stabilized around 0.48, with a ± 10% variation, indicating that all subreaches behaved similarly with a length scale larger than ~60-90 km (Figure 2.3a). They demonstrated that the variability of the river width to discharge could be "reduced to a single-digit uncertainty," and the site specificity declined with a sufficiently large enough length scale. They also, for the first time, provided direct mapping of the b exponent along a river course from space (Figure 2.3b). This result is of great importance, since it suggests the promising transferability of rating curves among different sites, and that with reach averaging, generalized hydraulic geometry can be retrieved through remote sensing. Especially with the new satellite mission, SWOT, producing three-dimensional images of surface water, numerous "universal rating curves" can be generated, which will enable estimates of river discharge in ungauged regions.



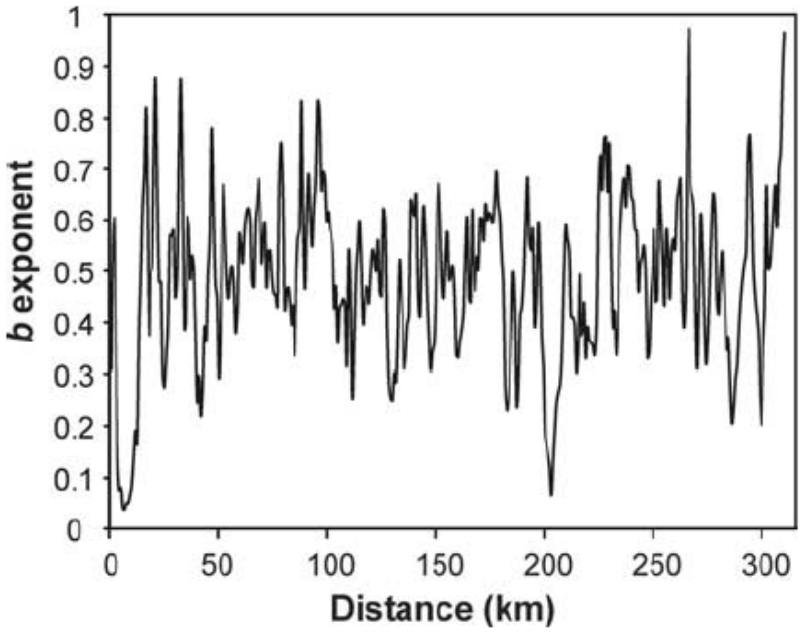


Figure 2.3 (a) Upper: Distribution of b exponent values for the full spectrum of reach length scales over Lena River (b) Bottom: The first continuous mapping of a classical hydraulic geometry parameter from space. *Smith and Pavelsky*, [2008]

Measurements from SWOT will include WSE, slope, inundation area, and surface water storage change. Several studies have estimated streamflow and river geometry from the SWOT virtual mission (VM). "Virtual" observations were generated based upon the outputs of LISFLOOD-FP, which were then corrupted by adding normally distributed errors. *Andreadis et al.*, [2007] assimilated virtual WSE into LISFLOOD-FP to estimate discharge and river depth over a segment of the Ohio River. They showed that the errors of simulation were reduced by 13.2%, 50% and 5.4% for discharge, river depth and inundated area, respectively, after assimilation. They also tested three different satellite observation frequencies, 8, 16 and 32 days, showing that the best simulations came with the shortest satellite repeat period. Similarly, using the Ensemble Kalman Filter (EnKF), *Durand et al.*, [2008] assimilated virtual WSE into a hydrodynamic model, showing that the bathymetric depth and slope in such a scheme can be estimated within

56 cm and 0.30 cm/km of the truth respectively over a 240 km reach of the Amazon Basin. They further indicated that the accuracy of their bathymetry estimation was less insensitive to the error in SWOT measurements than the uncertainty from LISFLOOD-FP. With continuity, kinematic assumptions and interpolation of depth estimates, *Durand et al.*, [2010] presented an algorithm to estimate river depth and discharge directly from the SWOT simulator over the Ohio River Basin. The relative error of the depth estimation is 4.1%, and the median instantaneous and monthly discharge error is 10.9% and 14.7%, respectively. Their approach indicated the potential to estimate river depth from SWOT observations directly. Furthermore, using the actual SWOT orbits repeat period (a three-day fast sampling orbit with three phases and a 22-day nominal orbit) for the first time, *Biancamaria et al.*, [2011] assimilated virtual WSE into LISFLOOD-FP with a Local Ensemble Kalman Smoother. They also showed the great improvement of the modeling of river depth in an Arctic river. All of the above results demonstrate the prospects of characterizing river discharge and geomorphology from SWOT.

3. A National-Scale, Catchment-Based Land Surface Modeling Framework with an Explicit Representation of River Network Dynamics

3.1 Introduction

Surface water bodies (rivers, lakes, reservoirs, wetlands, floodplains, and other inland waters) are key components of the terrestrial hydrological cycle with an important role in regulating climate both regionally and globally [*Famiglietti*, 2004]. Through interactions with the atmosphere and the corresponding exchange of CO_2 and methane, surface water dynamics also exert a strong impact on global biogeochemistry [*Richey et al.*, 2002]. Many existing studies hypothesize the intensification of the global hydrological cycle due to climate change [*Ohmura and Wild*, 2002; *Alsdorf and Lettenmaier*, 2003; *Huntington*, 2006]. Surface water is no exception, as evidenced by an estimated increasing trend of global freshwater discharge into the ocean during the past two decades [*Syed et al.*, 2010; *Chandanpurkar et al.*, 2014].

With population growth and the increasing demand on water supplies, human water management practices (dams, reservoirs, irrigation, surface water diversion, groundwater pumping, and land use change, etc.) have altered the natural hydrographs of nearly all the major river basins worldwide [*Nilsson et al.*, 2005; *Alsdorf et al.*, 2007]. Without a comprehensive understanding of both the seasonal and long-term variability and distribution of surface water, decision makers will be challenged to sustainably manage water resources or to adapt to the changing global waterscape [*Oki and Kanae*, 2006; *Famiglietti et al.*, 2009]. Therefore, the need for an integrated continental-to-global scale surface water dynamics monitoring system, relying on both

observations [*Lettenmaier and Famiglietti*, 2006; *Alsdorf et al.*, 2007] and models [*NRC*, 2008; *Famiglietti et al.*, 2009] is ever increasing.

Traditional streamflow monitoring relies on gauging stations to provide estimates of water discharge. Such gauge observations are highly resolved in time (minutes to days) but are generally sparse in space. Alone, these point-scale *in situ* measurements cannot adequately describe the complex three-dimensional features of surface river dynamics [*Alsdorf et al.*, 2007]. Alternatively, estimates of streamflow have also been developed from remote sensing over the past two decades [*Smith et al.*, 1996; *Birkett et al.*, 2002; *Bjerklie et al.*, 2003, 2005b; *Coe and Birkett*, 2004; *Kouraev et al.*, 2004; *Frappart et al.*, 2005; *Leon et al.*, 2006]. However, none of the current spaceborne technology is able to provide adequate information needed to represent the dynamics of inland surface water [*Alsdorf and Lettenmaier*, 2003]. The upcoming Surface Water Ocean Topography (SWOT) mission [*Alsdorf et al.*, 2007] will observe vertical and horizontal variations of surface water bodies globally, by providing direct measurements of water surface elevation, water surface slope and inundation area for the largest rivers, lakes, and wetlands of the world. Many studies are demonstrating the expected impact of the SWOT mission [*Andreadis et al.*, 2007; *Durand et al.*, 2008; *Biancamaria et al.*, 2011] which, by design, will provide measurements that are continuous in space, but sparse in time. As Such, existing and upcoming observing tools for surface water span a wide range of spatial and temporal scales. One way to bridge the gap is to associate them with models of surface hydrology. The development of continental and global surface water models that use existing *in situ* observations and that can fully leverage upcoming observations like those for SWOT will enable an improved understanding surface water dynamics.

Land Surface Models (LSMs) are powerful tools that allow for continuous simulation of the terrestrial hydrologic cycle. Early LSMs were developed as one-dimensional grid-based models designed to best fit the computational units of atmospheric general circulation models (GCMs) [*Manabe*, 1969], but they are not adequate for horizontal movement of surface water [*Koster et al.*, 2000]. *Koster et al.* [2000] proposed using catchments as modeling units in LSMs, However, neither the study of *Koster et al.*, [2000] nor its follow-on studies [*Reichle and Koster*, 2005] include an explicit representation of surface water bodies or of lateral water transport. Several grid-based routing models exist to simulate horizontal water transport at continental-to-global scales [*Vörösmarty et al.*, 1989; *Miller et al.*, 1994; *Oki et al.*, 1999; *Olivera et al.*, 2000; *Döll et al.*, 2003; *David et al.*, 2011a]. In contrast, routing within catchment-based LSMs is relatively younger [*Goteti et al.*, 2008; *Beighley et al.*, 2009; *David et al.*, 2011b]. Since catchment-based LSMs represent the land surface as a mosaic of catchments, the actual river paths can be used as computational elements. This offers the potential for a more realistic representation of river geometry and floodplain extent, and hence facilitates the inclusion of advanced surface flow, and storage dynamics and anthropogenic water management.

The goal of this study is to develop a continental-scale, catchment-based river routing model coupled with an LSM, that includes an explicit representation of river networks, and that can simulate flow rates, flow depths and inundation extents. Such a modeling framework development will facilitate the use of existing *in situ* observations and be suitable for integrating the upcoming SWOT measurements for a range of studies in climate, hydrology and water management. It will also allow for simulation of sediment and nutrient transport and trace gas exchange along rivers.

The remainder of this chapter is organized as follows: Section 3.2 provides further background on the methods for relating discharge with river geometry through empirical relationships and the current state of both grid and catchment-based river routing models. Section 3.3 describes the original CHARMS as developed by *Goteti et al.*, [2008], and the data needs for CHARMS implementation. Section 3.4 presents the data preparation for CHARMS, and Section 3.5 displays the results obtained. The discussion and conclusions are presented in Section 3.6 and Section 3.7.

3.2 Background

3.2.1 Methods of relating flow dynamics with channel geometry and landscape morphology

The development of empirical relationships linking flow dynamics with channel geometry and landscape morphology has been ongoing since the nineteenth century. The most notable early relationship is Manning's equation [*Gauckler*, 1867; *Manning*, 1891]. *Leopold and Maddock* [1953] then first introduced the concept of "hydraulic geometry" in which flow width (w), flow depth (d), and flow velocity (v) are all related to flow rate (Q) using a similar power law:

$$w = aQ^b; d = cQ^f; v = kQ^m \qquad (3.1)$$

where *a, b, c, f, k, m* are empirical parameters. Given access to flow measurements, these parameters can be determined based on observations of flow quantities and landscape morphology and the power law relationships can be used to continuously estimate hydraulic geometry as a function of flow rate, and *vice versa*. Early studies have also detected the close correlation between river bankfull discharge (Q_{full}) and drainage area (A_d) [*Leopold et al.*, 1964; *Dunne and Leopold*, 1978]:

$$Q_{full} = \mu A_d^{\gamma} \qquad (3.2)$$

where μ, r are empirical parameters. Thus, bankfull flow can easily be determined based on drainage area, which can be useful for regions where discharge estimates are not easily available (i.e. gauge uncertainty or ungauged areas). Despite the expected variations of the relationships shown in equation (3.1)-(3.2) in both time and space [*Leopold and Maddock*, 1953; *Knighton*, 1974, 1975; *Richards*, 1976; *Park*, 1977; *Rhodes*, 1977], many studies have demonstrated the transferability of these relationships to increasingly large areas such as New Zealand [*Jowett*, 1998], the U. S. Great Plains [*Dodov and Foufoula-Georgiou*, 2004], South Australia [*Stewardson*, 2005], 18 regions covering the continental US [*Faustini et al.*, 2009], and the Amazon Basin [*Beighley and Gummadi*, 2011].

For most existing large-scale river transport models, bankfull hydraulic variables are required to separate the main river channel and floodplain, and to estimate streamflow inside and outside channel banks [*Decharme et al.*, 2008, 2012; *Beighley et al.*, 2009; *Yamazaki et al.*, 2011]. In this paper, similar concepts are used to develop empirical relationships between bankfull discharge and drainage area, bankfull depth and bankfull discharge, and bankfull width and bankufll discharge/depth. The proposed work focuses on the nineteen water resource regions over the contiguous U. S. in the National Hydrography Dataset Plus (NHDPlus) [*Horizon Systems Corporation*, 2010] to determine hydraulic relationship and estimate numerous channel cross-section profiles needed by river routing models.

3.2.2 Current state-of-the art for grid-based and catchment-based river routing models

LSMs estimate surface and subsurface runoff within each modeling unit by considering meteorology, land cover, soil characteristics and topographic conditions [*Beven and Kirkby*,

1979; *Sivapalan et al.*, 1987; *Famiglietti and Wood*, 1994; *Stieglitz et al.*, 1997; *Niu and Yang*, 2003; *Niu et al.*, 2005; *Oleson et al.*, 2008]. Using these estimates of runoff, many grid-based river transport models have been developed to simulate river discharge, floodplain inundation, water depth, velocity or other hydraulic variables at different spatial scales[*Vörösmarty et al.*, 1989; *Miller et al.*, 1994; *Oki et al.*, 1999; *Bates and De Roo*, 2000; *Coe*, 2002; *Döll et al.*, 2003; *Wilson et al.*, 2007; *David et al.*, 2011a]. While most existing grid-based LSMs consider the heterogeneity of land cover and topography within each grid cell when simulating runoff, corresponding grid-based routing models do not, making it hard to represent surface water dynamics realistically, since variations of rivers and floodplains occur at sub-grid scale [*Goteti et al.*, 2008]. Efforts to incorporate subgrid features in grid-based models [*Coe*, 2002; *Döll et al.*, 2003; *Yamazaki et al.*, 2011] can improve the representation to enhance the model performance. However, it is not always feasible for grid-based models to simulate river channel and floodplains variation at continental or global scales with a detailed river network because of the corresponding high computational demand.

Alternatively, horizontal heterogeneity (e.g. soil moisture and runoff generation) within catchment-based LSMs can be parameterized using a numerical topographic index [*Famiglietti and Wood*, 1994; *Stieglitz et al.*, 1997; *Koster et al.*, 2000; *Niu et al.*, 2005]. Catchment-based routing models coupled to catchment-based LSMs can use accurate river geometry to capture the movement of streamflow across the actual river channel, and therefore floodplain storage can also be estimated through river geometry [*Goteti et al.*, 2008]. Taking into account sub-grid heterogeneity, this catchment-based approach is able to simulate discharge and surface water storage more realistically using less computational resources compared to grid-based model.

Goteti et al.[2008] presented a Catchment-based Hydrologic and Routing Model System (CHARMS) coupled with the NCAR Community Land Model (CLM) 3.0, with an application to the Wabash River basin to simulate river streamflow, depth, and corresponding floodplain inundation extent.

Based on the concept of CHARMS from *Goteti et al.*, [2008], our study builds a continental-scale catchment-based river routing model system coupled with an LSM and with the river network upscaled from NHDPlus. To our knowledge it is the first continental-scale catchment-based land surface modeling framework with an explicit representation of river networks, including corresponding flow depth and floodplain inundation extent.

3.3 Catchment-based land surface and river modeling with CHARMS

The Catchment-based Hydrologic And Routing Modeling System (CHARMS, [*Goteti et al.*, 2008]) is made of two components: a land surface model and a routing model both operating on a catchment template. The land surface model in CHARMS is adapted from version 3.5 of the Community Land Model (CLM, [*Oleson et al.*, 2007]), though updated version of CLM can be easily incorporated, to run on catchments instead of the traditional grid environment. Therefore, as opposed to running on a 2D grid of latitudes and longitudes, CLM is run within CHARMS on a 1D grid of unique catchment identifiers, while the river network is represented explicitly using discretized linear reaches. The routing model in CHARMS is presented in *Goteti et al.*, [2008] and includes treatment for transport of water from hillslopes to river channels (simplified here) and treatment for transport of water within the river channels and their floodplains. An explicit representation of river networks and river cross-section profiles allows for estimation of the

corresponding river depths, river widths, and floodplain inundation extent. Additional information on CHARMS that clarifies the work of [*Goteti et al.*, 2008] is available in the Appendices. This section briefly describes the characteristics of CHARMS that are of importance for the study presented here; i.e. the CHARMS template, the basics of surface and river dynamics in CHARMS, and the separation of total flow into channel and floodplain.

3.3.1 The CHARMS template

The main features of the CHARMS template are the catchment boundaries and the main river reach included within each catchment (Figure 3.1(a)). A unique identifier called the HydroID [*Maidment*, 2002] is used to relate a catchment to its main river reach. The hydrologic network connectivity is described using a pair of HydroIDs pointing to the corresponding upstream and downstream elements. Each main reach is further divided into sub-reaches (Figure 3.1(a)-(b)) which are ordered sequentially from upstream to downstream.

The surface area and slope (hillslope) of each catchment (Figure 3.1 (c)); and the length (L_{rch}), slope (S_{rch}) and drainage area of each sub-reach (A_{rch}) (Figure 3.1(b)) are also required for the routing. Finally, channel hydraulic geometry parameters (Figure 3.1(c)) composed of bankful depth (h_{full}), bankful width (w_{full}) and bankfull flow rate (Q_{full}) are also necessary for CHARMS, as is Manning's roughness coefficient for channel and floodplain.

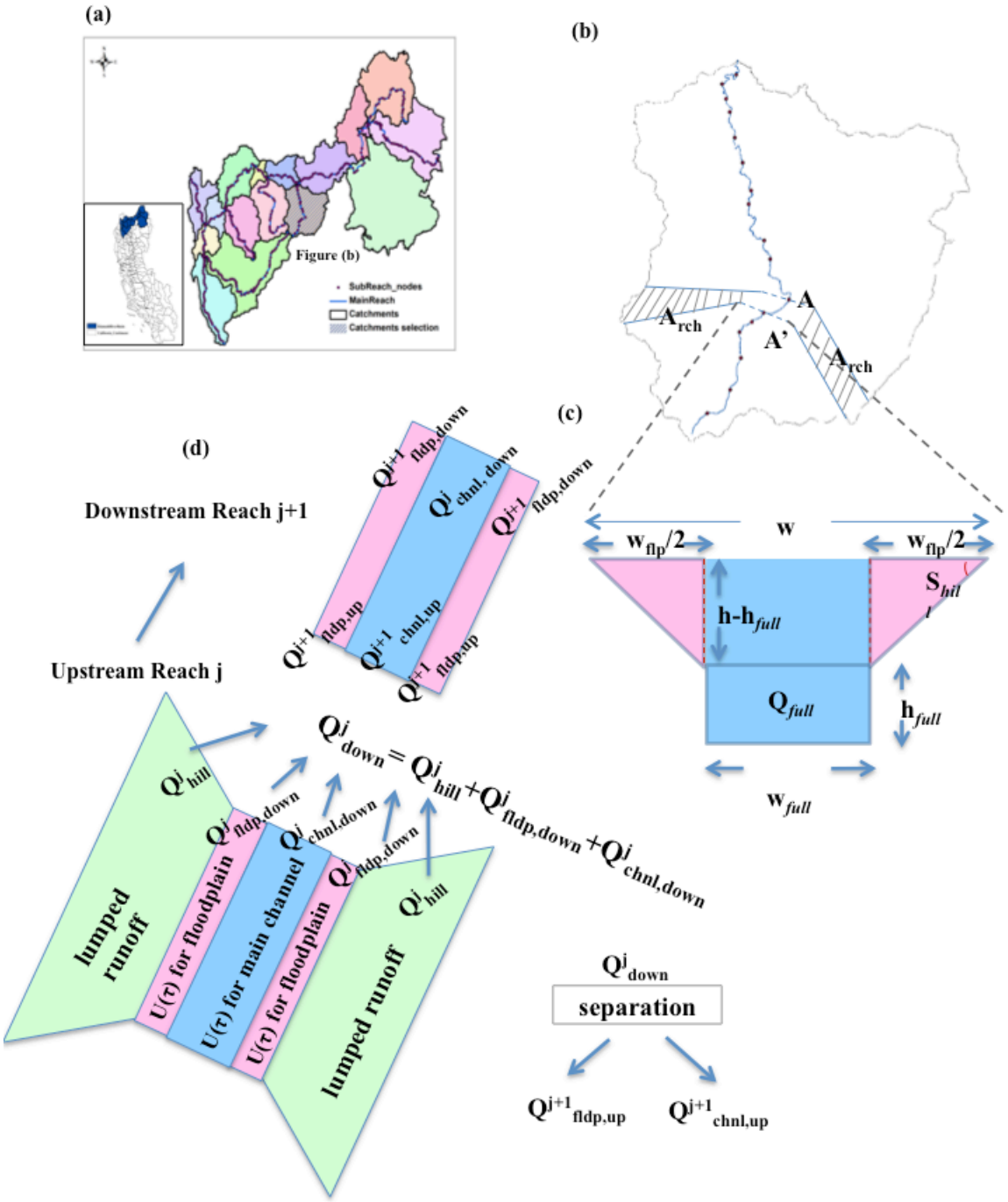


Figure 3.1 Schematic plot of (a) CHARMS representation of river networks; (b) CHARMS representation of the river network in one catchment; (c) cross-section profile and channel dimension; (d) river routing and separation of total stream flow into main channel and floodplain flow from upstream reach (j) to downstream reach (j+1).

3.3.2 Runoff generation and explicit river dynamics in CHARMS

Simulations of surface water dynamics generally start with runoff production. In this study, runoff is generated via surface runoff (saturation excess and infiltration excess) and subsurface runoff (baseflow), using the SIMTOP approach of [*Niu et al.*, 2005]. Details on the methods calculating surface and subsurface runoff with CLM in CHARMS can be found in Appendix 3.A.

The contribution by hillslope to each sub-reach uses a simplified version of that of *Goteti et al.*, [2008], and is calculated as the product of the drainage area of each sub-reach and the temporal averaged sum of surface and subsurface runoff during each routing period. This lumped runoff is added at the downstream end of each sub-reach (Figure 3.1(d)). More details on hillslope contribution to the river network are given in Appendix 3.B.

Routing in channels and floodplains is done separately but uses the same unit hydrograph approach. Total streamflow Q^{j}_{down} from the downstream end of all the upstream subreaches (j) is first separated into channel ($Q^{j+1}_{up,\,chnl}$) and floodplain ($Q^{j+1}_{up,\,fldp}$) at the upstream point of each downstream sub-reach $j+1$ before routing occurs in sub-reach $j+1$(Figure3.1 (d)). Separate unit hydrographs, which represent the fraction of the upstream flow that appears downstream are computed for channel routing and floodplain routing for each of sub-reach ($j+1$) (Figure 3.1(d)). The separate unit hydrographs and flows are used to route water from upstream to downstream in each sub-reach ($j+1$), both in the channel and floodplain. Details on how to calculate the unit response function are provided in Appendix 3.C. The total outflow from each sub-reach j is computed based on the contribution from hillslope transport from both surface runoff and

baseflow, and all the water transport from upstream sub-reaches from both the main river channel and the floodplain:

$$Q^{j}_{down}(t) = Q^{j}_{hill}(t) + Q^{j}_{chnl,down}(t) + Q^{j}_{fldp,down}(t) \qquad (3.3)$$

This summation is made downstream (Figure 3.1(d)). The routing process starts from the headwater catchment and proceeds sequentially downstream.

3.3.3 Separation of river flow into channel/floodplain components and estimation of river depth, width and floodplain extent

The separation of total upstream flow Q^{j}_{down} into channel ($Q^{j+1}_{chnl,up}$) and floodplain ($Q^{j+1}_{fldp,up}$) components of downstream sub-reaches is a key element of CHARMS. This process is only briefly mentioned in *Goteti et al.*, [2008] and therefore further developed here. The total water flow Q passing through the river cross-section of each sub-reach is separated at each time step based on bankfull hydraulic geometry (bankfull depth and bankfull width, and bankfull discharge). Two cases are considered depending on whether or not the total flow is greater in magnitude than the bankfull flow:

$$\begin{cases} if\,(Q \le Q_{full}) \quad Q_{chnl} = Q; \quad Q_{fldp} = 0; & 3.4(a) \\ if\,(Q > Q_{full}) \quad Q = Q_{full} + p \cdot (h - h_{full})^{q} & 3.4(b) \end{cases}$$

where h is the stage height, and p, q are parameters pre-defined using the power law method [*Garbrecht*, 1990]. This power method is an alternative form of the general power laws that consider main channel and over-bank flow together. The value of p and q are determined through linear regression between sets of increment values of Q (calculated using Manning's equation) and h. For each sub-reach, if the total flow Q passing through the cross-section is smaller than the bankfull flow (Q_{full}), river width w is equal to w_{full}, and stage height $h(t)$ can be estimated

through Manning's equation that relates Q to width and depth directly as Equation (3.5a). If the total flow Q is larger than bankfull flow (Q_{full}), then out-of-bank flow occurs on the floodplain. The stage height h is calculated by Equation (3.5b), and the river width w can be solved through geometry as:

$$if\ (Q(t) \le Q_{full}) \quad \begin{cases} h(t) = \left(\dfrac{Q(t) \cdot n}{w_{full} \cdot s_{rch}^{0.5}} \right)^{\frac{1}{1.67}} \\ w(t) = w_{full} \end{cases} \qquad (3.5a)$$

$$if\ (Q(t) > Q_{full}) \quad \begin{cases} h(t) = \left(\dfrac{Q(t) - Q_{full}}{p} \right)^{\frac{1}{q}} + h_{full} \\ w(t) = w_{full} + 2 \cdot \dfrac{h - h_{full}}{S_{hill}} \end{cases} \qquad (3.5b)$$

where n is the Manning's coefficient, S_{rch} is the river reach slope, and S_{hill} is the hillslope of each catchment (Figure 3.1(c)).

3.4 Data preparation for CHARMS

3.4.1 Building a national modeling template for CHARMS by upscaling NHDPlus data

3.4.1.1 The NHDPlus Dataset

Goteti et al., [2008] derived catchment boundaries and river flowlines from a high resolution (90m) Digital Elevation Model (DEM). However, this is excessively computationally demanding at the continental scale. Decreasing the resolution of the DEM can shorten processing time, but rivers with widths narrower than the resolution of DEM will not be captured. Instead, in this study, catchment boundaries and main river reaches corresponding to each catchment were extracted from version 1 of the National Hydrography Dataset Plus (NHDPlus) [*Horizon Systems*

Corporation, 2010]. NHDPlus is an integrated data suite of rivers and surface water bodies which includes over 3 million catchments boundaries and river flowlines over the United States. The NHDPlus dataset also provides river reach connectivity, relative upstream/downstream position, and the geolocation of all the USGS gauging stations on its river network. These unique properties make it well-suited to provide the backbone for our continental-scale modeling framework.

3.4.1.2 Upscaling NHDPlus data

NHDPlus provides valuable connectivity information but its dense description of surface hydrography makes it computationally demanding for continental-scale hydrologic modeling. Therefore, obtaining a more suitable resolution by upscaling NHDPlus data was performed here first. A combination of the Hydrologic Unit Codes (HUCs) of *Seaber et al.*, [1987] and Strahler stream order [*Strahler*, 1957] was used (Figure 3.2(a)). HUCs are a coding system used by the USGS to identify drainage basins in the U. S. The first level 2-digit HUCs (HUC2) divides the nation into 21 (18 over the contiguous U. S.) major drainage regions based on surface topography. The fourth level 8-digit HUCs (HUC8) partitions the nation into 2104 smaller watersheds with average area of 3890 km^2. We started here with the 2104 HUC8 units of the contiguous United States as the initial catchments (see Figure 3.2(a) for an example for the Klamath River Basin). We then sequentially overlaid river reaches of decreasing Strahler stream order on the catchment layer to find the corresponding main reach. For those catchments without an overlapping main river reach, the process was repeated with reaches of lower stream order. This process was repeated from the highest Strahler stream order (SO=10) in NHDPlus all the way upstream to the headwater (SO=1) until all the catchments had at least one main reach (Figure 3.2(b)). For those catchments with 2 or more overlapping reaches (Figure 3.2(c)), we

manually further divided the catchments according to the detailed drainage boundaries provided by NHDPlus (Figure 3.2(d)). The overlapping processing yielded a total of 2959 catchments with an average area of 2,773 km^2 for the contiguous U. S. (Figure 3.3(a)). Each main river reach has an average length of 110 km), resides in one catchment and is associated with one inlet and one outlet. The upscaled river network is composed of 198,633 sub-reaches of average length 1.67 km. In order to further limit the computational problem, we chose to set the minimum length of sub-reaches to 2.5km. In each catchment, sub-reaches with length shorter than 2.5km were merged together until the sub-reach length was 2.5km or longer. After merging, there are a total of 76,522 sub-reaches in the entire network and each catchment has up to 125 sub-reaches (see Figure 3.3(a)). All the other properties described in Section 3.3.1 were calculated with the information provided by NHDPlus.

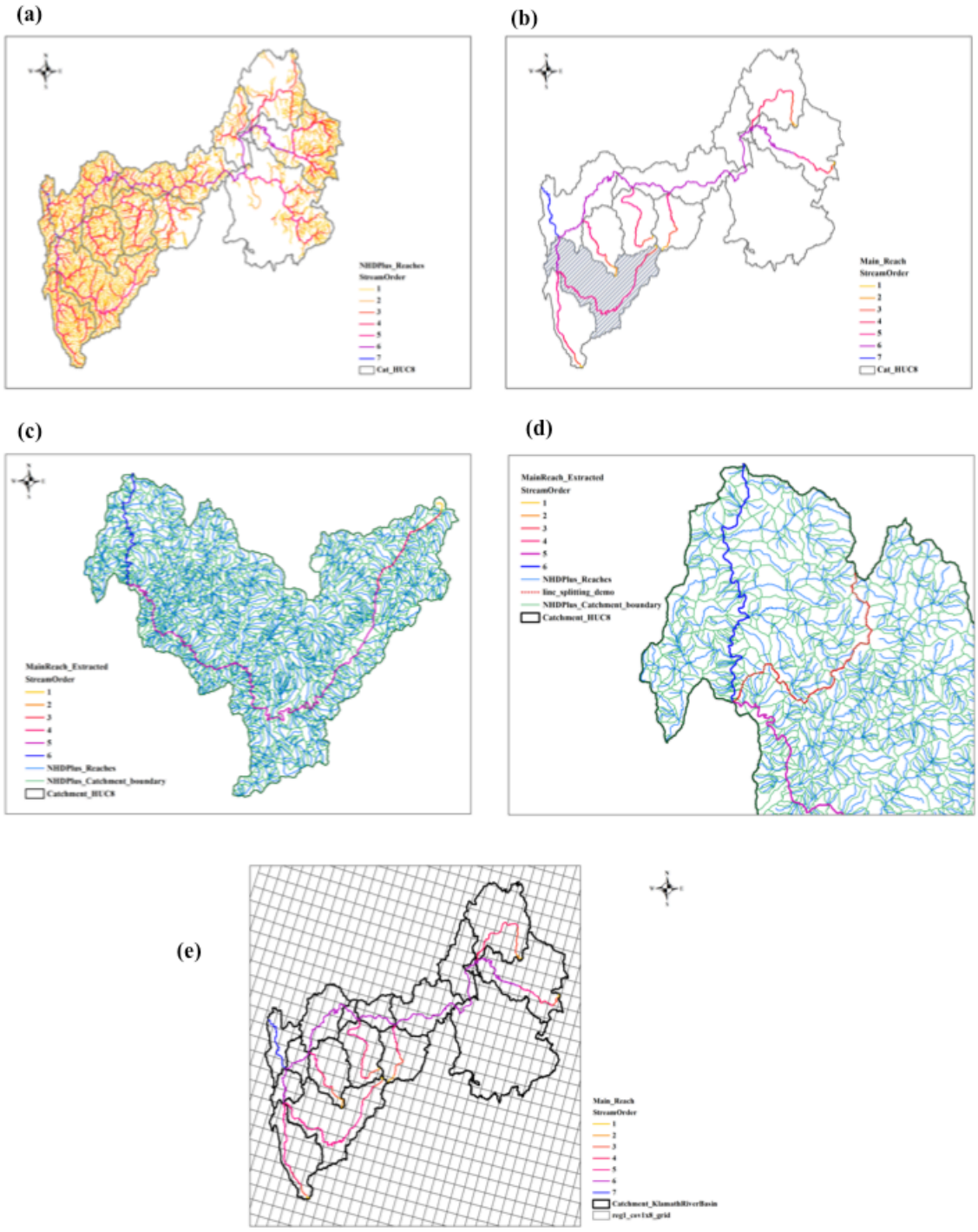
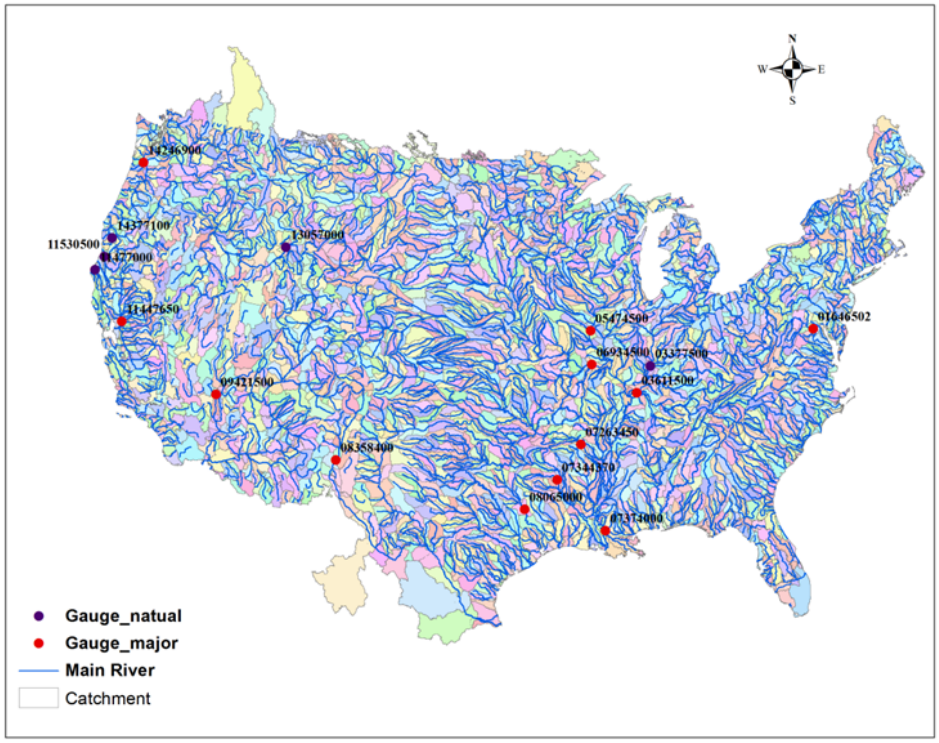


Figure 3.2 (a)-(d) Schematic plots of the upscaling process for the Klamath River basin with the NHDPlus dataset; (e) Schematic plot of the interpolation process to convert grid-based meteorological forcing and land surface input data into catchment-based input datasets.

(a)



(b)

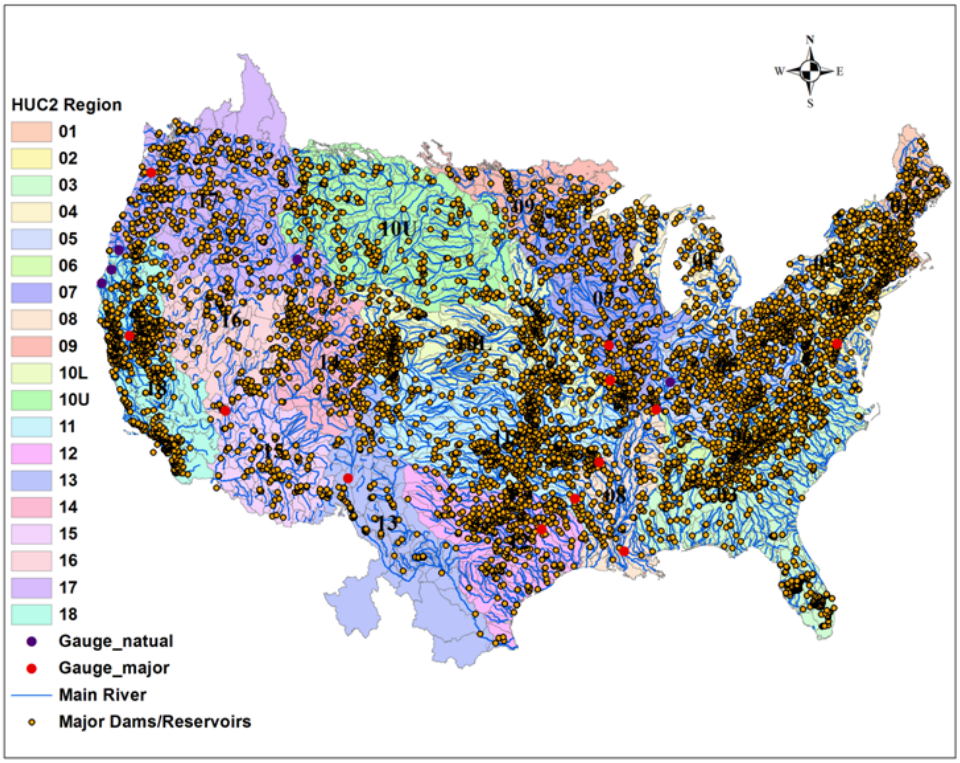


Figure 3.3 (a) Explicit representation of river networks for the continental-scale CHARMS modeling template with 17 USGS gauge sites for model validation. Blue lines represent the main river reaches in each catchment; (b) 19 HUC2 water resources regions by NHDPlus with the main river reaches and USGS gauge sites. The brown dots denote the major dams/reservoirs across the contiguous U.S.

3.4.2 Land surface data and atmospheric forcing for CHARMS

Gridded land surface model inputs must be interpolated to the catchment template before running the catchment-based version of CLM [*Goteti et al.*, 2008]. This interpolation was performed using an area-weighted sum based on the fractional coverage of a catchment by the regular grid. Three-hourly meteorological forcing data were derived and interpolated from the second phase of the North America Land Data Assimilation System (NLDAS2) [*Xia et al.*, 2012], an hourly 1/8° gridded dataset available from 1 Jan 1980 to 31 Mar 2010 for the United States and part of Canada and Mexico. The required atmospheric forcing variables include precipitation, air temperature, surface pressure, wind speed, specific humidity, and downward shortwave and longwave radiation. For comparison, after the grid-to-catchment interpolation, annual basin-averaged precipitation for the Mississippi River Basin is 826.90 mm/yr, which is comparable with the 835 mm/yr from published water budgets of the Mississippi River Basin [see, e.g. *Milly and Dunne*, 2001; *Milly*, 2005], and 821 mm/yr calculated from NLDAS2 by *Cai et al.*, [2013].

Surface properties including soil depth, soil properties, and vegetation characteristics were interpolated from the original surface data input of CLM3.5.

The modified 30 arc sec (~1km) DEM GTOPO30 [*Asante*, 2000] was used to calculate the topographic index and maximum fractional saturated area (fmax) of each catchment required for the runoff generation in CLM 3.5 [*Niu et al.*, 2005].

3.4.3 Extracting river cross-section profiles using empirical relationships

River geometry is needed to distinguish between the main channel and floodplain, and to estimate the corresponding river depth and width. Since there are nearly 80,000 sub-reaches in the CHARMS template used here, calculating the river bankfull depth and bankfull width from cross-sections derived from a high resolution (~90m) DEM as in previous studies would be excessively computationally demanding. However, given the average length of our main river reaches (110 km), there is potential transferability of rating curves among catchments in a large river basin through reach averaging, as suggested by *Smith and Pavelsky* [2008]. Following *Beighley and Gummadi*, [2011], we chose to derive empirical relationships between the drainage area and river dimensions for each of the 19 NHDPlus HUC2 water resources regions (region 10 from USGS HUC2 is divided to region10U and region 10L in NHDPlus, Figure 3.3(b)).

For each HUC2, USGS observations (http://waterdata.usgs.gov/nwis/measurements) from 1990-01-01 to 2010-03-31 were used to fit a rating curve (fourth order polynomial) between stage and discharge (Figure 3.4(a)). Bankfull discharge (Q_{full}) was defined as the value at the inflection point of the stage-discharge relationship based on the assumption that it represents the point of overflow onto the floodplain [*Beighley and Gummadi*, 2011]. The inflection point was determined by setting the second derivative of the 4th order polynomial fit to zero (Figure 3.4(a)). The bankfull depth h_{full}, was chosen as the value of the depth corresponding to Q_{full} on the rating curve. The drainage area of each gauge station was also determined from USGS data. With Q_{full}, h_{full}, and the drainage area A_d of different gauge sites, the Q_{full}-A_d and h_{full}-Q_{full} relationships for the main channel were calculated as:

$$Q_{full} = \mu \cdot A_d^{\gamma}; \quad h_{full} = c \cdot Q_{full}^{f} \qquad (3.6)$$

where *μ, r, c, and f* are empirical parameters. The parameter sets for the different regions are listed in Table 3.1.

HUC2 Region	Region Name	Number of Gauges	Q_{full} vs A	R^2	Q_{full} vs h_{full}	R^2
01	New England	301	$Q_{full}=0.0772A^{0.9943}$	0.78	$h_{full}=0.8699Q_{full}^{0.1846}$	0.45
02	Mid-Atlantic	649	$Q_{full}=0.0804A^{0.9928}$	0.71	$h_{full}=0.7238Q_{full}^{0.2249}$	0.51
03	South Atlantic-Gulf	892	$Q_{full}=0.4789A^{0.7735}$	0.58	$h_{full}=1.0129Q_{full}^{0.2365}$	0.38
04	Great Lakes	371	$Q_{full}=0.0644A^{0.8774}$	0.59	$h_{full}=0.8733Q_{full}^{0.2220}$	0.42
05	Ohio	491	$Q_{full}=0.3803A^{0.7922}$	0.73	$h_{full}=0.7792Q_{full}^{0.2687}$	0.52
06	Tennessee	160	$Q_{full}=0.0932A^{1.0054}$	0.69	$h_{full}=0.6401Q_{full}^{0.3018}$	0.65
07	Upper Mississippi	444	$Q_{full}=0.3459A^{0.7706}$	0.68	$h_{full}=1.2601Q_{full}^{0.2146}$	0.44
08	Lower Mississippi	134	$Q_{full}=1.8866A^{0.6112}$	0.46	$h_{full}=1.9942Q_{full}^{0.1653}$	0.28
09	Souris-Red-Rainy	96	$Q_{full}=0.1524A^{0.7021}$	0.69	$h_{full}=1.1168Q_{full}^{0.3115}$	0.63
10U	Missouri	306	$Q_{full}=0.1225A^{0.6846}$	0.55	$h_{full}=0.9504Q_{full}^{0.2049}$	0.35
10L	Missouri	223	$Q_{full}0.3916A^{0.0638}$	0.24	$h_{full}=0.8900Q_{full}^{0.3178}$	0.72
11	Arkansas-White-Red	427	$Q_{full}=1.5324A^{0.4874}$	0.27	$h_{full}=1.0887Q_{full}^{0.2465}$	0.56
12	Texas-Gulf	295	$Q_{full}=26.14A^{0.385}$	0.22	$h_{full}=0.7462Q_{full}^{0.2887}$	0.51
13	Rio Grande	109	$Q_{full}=0.0662A^{0.5717}$	0.49	$h_{full}=0.7879Q_{full}^{0.2106}$	0.42
14	Upper Colorado	290	$Q_{full}=0.3267A^{0.7387}$	0.66	$h_{full}=0.5778Q_{full}^{0.1839}$	0.46
15	Lower Colorado	173	$Q_{full}=0.3487A^{0.7383}$	0.33	$h_{full}=0.9439Q_{full}^{0.1512}$	0.29
16	Great Basin	208	$Q_{full}=0.2856A^{0.7559}$	0.63	$h_{full}=0.8364Q_{full}^{0.1358}$	0.27
17	Pacific Northwest	667	$Q_{full}=1.3611A^{0.7563}$	0.53	$h_{full}=0.7285Q_{full}^{0.1948}$	0.31
18	California	361	$Q_{full}=1.4191A^{0.7679}$	0.50	$h_{full}=0.5714Q_{full}^{0.2488}$	0.55

Table 3.1 Empirical power law relationships between bankfull discharge (Q_{full}) and drainage area (A), and between bankfull discharge (Q_{full}) and bankfull depth (h_{full}) for each HUC2 water resource region with USGS field measurements between 01/01/1990 to 03/31/2010.

With drainage area calculated from NHDPlus, the corresponding bankfull flow and bankfull depth of each sub-reach can be determined. Bankfull width w_{full} for each river reach was determined using a modification of Manning's equation (Equation (3.1)) accounting for flow area in a rectangular channel:

$$Q = \frac{1}{n} \cdot w \cdot h^{1.67} \cdot S_{rch}^{0.5} \qquad (3.7)$$

where Q is the flow passing through a river cross-section, n is Manning's coefficient, w is the channel top width, h is the mean flow depth, and S_{rch} is the water surface slope along each reach. Maps of derived Q_{full}, h_{full}, w_{full} for the U. S. are shown in Figure 3.4(b, c, d). The derived value of bankfull depth and width compared reasonably well with the dataset of [*Andreadis et al.*, 2013] in Figure 3.4(e, f). The spatial patterns of both the bankfull depth and bankfull width derived in this study match well. The magnitude of both derived bankfull depth with different relationships is also comparable. The magnitude of the derived bankfull width in this study is 20-30% smaller than that of *Andreadis et al.*, [2013] for several major rivers in the Mississippi river basin. This is likely due to their use of one uniform hydraulic geometry relationship globally.

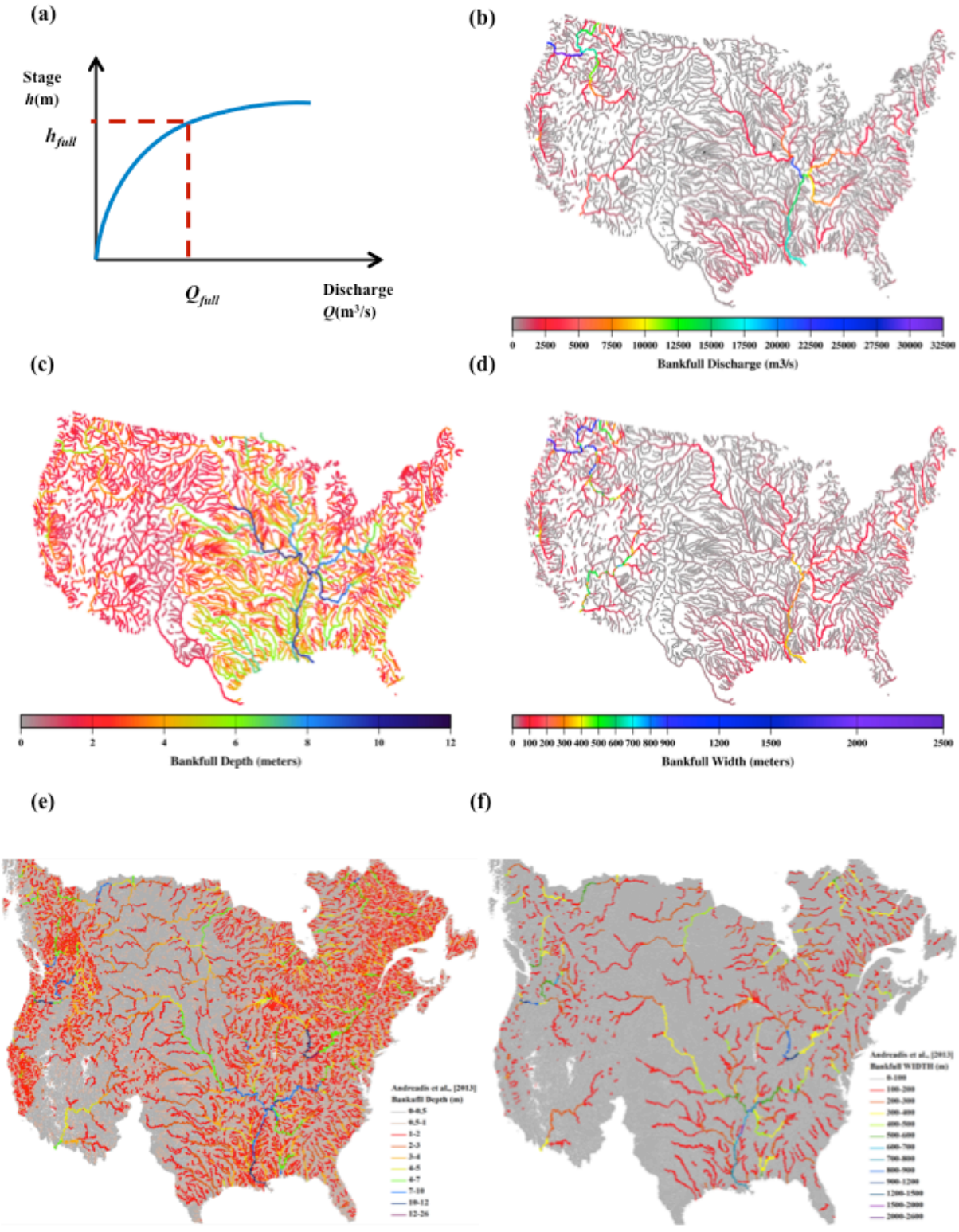


Figure 3.4 (a) Schematic plot of a stage-discharge relationship at a hypothetical gauging station; (b), (c), (d) bankfull depth, bankfull width, and bankfull discharge derived based the empirical relationship summarized in Table 3.1; (e-f) bankfull depth and bankfull width product by *Andreadis et al.*, [2013] for comparison.

3.5 Results

CHARMS was run from 1 Jan 1980 to 31 Mar 2010, spanning most of the NLDAS2 atmospheric forcing data availability. However, allowing for the substantial model spin-up that is necessary for sub-surface hydrology (see, e.g. [*Cai et al.*, 2013]), the calibration and analysis presented here focus on the last five water years (from October of the previous year to September of the following year) of the simulation (2004-10-01 to 2009-09-30). Daily discharge estimates and periodic field observations of river depth and width were obtained from the U. S. Geological Survey National Water Information System (NWIS, http://waterdata.usgs.gov/usa/nwis/) for comparison and validation purposes. Model performance was therefore evaluated by comparing simulated and observed daily discharge, and water depth and inundation extent for days when such data were available.

3.5.1 Land Surface Model Calibration

Runoff generation (see Section 3.3.2.) is a critical component of any study focusing on the simulation of river flow dynamics. Previous work has shown that the land surface model in CHARMS (CLM) tends to overestimate runoff, to underestimate evapotranspiration, and consequently results in poor simulations of peak flows [*Goteti et al.*, 2008]. CLM also typically produces higher runoff with larger temporal variability and lower evapotranspiration over mountainous and wet regions [*Zaitchik et al.*, 2010; *Li et al.*, 2011] and during the winter [*Kumar and Merwade*, 2011]. However, detailed analysis of the land surface modeling component of CHARMS is not the focus of this study: rather it is on the explicit representation of water dynamics within river networks. Therefore, the emphasis of CLM here is on an initial tuning of the parameters that have previously been identified as crucial in controlling runoff generation

and evaporation in CLM [*Niu et al.*, 2007; *Li et al.*, 2011] and other land surface models [*Cai et al.*, 2013]. These parameters include the saturated hydraulic conductivity (k_{sat}), the exponential decay factor of subsurface runoff (f), the surface dryness factor (α), soil resistance (R_{soil}), and volumetric water content at saturation (porosity) (θ_{sat}). Details on the calculation of the above parameters in CLM runoff generation are provided in Appendix 3.A. Parameters were tuned for the Mississippi River Basin since it occupies almost half of the contiguous U. S. by area. Starting with CLM default parameter values, different combinations of alternative values were tested following the procedure of *Cai et al.*, [2013]: default parameter values were varied manually by fixed amounts or by scaling factors as summarized in Table 3.2.

Parameters	Value/Ranges
Ksat	Default value multiplied by 0.01, 0.5, 1.0, 2.0 , **5.0**, 10 ,20, 100
f	2.5, **3.0**, 4.5, 5.5, 6.5
α	4.25, 5.5,6.5,**8.0**
Rsoil	Default value multiplied by 0.05, **0.2**, 0.4, 0.6, 0.8
θsat	Default value multiplied by 1.0, 1.5, **2.0**

Table 3.2 Manual calibration of key parameters. Variation of values described in text. Red underscored values were those selected for model simulation.

The combination of model parameters leading to total annual basin-averaged runoff that is closest to published values was selected. Table 3.3 shows the water budget of the Mississippi River Basin after this initial parameter tuning, along with corresponding values from *Kumar and Merwade*, [2011] and *Milly*, [2005]. The total yearly-accumulated basin-averaged runoff obtained here in the Mississippi River Basin is 310.19 mm/yr for 2004-2010, which is comparable to the 281mm/yr for 1988-1999 obtained by *Kumar and Merwade*, [2011] although

it is over 50% higher than the 198mm/yr obtained by *Milly*, [2005] for 1949-1997. Conversely, the evapotranspiration, 637 mm/yr in *Milly*, [2005] is higher than that obtained in this study (489.89 mm/yr). Differences may be due to different lengths of study, variations in forcing data, and parameter values etc.; but are satisfactory given that the focus of this study is on river transport and not runoff generation.

Water Budget (mm/yr)	This Study (Year 2004-2010)	*Milly et al.*, [2005] (Year 1949 - 1997)	Kumar and Merwade, [2011] (Year 1988-1999)
Precipitation	826.91	835	N/A
Total Runoff	310.20	198	281
Surface Runoff	54.16	N/A	N/A
SubSurface Runoff	256.04	N/A	N/A
Total Evapotranspiration	489.89	637	N/A
Soil Evaporation	355.16	N/A	N/A
Canopy Evaporation	10.15	N/A	N/A
Vegetation Transpiration	124.58	N/A	N/A

Table 3.3 Water budget of the Mississippi River basin from CHARMS after initial tuning. Comparisons are to the studies of *Milly et al.,* [2005] and *Kumar and Merwade* [2011].

3.5.2 Model Simulations

3.5.2.1 Choice of gauging stations

A total of seventeen USGS gauging stations were selected as validation sites for the CHARMS simulation. Twelve stations that are widely used (see, e.g. [*Xia et al.*, 2012; *David et al.*, 2013]) were chosen near the outlets of major river basins involved with active human management, and are considered as major rivers at "managed" regions. Given the current lack of representation of

lakes and reservoirs in CHARMS, five additional sites were selected that did not include major dams, and are considered here as relatively free of anthropogenic effects and as natural rivers at "unmanaged" regions. Figure 3.3(a) shows the locations of the seventeen gauging stations considered in this study, and Figure 3.3(b) shows the major dams and reservoirs as described in the National Inventory of Dams of the US Army Corps of Engineers. The USGS station code, name, location (latitude and longitude), and the corresponding HUC 2 region of each site are all listed in Table 3.4.

Station Number	Station Name	Long	Lat	HUC2	Mean flow Simulation (m^3/s)	Mean flow Observations (m^3/s)	Relative Bias	Correlation coefficient	RMSE (m^3/s)	NS Efficiency
Natural:										
03377500	WABASH RIVER AT MT. CARMEL, ILL.	-87.75	38.40	5	1451.30	1010.00	32%	0.53	1175.44	-0.10
11477000	EEL R A SCOTIA CA	-124.10	40.49	18	336.09	264.50	27%	0.33	551.97	-0.67
11530500	KLAMATH R NR KLAMATH CA	-124.00	41.51	18	800.11	472.83	69%	0.53	818.95	-1.28
13057000	SNAKE RIVER NR MENAN ID	-111.98	43.75	17	131.87	161.87	-19%	0.61	105.16	0.30
14377100	ILLINOIS RIVER NEAR KERBY, OR	-123.66	42.23	17	38.75	34.51	12%	0.43	67.05	-0.02
Major:										
03611500	OHIO RIVER AT METROPOLIS, IL	-88.74	37.15	5	9700.00	7908.50	23%	0.64	5291.40	0.29
01646502	POTOMAC RIVER (ADJUSTED) NEAR WASH, DC	-77.13	38.95	2	512.53	304.12	69%	0.19	486.50	-0.85
06934500	Missouri River at Hermann, MO	-91.44	38.71	10U	3784.70	2282.20	66%	0.44	2784.80	-2.20
07263450	Arkansas River at Murray Dam near Little Rock, AR	-92.36	34.79	11	2032.22	1495.10	36%	0.42	1755.90	-0.14
07344370	Red River at Spring Bank, AR	-93.86	33.08	11	796.70	552.75	44%	0.41	770.71	-0.15
07374000	Mississippi River at Baton Rouge, LA	-91.19	30.45	8	18190.00	15123.00	20%	0.65	7250.90	0.02
08065000	Trinity Rv nr Oakwood, TX	-95.79	31.65	12	306.72	142.03	116%	0.35	342.81	-1.29
08358400	RIO GRANDE FLOODWAY AT SAN MARCIAL, NM	-106.99	33.68	13	51.75	22.71	128%	0.36	98.80	-11.52
11447650	SACRAMENTO R A FREEPORT CA	-121.50	38.46	18	615.33	584.92	5%	0.58	524.61	-0.27
14246900	COLUMBIA RIVER @ BEAVER ARMY TERMINAL NR QUINCY,OR	-123.18	46.18	17	5207.1	6239.2	-17%	0.3781	3064.10	-0.40
09421500	Colorado River blw Hoover Dam, AZ-NV	-114.74	36.02	15	260.97	355.70	-27%	0.45	296.25	-4.15
05474500	Mississippi River at Keokuk, IA	-91.37	40.39	7	4984.60	2215.20	125%	0.31	4342.60	-3.36

Table 3.4 List of validation sites of USGS gauging stations and CHARMS performance statistics for daily simulated discharge, compared to gauge observations (10/1/2004-9/30/2009).

3.5.2.2 Temporal variations of simulated streamflow

Daily flow statistics consisting of the mean observed flow, mean modeled flow, relative bias, correlation coefficient, root mean square error (RMSE) and Nash-Sutcliffe efficiency (NSE) for each of the seventeen gauging stations considered are summarized in Table 3.4. The upper part of Table 3.4 contains statistics for natural rivers within unmanaged regions and the lower part contains those of managed regions. Hydrographs of observed and modeled daily flows for ten representative locations are plotted in Figure 3.5. The left-hand side of Figure 3.5 displays natural rivers within unmanaged regions and the right-hand side exhibits major rivers in managed regions. Daily flow statistics and hydrographs are presented for the last five water years of simulation (2004-10-01 to 2009-09-30).

Simulations of daily discharge over unmanaged regions show a close match with observations. The absolute values of the relative biases range from 12% for the Illinois River near Kerby, OR, to 69% for the Klamath River near Klamath, CA. The values of the NSE range from -1.28 to 0.30, but the negative efficiencies are likely related to inaccurate reproduction of the mean rather than to poor dynamics, as evidenced by correlation coefficients ranging from 0.33 to 0.61. The performance statistics therefore indicate fair agreement between the CHARMS simulation and the available observations, and demonstrate the capability of CHARMS to capture both the long term and seasonal variability of daily flows within unmanaged regions. The hydrographs of Figure 3.5 (left) show that CHARMS is able to capture the timing and magnitude of low flows, but sometimes does not capture high flows. Such discrepancies are likely due to the tendency of CLM to generate higher runoff during peak flow seasons [*Goteti et al.*, 2008; *Zaitchik et al.*, 2010]. Generally, daily discharge simulations over managed regions follow observed seasonal

patterns Figure 3.5 (right). Absolute values of the relative biases between simulations and observations range from 5% for the Sacramento River at Freeport, CA to 128% at for the Rio Grande Floodway at San Marcial, NM. The NSE over these locations is up to 0.29 for the Ohio River at Metropolis, IL, but can reach values as low as -11.52 for the Rio Grande Floodway at San Marcial, NM. Again the correlation coefficients ranging from 0.19 to 0.64 indicate that the inaccuracy of the mean has a large impact on efficiencies. These statistics indicate the capability of CHARMS to satisfactorily reproduce observed daily flows despite some relatively large biases at several gauging stations. Such discrepancies between modeled and observed daily flow can be explained in part by heavy water management of the major rivers of the U. S. [*Graf*, 1999], and by the lack of their representation in the current version of CHARMS. For example, approximately seventy-five percent of the flow from the Rio Grande River is currently diverted to satisfy the agriculture demands of nearby basins [*Douglas*, 2009; *Ward and Pulido-Velazquez*, 2012]. Additionally, the large reservoir storage (*Graf* [1999] estimated that nearly 2.5-4 times of the mean annual runoff was stored along the rivers of the U. S. Great Plains, the Rio Grande, Texas, and the American southwest) could further explain the poor average flow (and hence efficiency) obtained for the Rio Grande River. Similarly, the overestimated winter flow and underestimated summer flow near the mouth of the Sacramento River may be linked to water management of the California State Water Project (SWP), an intricate system of dams, reservoirs, aqueducts, and pumping plants to distribute water from northern to southern California (http://www.water.ca.gov/swp/). Despite such limitations in the modeling of large rivers, the daily flow simulations obtained here are to demonstrate the potential of a large-scale hydrologic modeling system such as CHARMS.

Overall, the simulation of daily flows in CHARMS for the U. S. is satisfactory in its ability to reproduce seasonal and inter-annual variability, particularly when considering the large extent of the domain studied, the limitations that are inherent to the current version of CHARMS, and the limited calibration that was performed in this study.

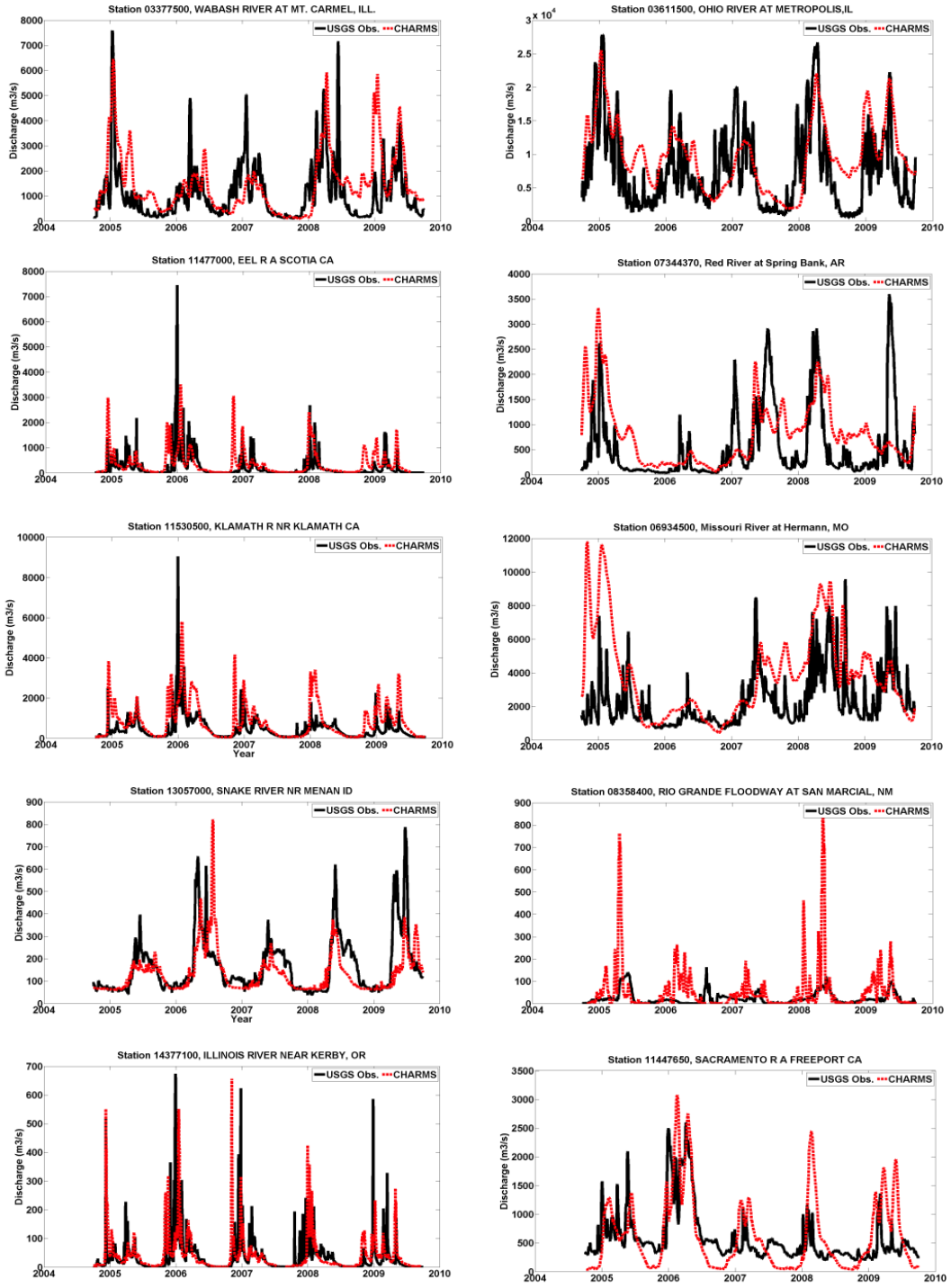


Figure 3.5 Comparison between CHARMS simulated daily discharge (red dotted line) and USGS observations (black solid line) at gauging stations over natural rivers relatively free of human impact (left) and major rivers (right) across the country.

3.5.2.3 Temporal variations of simulated water depth and inundation extent

Periodic USGS field measurements of river depth and width available during the last five water years of the simulation were obtained for five of the seventeen gauges shown in Table 3.4. They are shown in Figure 3.6 along with the corresponding daily averages of modeled quantities. One should note that despite being shown at regular intervals in Figure 3.6, the frequency of field measurements is not constant, and only those days for which measurements are available are compared to simulated results. Of the five gauges shown in Figure 3.6, two are from natural rivers in unmanaged regions, and three are major rivers within managed regions. Although only a subset is selected here for clarity of graphics, the five locations are representative of all available results. Table 3.5(a) shows averaged values of observed and modeled river depth, relative bias, correlation coefficient, RMSE of modeled depth, and the standard deviation of observed and modeled depth. Table 3.5(b) shows the same statistics but for river width instead of river depth. The river width (interchangeably referred to here as inundation extent) is defined as the surface width of the river (Figure 3.1(c)).

(a)

Station Number	Mean Depth Observation (m)	Mean Depth Simulation (m)	Relative Bias	Correlation Coefficient	RMSE (m)	Standard Dev Observation	Standard Dev Simulation
Natural:							
03377500	3.00	3.73	24%	0.70	1.87	2.26	2.29
11477000	4.55	1.23	-72%	0.38	4.05	2.60	1.17
11530500	4.38	1.99	-54%	0.44	2.95	1.93	1.03
13057000	1.05	0.39	-62%	0.11	0.91	0.57	0.35
14377100	1.39	0.51	-63%	0.58	1.55	1.56	0.70
Major:							
03611500	9.40	9.73	3%	0.31	3.55	3.55	2.37
01646502	N/A	1.82	N/A	N/A	N/A	N/A	0.78
06934500	3.30	13.53	310%	0.32	10.66	2.06	2.91
07263450	70.86	9.70	-86%	0.11	61.12	1.52	2.31
07344370	6.01	6.27	4%	0.28	2.37	2.44	1.15
07374000	6.78	12.98	91%	0.38	6.96	3.22	2.03
08065000	5.09	2.67	-47%	0.25	4.40	3.84	1.45
08358400	5.64	1.22	-78%	0.31	4.61	0.63	1.37
11447650	31.62	1.07	-97%	0.70	30.56	1.29	0.77
14246900	1.40	0.91	-35%	0.54	0.70	0.45	0.61
09421500	8.51	0.45	-95%	0.06	9.41	4.96	0.41
05474500	N/A	7.32	N/A	N/A	N/A	N/A	2.79

(b)

Station Number	Mean Width Observation (m)	Mean Width Simulation (m)	Relative Bias	Correlation Coefficient	RMSE (m)	Standard Dev Observation	Standard Dev Simulation
Natural:							
03377500	300.58	275.19	-8%	0.60	402.95	143.61	483.58
11477000	114.45	130.83	14%	0.15	41.23	38.61	6.20
11530500	144.65	122.58	-15%	NaN	35.48	27.99	0.00
13057000	92.21	101.88	10%	NaN	12.17	7.46	0.00
14377100	26.80	18.08	-33%	0.07	26.13	24.65	6.25
Major:							
03611500	1258.00	586.88	-53%	-0.18	929.43	259.65	554.24
01646502	N/A	71.75	N/A	N/A	N/A	N/A	1.68
06934500	341.37	533.94	56%	0.26	450.58	68.57	424.02
07263450	330.78	997.39	202%	-0.32	917.01	83.33	611.05
07344370	154.90	672.31	334%	0.28	652.58	48.36	413.71
07374000	4470.92	7533.50	69%	-0.05	26297.00	25671.80	4299.20
08065000	95.06	64.78	-32%	NaN	157.95	157.95	0.00
08358400	32.78	24.64	-25%	0.10	50.52	21.42	47.56
11447650	184.09	384.77	109%	NaN	200.78	6.42	0.00
14246900	625.51	1740.76	178%	NaN	1115.46	22.47	0.00
09421500	98.29	147.17	50%	NaN	50.89	14.46	0.00
05474500	756.81	514.44	-32%	0.14	623.97	33.30	589.98

Table 3.5 Model performance statistics of (a) simulated river depth, and (b) simulated inundation extent compared to USGS field measurements.

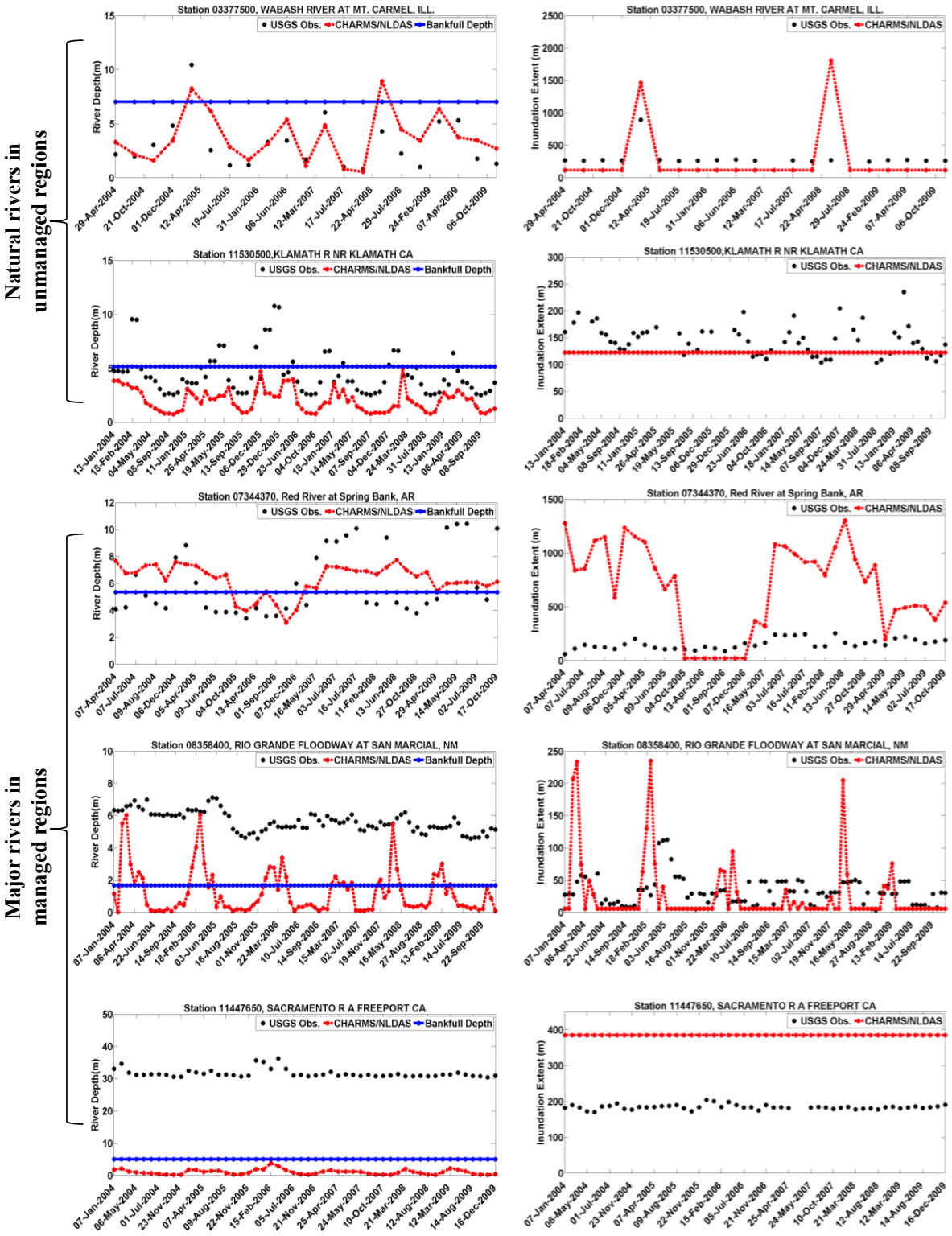


Figure 3.6 Comparison between CHARMS simulated (red dotted line) river depth (left) and inundation extent (right) and USGS gauge field measurements (black dots). The blue lines in the figures on the left are the derived bankfull depth of each corresponding river reach.

Figure 3.6 show that the river inundation extent remains constant at bankfull conditions W_{full} as long as the river depth is below the bankfull height h_{full}, which can be anticipated from the rectangular channel geometry (Figure 3.1(c)) used in the model formulation. Only when the river depth exceeds bankfull height h_{full} does water flow over bank onto the flood plain.

Figure 3.6 (top) shows that CHARMS captures the observed patterns of water depth and width fairly well over unmanaged regions. The absolute values of the relative biases in depth range from 24% for the Wabash River at Mount Carmel, IL to 72% for the Eel River at Scotia, CA; and correlation coefficients reach values as high as 0.70. The absolute values of the relative biases in width range from 8% for the Wabash River at Mount Carmel, IL to 33% for the Illinois River near Kerby, OR. Therefore despite some biases likely due to the accuracy of the channel geometry used, CHARMS displays some strength in reproducing observed depth and width in natural rivers.

Plots of water depth and width for major rivers over managed regions presented in Figure 3.6 (bottom) show larger discrepancies than for those over unmanaged regions. The absolute values of the relative biases in depth range from 3% for the Ohio river at Metropolis, IL to 310% for the Missouri River at Hermann, MO. The absolute values of the relative biases in width range from 25% for the Rio Grande Floodway at San Marcial, NM to 334% for the Red River at Spring Bank, AR. The large differences for rivers over managed regions have at least three explanations. First, the mismatch between simulated and observed flow resulting from the lack of representation of anthropogenic effects in CHARMS (see Section 3.5.2.2.) likely contributes to these poorer results. Second, the empirical relationships derived between the river cross-

section profile and drainage area that are crucial for flow dynamics are mainly based on the assumption of a natural river system. Such an assumption is likely violated in regions like Arkansas, the Rio Grande River Basin, and the Sacramento River Basin. Third, one can see that – for some high flow events – the magnitude of the inundation extent is largely overestimated (up to 10 times higher than the observed river width). This appears to be due to the combined effects of underestimated bankfull width (Equation 18) and underestimated hillslope of each catchment (Figure 3.1c) derived from 1km DEM. Combined, these lead to earlier flooding and flatter terrain, hence generating greater inundation extent during flood events.

3.5.2.4 Spatial variation of simulated river depth and inundation extent

The capacity to model spatial variability in river depth and inundation extent is one of the key attributes of CHARMS. To investigate such dynamics at the continental scale, two consecutive water years of the simulation period were selected based on opposite hydrological conditions. A weak El Niño signal, starting in September 2006 and lasting till early 2007, identified by the Climate Prediction Center (CPC), which tends to bring more precipitation to northern California, and dry conditions to the Ohio Valley [*Mo*, 2010; *St. George et al.*, 2010], contributed to the dry 2006-2007 water year in the Mississippi River Basin; whereas continuous heavy precipitation in the spring/summer of 2008 made June 2008 among the wettest months on record over the majority of the Upper Mississippi and Ohio River Basins [*Gleason*, 2008], and 2007-2008 a wet water year.

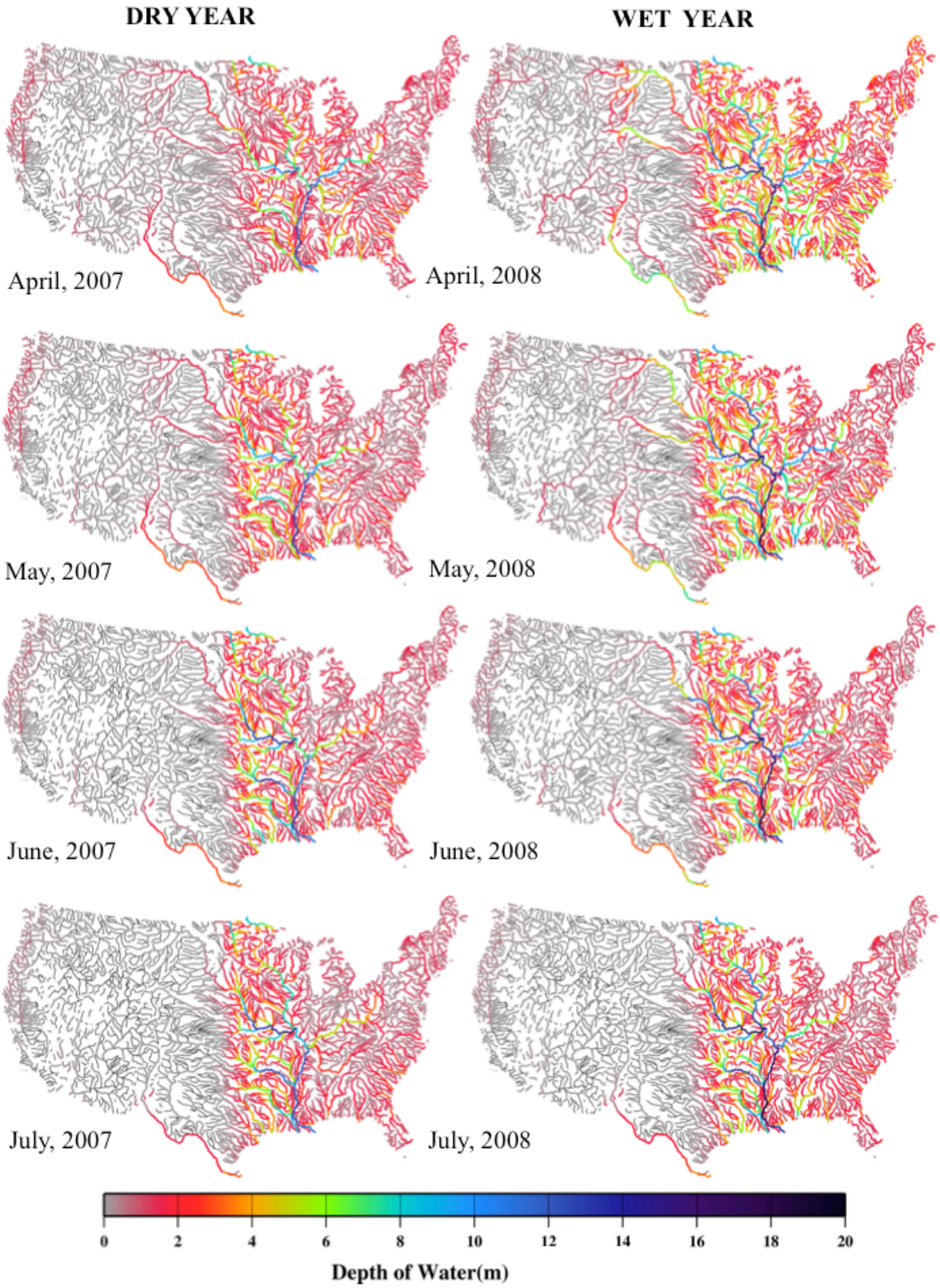


Figure 3.7 CHARMS simulated monthly (from April to July) river depth for the U.S. in year 2007 (left) and 2008 (right).

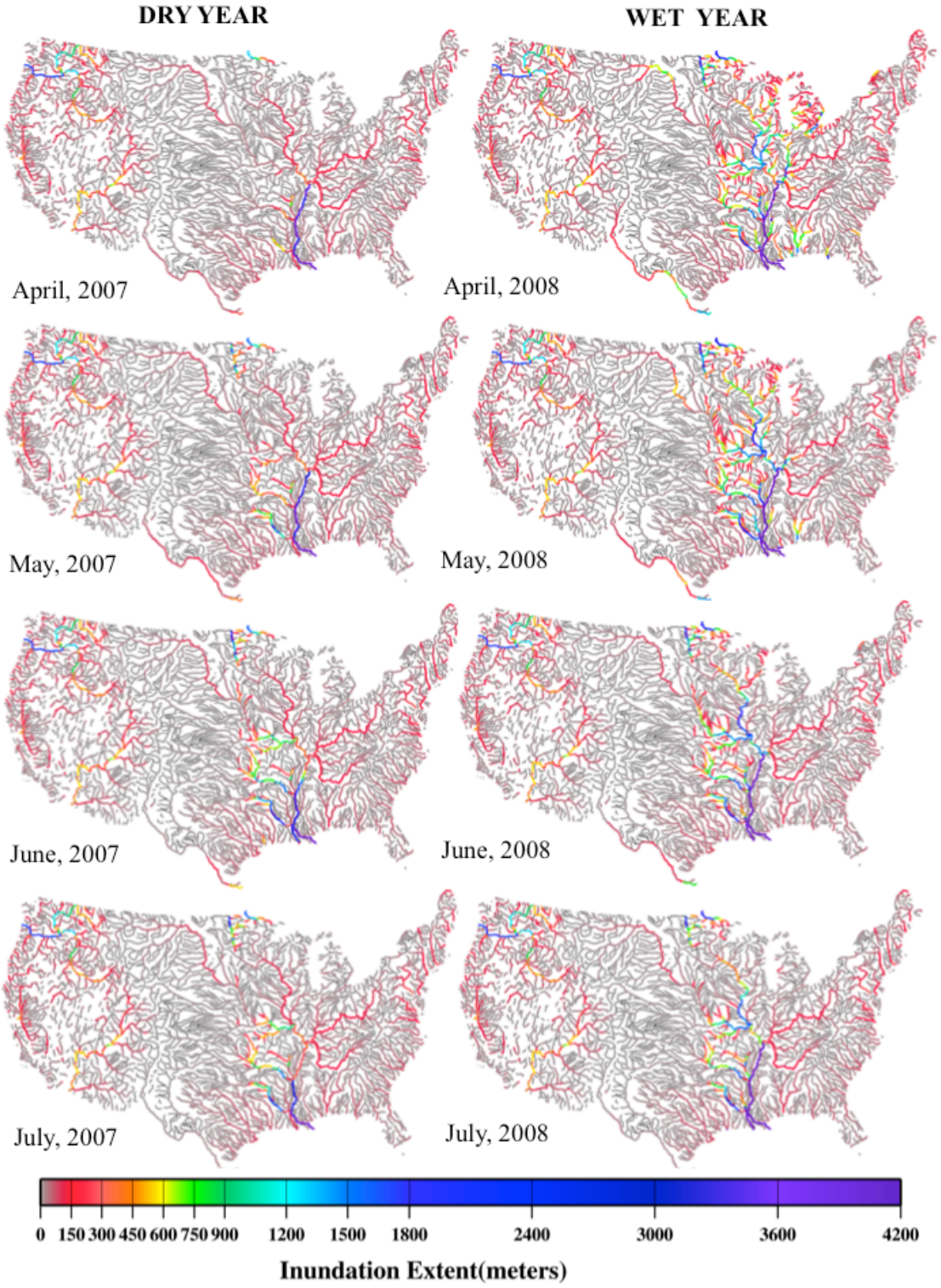


Figure 3.8 CHARMS simulated monthly (from April to July) inundation extent for the U.S. in 2007 (left) and 2008 (right).

Figure 3.7 shows simulated water depth for the summer of the dry water year of 2006-2007, and for the wet water year of 2007-2008. For display purposes, reaches with river depths higher than 20m are set to 20m and reaches with river depths lower than 0.01m are shown using a thin black line. Figure 3.7 shows the division between eastern and western regions of the U. S., following the geographical contrast between the cooler and more humid eastern region and warmer and drier western region [*Portmann et al.*, 2009]. The averaged water depth over the eastern region is 3-5m deeper than that of the western area. Figure 3.7 also shows that water depth generally increases from upstream to downstream along river channels. The seasonal variation of water depth is also apparent within each year, and higher water depths follow higher flows leading to the spring season. Comparing between the summer period of 2007 and 2008, the effects of the severe floods around June 2008 in the Midwestern U. S. including part of Iowa, Indiana, Illinois, Wisconsin, and Missouri [*Gleason*, 2008] are apparent. Simulated water depth along the Mississippi river for these regions during the spring/summer 2008 is higher than the corresponding periods of 2007 by 3-5 m.

Simulated monthly-averaged inundation extents for the dry year of 2006-2007 and the wet year of 2007-2008 are shown in Figure 3.8. For display purposes, reaches with inundation extents wider than 4200m were set to 4200m and reaches with inundation extents less than 1m are shown using a thin black line. Within each river basin, the inundation extent generally increases from upstream to downstream along river channels. Inundation extent is typically smaller during low flow season than high flow season, where most of the water flow remains within river banks. The east-west pattern that is quite apparent for river depth is not as marked for river width. However, such a pattern is also lacking in bankfull width variations presented in Section 3.4.3. The lack of apparent pattern is likely due to that the increase rate of width with

increasing flow is faster in rivers with sandy bed materials within arid and semiarid eastern regions than that of rivers with cohesive bank material under more humid climate [*Leopold et al.*, 1964]. Comparisons between the summer periods of years 2007 and 2008 show evidence of flood events in the Midwest along the Mississippi River around the summer 2008 with an increase in width of 600-900m. These results show that although adjustments and modifications could allow a more accurate description of river cross-section profiles, CHARMS is able to reproduce some seasonal and intern-annual spatial variability in the dynamics of river depth and inundation extent.

3.5.2.5 The challenge of validating spatial variations of river widths

Among the most notable datasets for spatial variations of surface water extent is the multi-satellite products of inundation extent by *Papa et al.*, [2010] and *Prigent et al.*, [2007] which combines a suite of satellite observations, including passive/active microwave observations and visible/near-infrared images, in order to generate a ~0.25° gridded monthly global surface water extent from 1993 to 2004. This multi-sensor estimate of surface water extent includes inundated wetland, rivers, lakes, irrigated regions, and saturated wet soil [*Papa et al.*, 2010].

Since the simulated river widths from CHARMS are represented by a width associated with each river reach (see Figure 3.1(c)), a transformation of CHARMS outputs into a gridded product of inundated area is needed prior to comparison with the dataset of *Papa et al.*, [2010]. To do so, the 0.25° grid was intersected with the river reach centroids of the hydrographic network used in this study. For each grid cell, the inundated area (river width multiplied by reach length) was summed for all the reaches which centroid resides inside the grid cell. Since

the CHARMS simulations presented herein only compute the main river reaches, so does the transformed gridded dataset.

Figure 3.9 shows the comparison over the U. S. between the simulated monthly inundation extent area from CHARMS and the dataset of *Papa et al.*, [2010] for June 2004. It indicates that the CHARMS simulations and the remotely-sensed estimates share similar spatial patterns. However, the magnitude of the simulated inundation area can be up to 10 times smaller than that reported from satellite observations. One can argue that these large differences can be explained by the much-coarser river network simulated in CHARMS than is included in the estimates of *Papa et al.*, [2010]. Regardless, until observations such as those expected from SWOT are available, a quantitative comparison of simulated and remotely-sensed spatial variations of river widths will remain a challenge.

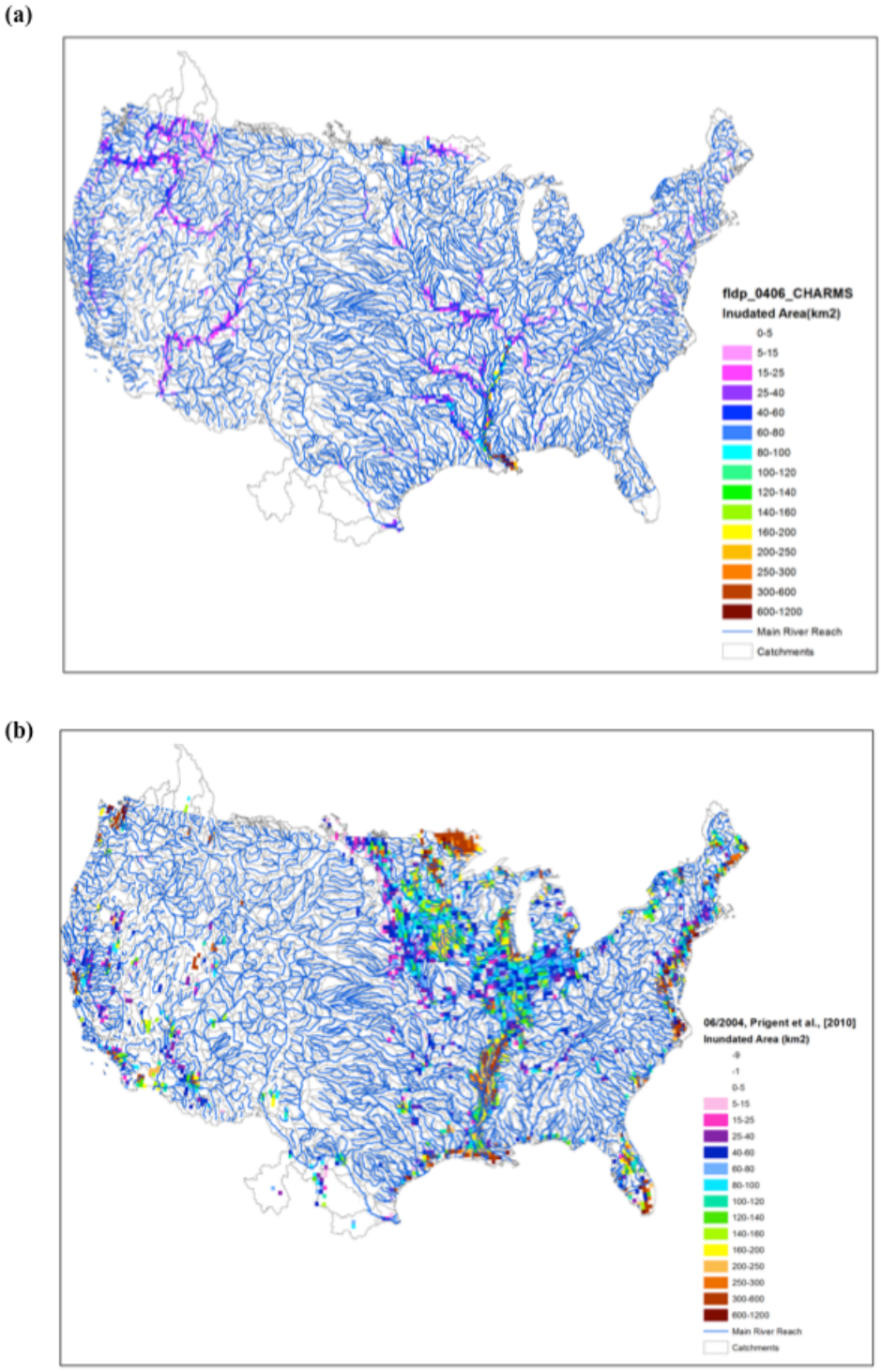


Figure 3.9 (a) Simulated inundation extent for the U.S.; (b) Satellite observation of inundation extent by *Prigent et al.*, [2007].

3.6 Discussion

The main objective of this study is to build a continental-scale, catchment-based land surface modeling and river routing framework that uses an explicit, spatial representation of river networks, and that is able to simulate flow rates, flow depths and the corresponding flow widths. Our experience suggests that the complexity of such an endeavor is three-fold: 1) there are technical difficulties related to preparing suitable datasets for such a model, 2) the broad inclusion of all processes, both natural and anthropogenic, involved in surface water dynamics is still limited in current hydrologic models; and 3) challenges exist that are due to the general lack of detailed data products necessary to validate the quality of the results obtained.

Despite the increasing availability of hydrographic datasets describing river networks at the continental scale, such as NHDPlus [*Horizon Systems Corporation*, 2010] or HydroSHEDS [*Lehner et al.*, 2008], the preparation of modeling templates from such datasets remains a challenge. The first challenge is related to the high resolution of these datasets and the corresponding computational burden if used as-is. NHDPlus is valuable for continental-scale modeling of the U. S. because it includes a detailed description of the mapped river reaches and some of their properties nationwide. However, the 3 million NHDPlus rivers reaches and corresponding catchments in the contiguous U. S. make it computationally intensive to use of-the-shelf. Our proposed upscaling process (Figure 3a) designed to coarsen the dataset from 3 million reaches and catchments to approximately 80,000 reaches and 3,000 catchments is a preliminary step towards decreasing the computational burden while keeping mapped rivers as computational elements. However, it leads to a loss of density in the description of mapped river networks. The second challenge is the general lack of detailed river cross-section profile information at the continental scale, which affects the ability to separate flow in the main river

channel and the floodplain within a simulation model. Our attempt at generating such data (Figure 3.4c and 3.4d) using classic empirical relationships (Table 3.1) to describe the river bed geometry for each water resource region is an initial step towards addressing this lack of data. Shortcomings of the work shown here are the strong assumptions about the applicability of hydraulic geometry relationships over large areas, and that we ignore both natural and anthropogenic modifications of river beds. Our results suggest that inaccuracies in channel geometry influence the quality of model simulations and that our estimates of channel shape and dimensions can be further improved.

The proposed CHARMS model simulations generally show better performance in unmanaged regions that are relatively free of anthropogenic modifications of surface water than in managed regions located along major river basins that commonly include man-made structures. This suggests that treatment of reservoirs, dams, and other anthropogenic modifications of surface water processes would be beneficial for the simulation of streamflow. Our model results can also likely be improved even in regions where natural processes dominate. Our calibration was focused solely on a few key parameters that were tuned only within the Mississippi River Basin. Further refinement of land surface model parameters, through automated calibration procedures or enhanced spatial variability, would likely improve simulations. Regardless, the strengths and weaknesses of these results should be put in the perspective of the broad goal of this study, namely to demonstrate the feasibility of continental-scale modeling of river flow, river depth, and river width using mapped hydrography. Results shown here are an important step toward building such a modeling framework, and our results inform the successive steps necessary to create and improve it.

Quantitative validation of our CHARMS model results is also challenging because detailed *in situ* observations of river depth and width are site-specific and their temporal availability is very limited (the USGS field measurements are only provided at punctual times). Our comparison of CHARMS simulations with remotely-sensed estimates of inundation extent (Section 3.5.2.5) highlights the necessity of developing models that can account for the processes observed by satellites, and at the same spatial resolution. Surface water models that can be used, jointly with data for the upcoming SWOT mission at continental and global scales, will be crucial in order to fully utilize mission information and to enable significant improvement in our understanding of surface water dynamics.

3.7 Conclusions

In order to bridge the gap between the spatial and temporal scales of existing *in situ* and upcoming satellite observations, and to provide a seamless space-time calculation of surface water dynamics, this study presents a continental-scale, catchment-based hydrologic and river routing modeling system using an explicit representation of river networks and capable of estimating flow rate, flow depth and flow width. A catchment-based model template was upscaled from version 1 of the NHDPlus dataset and consists of approximately 3,000 catchments and 80,000 river reaches. River cross-section profiles were determined by establishing empirical relationships between river dimension and drainage area, allowing for simulation of the corresponding river water depth and floodplain. The land surface model is a catchment-based version of the gridded CLM 3.5. Horizontal routing within the river networks was performed using a unit hydrograph approach with separate parameters for channels and floodplains. The seasonal and inter-annual variability of the simulated stream flow compares fairly well with USGS observations, although the inclusion of anthropogenic modifications on surface water

processes can be seen as a potential way to improve the proposed approach. Seasonal variations of monthly-averaged simulated water depth and width follow the observed dry and wet patterns, but a detailed validation of these quantities is limited by a general lack of detailed observational datasets. The planned SWOT mission will likely offer new opportunities to validate model results, and further justifies the future development of continental-scale surface hydrologic modeling systems such as the CHARMS framework described here.

3.8 Appendix A - Runoff generation in CHARMS

Runoff generation in CHARMS is produced by a modified version of CLM 3.5. The meteorological data are needed for running CLM, including precipitation, air temperature, surface pressure, specific humidity, wind speed, longwave radiation and downward shortwave radiation [*Oleson et al.*, 2007]. Land surface data describing land topography, soil properties and vegetation characteristics are also necessary [*Oleson et al.*, 2007]. Since land surface modeling with CLM in CHARMS is catchment-based, interpolation of input data from grids to catchments is needed. Other than using catchments instead of grids as modeling unit, the modified catchment-based CLM3.5 performs similar to the grid-based version.

Runoff generation in CLM3.5 is based on TOPMODEL-based runoff [*Beven and Kirkby*, 1979], proposed by [*Famiglietti and Wood*, 1994] for use in LSMs. Surface runoff from simple TOPMODEL-based runoff parameterization (SIMTOP) mechanism of *Niu et al.*, [2005] includes saturation excess runoff (Dunne mechanism) and infiltration excess runoff (Horton Mechanism). Subsurface runoff is parameterized based upon maximum subsurface runoff, water table depth, and an exponential decay factor. The mathematical representation of SIMTOP-based surface runoff q_{over} is

$$q_{over} = f_{sat} q_{liq,0} + (1 - f_{sat}) \max(0, q_{liq,0} - q_{\inf l,\max}) \qquad (3.8)$$

where f_{sat} is saturated fraction of each modeling unit; $q_{liq,0}$ is the total input of precipitation, snowmelt and dewfall on the ground. $q_{infl,max}$ is the maximum soil infiltration capacity, determined by soil moisture [*Entekhabi and Eagleson*, 1989] and soil characteristics, and is calculated as

$$q_{\inf l,\max} = k_{sat,1}[1 + v(s-1)] \qquad (3.9)$$

where $k_{sat,1}$ is the saturated hydraulic conductivity, determined from

$$k_{sat,i} = 0.0070556 \times 10^{-0.884+0.0153(\%sand)_i} \qquad (3.10)$$

where %*sand* is the sand fraction of each soil layer. v is a parameterized variable dependent on saturated soil matric potential and top soil layer thickness; s is the relative liquid moisture of the first soil layer to the effective porosity, and is also adjusted for saturated fraction, calculated as

$$s = \frac{\dfrac{\theta_{liq,1}}{\max(\theta_{imp,}\ \theta_{sat} - \theta_{ice,1})} - f_{sat}}{1 - f_{sat}} \qquad (3.11)$$

where $\theta_{liq,1}$ is the volumetric liquid water content of the first soil layer, and $\theta_{ice,1}$ is the volumetric ice content of the top soil layer; θ_{imp}=0.05 is a minimum effective porosity. θ_{sat} is volumetric water content at saturation/porosity, calculated as

$$\theta_{sat,i} = 0.489 - 0.00126(\%sand)_i \qquad (3.12)$$

The subsurface runoff/baseflow q_{drain} is calculated as

$$q_{drain} = (1 - f_{imp}) q_{drain,\max} \exp(-f z_{\nabla}) \qquad (3.13)$$

where $q_{drain,\ max}$ is the predefined maximum (=4.5x10^{-4}kg m^{-2} s^{-1}) subsurface runoff; f_{imp} is the fractional impermeable area. f is the exponential decay factor of subsurface runoff equation, with a default value of 2.5 m^{-1}; and z_{∇} is the water table depth of each modeling unit. The surface and

subsurface runoff data generated from catchment-based CLM in one catchment is represented as depth per unit time (mm/s) and is considered constant within each catchment.

Moreover, our study shows that runoff can also be affected by the soil resistance term R_{soil}, which represents the resistance to the transport by water vapor from the water surface of soil pores to the soil surface [*Sellers et al.*, 1992], thus affecting soil evaporation.

$$R_{soil} = (1 - f_{sno})\exp(8.206 - \alpha s_1) \qquad (3.14)$$

where f_{sno} is the percent of soil covered by snow in each modeling unit, and s_1 is the relative soil moisture to saturation of the first layer. α is surface dryness factor, with a default value of 4.255. Studies by *Cai et al.*, [2013] demonstrate that value of α can also affect the runoff generation.

Description of equations (3.8)-(3.14) is largely withdrawn from CLM3.5 technical description [*Oleson et al.*, 2007]. Readers are referred to [*Oleson et al.*, 2007] for more detail.

3.9 Appendix B- Routing from hillslope to river channel in CHARMS

Goteti et al., [2008] considered the temporal lag occurring in the transport of water from the hillslope to the river channel. The formulations of *Lee and Chang* [2005] and Darcy's law were used to estimate separate travel times corresponding to transport of surface runoff and subsurface runoff, respectively. *Goteti et al.*, [2008] focused on the Wabash River Basin of the central United States (drainage area 77,282 km^2), and used an average length of ~20km for sub-reaches. This study focuses on the much larger contiguous U. S., and the average length of sub-reaches is ~2.5km (see Section 3.4.1.2). Therefore, a simplified approach for the contribution of water from the hillslope and neglecting overland travel times is used here.

The contribution by hillslope to each sub-reach is calculated as the product of the drainage area of each sub-reach and the averaged sum of surface and subsurface runoff during each routing period τ

$$Q_{hillslope}(t) = A_{rch} \sum_{i=0}^{i=\frac{\tau}{\Delta t}-1} (r_{surf}(t + i \cdot \Delta t) + r_{base}(t + i \cdot \Delta t)) / 6 \qquad (3.15)$$

where A_{rch} is the contributing drainage area of each sub-reach (Figure 3.1(b)). τ is a generic routing model time interval (6 hour), q_{over} and q_{drai} are surface runoff and baseflow generated within τ, and Δt is the simulation time step (1 hour) of the catchment-based CLM.

3.10 Appendix C - Routing within river channels and floodplains in CHARMS

The routing model is largely based on the work of *Asante et al.*, [2008]. The determination of the unit hydrograph $U(\tau)$ is based on the following equations [*Goteti et al.*, 2008]

$$V = \frac{dQ}{dA_c} = \frac{1}{W}\frac{dQ}{dh} \qquad (3.16)$$

$$D = \frac{Q}{2WS_{rch}} \qquad (3.17)$$

$$T = (\frac{L_{rch}}{V}) / \tau \qquad (3.18)$$

$$\Pi = \frac{L_{rch}V}{D} \qquad (3.19)$$

$$U(\tau) = \frac{1}{2\tau\sqrt{\pi(\tau/T)/\Pi}} \exp\left\{-\frac{[1-(\tau/T)]^2}{4(\tau/T)/\Pi}\right\} \qquad (3.20)$$

A_c is cross section area of each sub-reach. V and D are the convective velocity and diffusion coefficient respectively, and are both expressed as a function of streamflow Q and water

stage h. T and Π represent the convective and diffusive processes (respectively) in the response function.

Separate unit hydrographs are computed for channel routing and floodplain routing for each of sub-reach (j+) (Figure 3.1(d)). Total streamflow Q^{j}_{down} from the downstream end of all the upstream reaches (j) is first separated into channel ($Q^{j+1}_{up,\,chnl}$) and floodplain ($Q^{j+1}_{up,\,fldp}$) at the upstream point of each downstream sub-reach $j+1$ before routing occurs in sub-reach $j+1$(Figure 3.1(d)).

The separated unit hydrographs and flows are used to route water flow from upstream to downstream in each sub-reach ($j+1$), both in the channel and floodplain

$$Q^{j+1}_{chnl,down}(t) = \sum_{\tau=0}^{\tau=\Lambda} Q^{j+1}_{chnl,up}(t-\tau)U^{j+1}_{chnl}(t-\tau) \tag{3.21}$$

$$Q^{j+1}_{fldp,down}(t) = \sum_{\tau=0}^{\tau=\Lambda} Q^{j+1}_{fldp,up}(t-\tau)U^{j+1}_{fldp}(t-\tau) \tag{3.22}$$

where $U(t-\tau)$ is the unit hydrograph, hence representing the fraction of upstream flow that appears downstream at time t-τ for each sub-reach ($j+1$). To consider the time delay from the previous routing intervals, both $Q^{j+1}_{chnl,down}$ and $Q^{j+1}_{fldp,down}$ are computed over a pre-defined time period Λ. The routing process starts from the headwater catchment and proceeds sequentially downstream. Note that the unit hydrographs are computed based on upstream flow quantities (Equation (3.16)-Equation (3.20)). However, the total upstream flow from the downstream end of the upstream reach (j) is composed of water coming from the upstream hillslope, from the upstream channel and from the upstream floodplain (sees Section 3.3.2, Figure 3.1(d)). Therefore, since routing is done in the channel and floodplain separately, one needs to first

redistribute the total upstream flow into channel ($Q^{j+1}_{chnl,up}$) and floodplain ($Q^{j+1}_{fldp,up}$) components before the routing process in each downstream sub-reaches ($j+1$).

3.11 Acknowledgments

This work was supported by the NASA Earth and Space Science Fellowship program by the University of California Office of the President Multicampus Research Programs and Initiatives. Both sponsors are gratefully acknowledged. The practical application in this study was made possible using the following freely available data: river network information from the National Hydrography Dataset Plus, estimates of runoff from phase 2 of the North American Land Data Assimilation System and gauge observations from the U. S. Geological Survey National Water Information System.

4. Further Exploration of Hydraulic Geometry Relationships

River cross-section profiles describing river shape has been proven to be important for large-scale hydrologic and river routing models [*Goteti et al.*, 2008; *Beighley et al.*, 2009; *Yamazaki et al.*, 2011] to separate total flow into main channel and floodplain, and to estimate river depth and corresponding floodplain inundation extent. However, river cross-section profiles are hard to obtain in many regions. Even over most gauged regions like U.S and Germany, there is still large lack of detailed river-cross section observations directly available to satisfy the need of large-scale river routing models.

As described in Chapter 2 and Chapter 3, empirical relationships relating river cross-section profiles with streamflow have been widely explored since the 1960s. As a continues discussion of the 19 distinct sets of power relationships described in Section 3.4.3, this Chapter first shows an updated version of the relationship Table 3.1, and explores the possibility of generating one uniform relationship over the entire continental U.S. Impact of basin sizes on the distinct relationship is then discussed. Next, discussion on the impact of anthropogenic effect on these empirical hydraulic relationships are also presented. Lastly, feasibility of deriving the hydraulic relationship for each separate group based on the streamflow variability (natural or managed regions) is shown.

4.1 Updated Relationship Table

During the initial process establishing the empirical relationships in Table 3.1 with USGS gauge observations, one criteria is to only keep the gauging stations with at least more than 80 days of field measurements. We notice that with this selection criteria, some of the gauge stations at

relatively downstream or near the river outlet were eliminated over several water resources regions. Losing downstream gauging stations with larger drainage area can lead to a miss representing the empirical relationship based on drainage area. Thus, a lower criteria that keep gauging stations with at least 40 days of field measurements is used to updated the relationship. Table 4.1 shows the updated relationship. Compared with Table 3.1, it is noticeable that with more gauging stations, the correlation coefficients between Q and A increases over Ohio, Tennesee, Upper, and lower Mississippi region, and lower Missouri from 0.24-0.70 to 0.78-0.90. This can be due to the new criteria leading to include the gauging stations at downstream end of the water resource region with a much larger drainage area. As expected, those large number of drainage area can result in all the rest of data points squeezed at one side, leading to a much higher R^2 value. By contrast, the correlation coefficient of the power relationship between Q and A drops dramatically after the update over lower Colorado and Pacific North West regions. This drop might be related to the fact that the downstream gauging stations are largely affected by anthropogenic effect. While the power relationship are based on the behavior of natural rivers. Therefore, adding those heavily regulated gauging stations will lead to a much lower correlation coefficient.

To include as much as gauging stations to keep the data completeness, for Section 4.2-4.5, all the analysis is based on the updated relationship in Table 4.1.

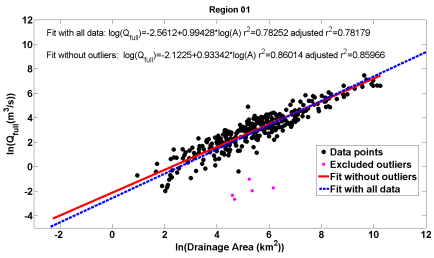
Region Number	Region Name	Number of Gauges	Qfull vs A	R^2	hfull vs Qfull	R^2
01	New England	301	$Qfull=0.0772A^{0.9983}$	0.78	$h_{full}=0.8699Q_{full}^{0.1846}$	0.45
02	Mid-Atlantic	652	$Qfull=0.0851A^{0.9802}$	0.62	$h_{full}=0.7305Q_{full}^{0.2263}$	0.46
03	South Atlantic-Gulf	893	$Qfull=0.5018A^{0.7630}$	0.57	$h_{full}=0.999Q_{full}^{0.2389}$	0.41
04	Great Lakes	371	$Qfull=0.0644A^{0.8774}$	0.35	$h_{full}=0.8733Q_{full}^{0.2220}$	0.47
05	Ohio	502	$Qfull=0.3817A^{0.7915}$	0.92	$h_{full}=0.7786Q_{full}^{0.2690}$	0.54
06	Tennessee	161	$Qfull=0.0941A^{1.00034}$	0.94	$h_{ull}=0.6414Q_{full}^{0.3007}$	0.67
07	Upper Mississippi	446	$Qfull=0.3627A^{0.7624}$	0.92	$h_{full}=1.2598Q_{full}^{0.2146}$	0.48
08	Lower Mississippi	142	$Qfull=1.6349A^{0.6346}$	0.91	$h_{full}=1.8707Q_{full}^{0.1758}$	0.40
09	Souris-Red-Rainy	97	$Qfull=0.1375A^{0.7176}$	0.66	$h_{full}=1.1063Q_{full}^{0.3149}$	0.71
10U	Missouri	306	$Qfull=0.1225A^{0.6846}$	0.46	$h_{full}=0.9504Q_{full}^{0.2049}$	0.35
10L	Missouri	279	$Qfull=0.5959A^{0.5546}$	0.78	$h_{full}=0.8703Q_{full}^{0.2966}$	0.57
11	Arkansas-White-Red	429	$Qfull=1.6402A^{0.4766}$	0.27	$h_{full}=1.0857Q_{full}^{0.2497}$	0.20
12	Texas-Gulf	295	$Qfull=26.14A^{0.385}$	0.27	$h_{full}=0.7462Q_{full}^{0.2887}$	0.48
13	Rio Grande	109	$Qfull=0.0662A^{0.5717}$	0.47	$h_{full}=0.7879Q_{full}^{0.2106}$	0.38
14	Upper Colorado	290	$Qfull=0.3267A^{0.7387}$	0.68	$h_{full}=0.5778Q_{full}^{0.1839}$	0.44
15	Lower Colorado	183	$Qfull=1.4921A^{0.5150}$	0.005	$h_{full}=0.9687Q_{full}^{0.1586}$	0.09
16	Great Basin	208	$Qfull=0.2856A^{0.7559}$	0.12	$h_{full}=0.8364Q_{full}^{0.1358}$	0.29
17	Pacific Northwest	681	$Qfull=1.8252A^{0.7041}$	0.26	$h_{full}=0.7116Q_{full}^{0.2001}$	0.17
18	California	361	$Qfull=1.4191A^{0.7679}$	0.42	$h_{full}=0.5714Q_{full}^{0.2488}$	0.55

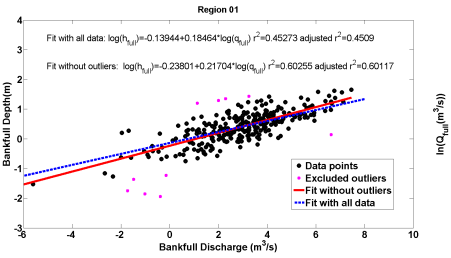
Table 4.1 Updated empirical power law relationships between bankfull discharge (Q_{full}) and drainage area (A), and between bankfull discharge (Q_{full}) and bankfull depth (h_{full}) for each HUC2 water resource region with USGS field measurements between 01/01/1990 to 03/31/2010 with new selection criteria

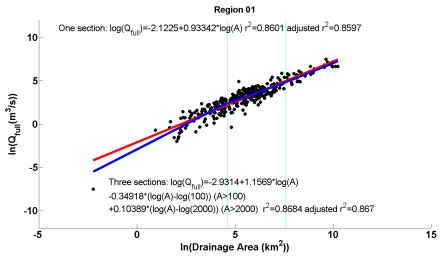
4.2 Log-scale transformation and Outlier analysis

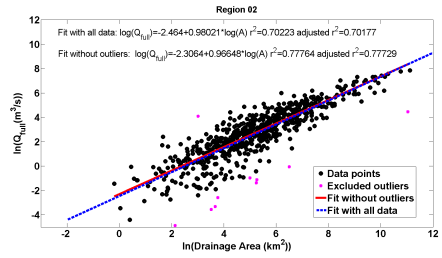
Studies have shown that over the U.S., most of the streamflow follows a log-normal distribution, therefore, log transformation is done to make sure that *logQ* will have a normal distribution, and thus the error information of *logQ* for each gauging station are random and independent with

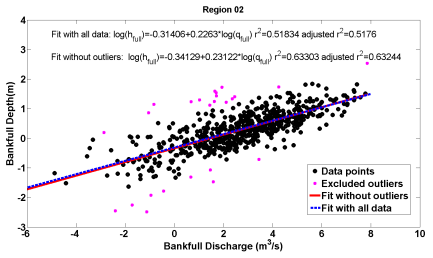
each other. Another update with the empirical relationship is that during the power relationship fitting, we noticed that there are different data points far away from the fitted power line. For example, one data point in Arkansas Region 11 has a value of bankfull depth with an averaged value of 120m, which is far away from the valued of bankfull depth of other data points in Region11, and largely decrease the correlation coefficient. Therefore, to exclude the outlier effect, an outlier analysis is proceeded. Here, we define the outliers as the points that have a distance over 1.5 times the standard deviation from the fitted model. For each region, after fitting the initial power relationship between *log(Qfull)* and *log(A),* and *log(Qfull)* and *log(hfull),* all the outliers are excluded and a new power relationship is then generated. Figure 4.1 shows all comparison of the fitted power relationship with and without outlier. As expected, the correlation coefficients of the fitted power relationship have been all increased compared to the original with all the gauging stations included.

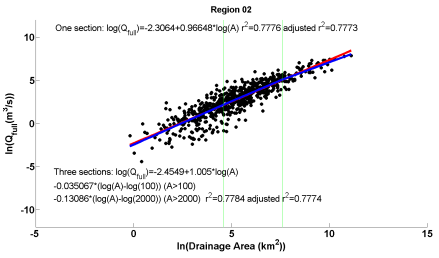

Region 01
Fit with all data: log(Q_full)=-2.5612+0.99428*log(A) r²=0.78252 adjusted r²=0.78179
Fit without outliers: log(Q_full)=-2.1225+0.93342*log(A) r²=0.86014 adjusted r²=0.85966
Data points
Excluded outliers
Fit without outliers
Fit with all data
ln(Q_full(m³/s))
ln(Drainage Area (km²))

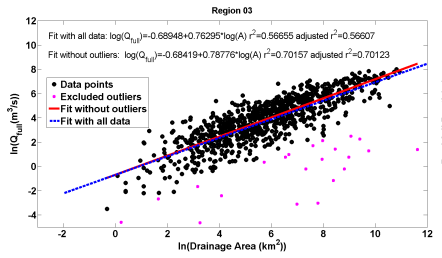

Region 01
Fit with all data: log(h_full)=-0.13944+0.18464*log(q_full) r²=0.45273 adjusted r²=0.4509
Fit without outliers: log(h_full)=-0.23801+0.21704*log(q_full) r²=0.60255 adjusted r²=0.60117
Data points
Excluded outliers
Fit without outliers
Fit with all data
Bankfull Depth(m)
Bankfull Discharge (m³/s)

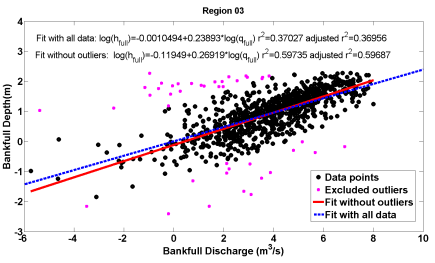

Region 01
One section: log(Q_full)=-2.1225+0.93342*log(A) r²=0.8601 adjusted r²=0.8597
Three sections: log(Q_full)=-2.9314+1.1569*log(A)
-0.34918*(log(A)-log(100)) (A>100)
+0.10389*(log(A)-log(2000)) (A>2000) r²=0.8684 adjusted r²=0.867
ln(Q_full(m³/s))
ln(Drainage Area (km²))

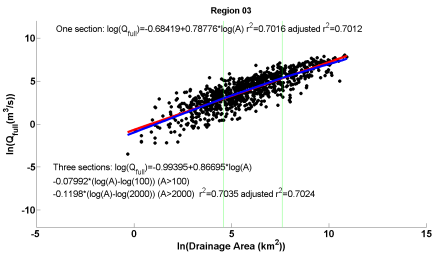

Region 02
Fit with all data: log(Q_full)=-2.464+0.98021*log(A) r²=0.70223 adjusted r²=0.70177
Fit without outliers: log(Q_full)=-2.3064+0.96648*log(A) r²=0.77764 adjusted r²=0.77729
Data points
Excluded outliers
Fit without outliers
Fit with all data
ln(Q_full(m³/s))
ln(Drainage Area (km²))

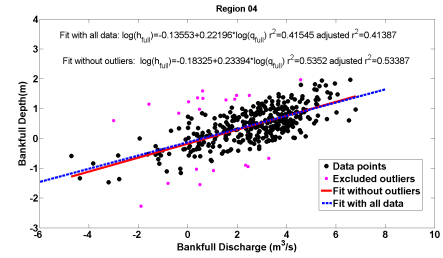

Region 02
Fit with all data: log(h_full)=-0.31406+0.2263*log(q_full) r²=0.51834 adjusted r²=0.5176
Fit without outliers: log(h_full)=-0.34129+0.23122*log(q_full) r²=0.63303 adjusted r²=0.63244
Data points
Excluded outliers
Fit without outliers
Fit with all data
Bankfull Depth(m)
Bankfull Discharge (m³/s)

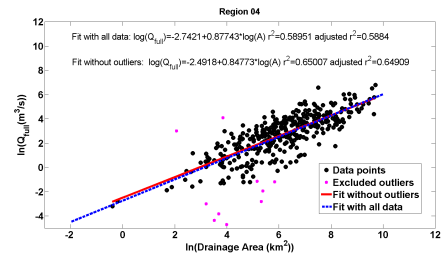

Region 02
One section: log(Q_full)=-2.3064+0.96648*log(A) r²=0.7776 adjusted r²=0.7773
Three sections: log(Q_full)=-2.4549+1.005*log(A)
-0.035067*(log(A)-log(100)) (A>100)
-0.13086*(log(A)-log(2000)) (A>2000) r²=0.7784 adjusted r²=0.7774
ln(Q_full(m³/s))
ln(Drainage Area (km²))

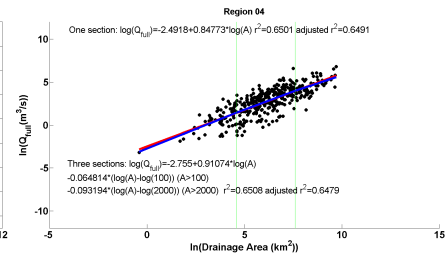

Region 03
Fit with all data: log(Q_full)=-0.68948+0.76295*log(A) r²=0.56655 adjusted r²=0.56607
Fit without outliers: log(Q_full)=-0.68419+0.78776*log(A) r²=0.70157 adjusted r²=0.70123
Data points
Excluded outliers
Fit without outliers
Fit with all data
ln(Q_full(m³/s))
ln(Drainage Area (km²))

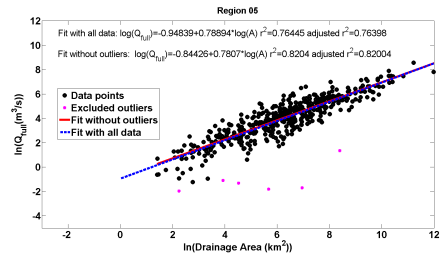

Region 03
Fit with all data: log(h_full)=-0.0010494+0.23893*log(q_full) r²=0.37027 adjusted r²=0.36956
Fit without outliers: log(h_full)=-0.11949+0.26919*log(q_full) r²=0.59735 adjusted r²=0.59687
Data points
Excluded outliers
Fit without outliers
Fit with all data
Bankfull Depth(m)
Bankfull Discharge (m³/s)

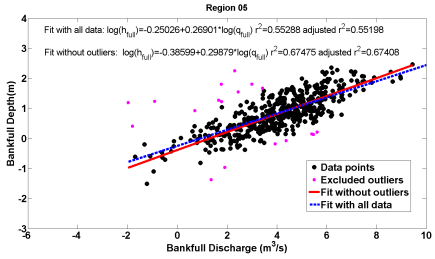

Region 03
One section: log(Q_full)=-0.68419+0.78776*log(A) r²=0.7016 adjusted r²=0.7012
Three sections: log(Q_full)=-0.99395+0.86695*log(A)
-0.07992*(log(A)-log(100)) (A>100)
-0.1198*(log(A)-log(2000)) (A>2000) r²=0.7035 adjusted r²=0.7024
ln(Q_full(m³/s))
ln(Drainage Area (km²))

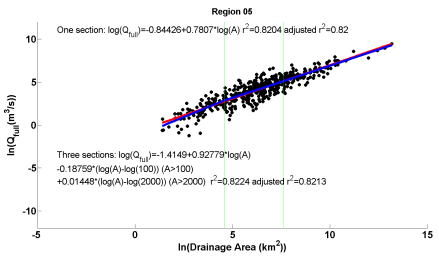

Region 04
Fit with all data: log(h_full)=-0.13553+0.22196*log(q_full) r²=0.41545 adjusted r²=0.41387
Fit without outliers: log(h_full)=-0.18325+0.23394*log(q_full) r²=0.5352 adjusted r²=0.53387
Data points
Excluded outliers
Fit without outliers
Fit with all data
Bankfull Depth(m)
Bankfull Discharge (m³/s)

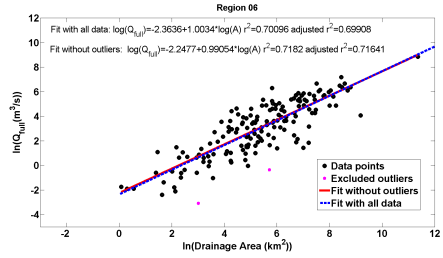

Region 04
Fit with all data: log(Q_full)=-2.7421+0.87743*log(A) r²=0.58951 adjusted r²=0.5884
Fit without outliers: log(Q_full)=-2.4918+0.84773*log(A) r²=0.65007 adjusted r²=0.64909
Data points
Excluded outliers
Fit without outliers
Fit with all data
ln(Q_full(m³/s))
ln(Drainage Area (km²))

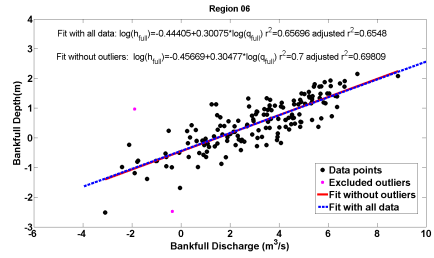

Region 04
One section: log(Q_full)=-2.4918+0.84773*log(A) r²=0.6501 adjusted r²=0.6491
Three sections: log(Q_full)=-2.755+0.91074*log(A)
-0.064814*(log(A)-log(100)) (A>100)
-0.093194*(log(A)-log(2000)) (A>2000) r²=0.6508 adjusted r²=0.6479
ln(Q_full(m³/s))
ln(Drainage Area (km²))

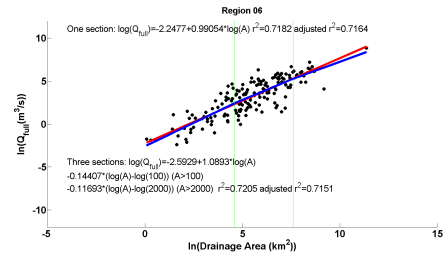

Region 05
Fit with all data: log(Q_full)=-0.94839+0.78894*log(A) r²=0.76445 adjusted r²=0.76398
Fit without outliers: log(Q_full)=-0.84426+0.7807*log(A) r²=0.8204 adjusted r²=0.82004
Data points
Excluded outliers
Fit without outliers
Fit with all data
ln(Q_full(m³/s))
ln(Drainage Area (km²))

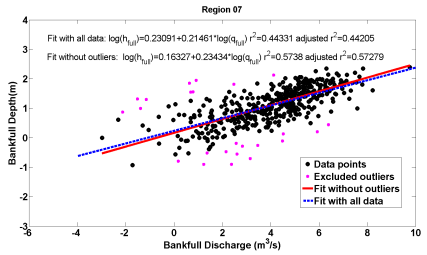

Region 05
Fit with all data: log(h_full)=-0.25026+0.26901*log(q_full) r²=0.55288 adjusted r²=0.55198
Fit without outliers: log(h_full)=-0.38599+0.29879*log(q_full) r²=0.67475 adjusted r²=0.67408
Data points
Excluded outliers
Fit without outliers
Fit with all data
Bankfull Depth(m)
Bankfull Discharge (m³/s)

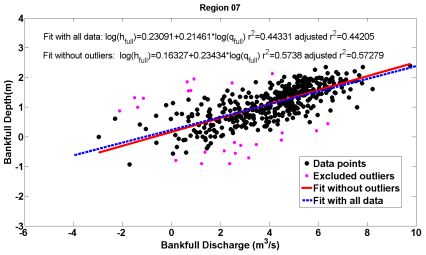

Region 05
One section: log(Q_full)=-0.84426+0.7807*log(A) r²=0.8204 adjusted r²=0.82
Three sections: log(Q_full)=-1.4149+0.92779*log(A)
-0.18759*(log(A)-log(100)) (A>100)
+0.01448*(log(A)-log(2000)) (A>2000) r²=0.8224 adjusted r²=0.8213
ln(Q_full(m³/s))
ln(Drainage Area (km²))

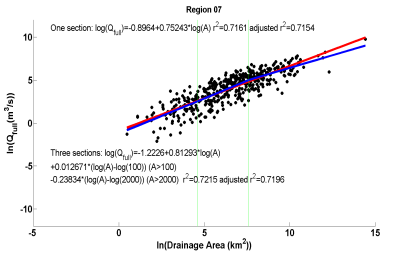

Region 06
Fit with all data: log(Q_full)=-2.3636+1.0034*log(A) r²=0.70096 adjusted r²=0.69908
Fit without outliers: log(Q_full)=-2.2477+0.99054*log(A) r²=0.7182 adjusted r²=0.71641
Data points
Excluded outliers
Fit without outliers
Fit with all data
ln(Q_full(m³/s))
ln(Drainage Area (km²))

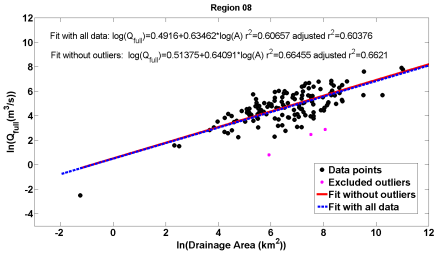

Region 06
Fit with all data: log(h_full)=-0.44405+0.30075*log(q_full) r²=0.65696 adjusted r²=0.6548
Fit without outliers: log(h_full)=-0.45669+0.30477*log(q_full) r²=0.7 adjusted r²=0.69809
Data points
Excluded outliers
Fit without outliers
Fit with all data
Bankfull Depth(m)
Bankfull Discharge (m³/s)

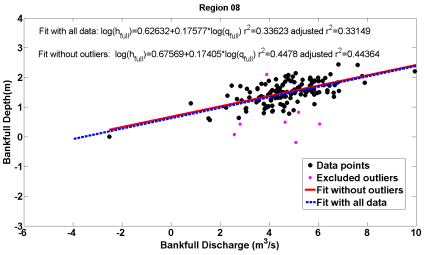

Region 06
One section: log(Q_full)=-2.2477+0.99054*log(A) r²=0.7182 adjusted r²=0.7164
Three sections: log(Q_full)=-2.5929+1.0893*log(A)
-0.14407*(log(A)-log(100)) (A>100)
-0.11693*(log(A)-log(2000)) (A>2000) r²=0.7205 adjusted r²=0.7151
ln(Q_full(m³/s))
ln(Drainage Area (km²))

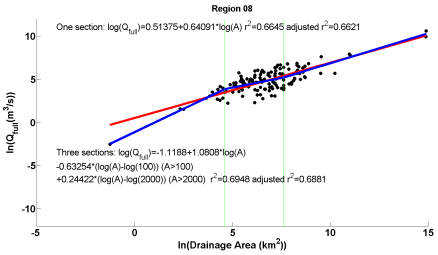

Region 07
Fit with all data: log(h_full)=0.23091+0.21461*log(q_full) r²=0.44331 adjusted r²=0.44205
Fit without outliers: log(h_full)=0.16327+0.23434*log(q_full) r²=0.5738 adjusted r²=0.57279
Data points
Excluded outliers
Fit without outliers
Fit with all data
Bankfull Depth(m)
Bankfull Discharge (m³/s)

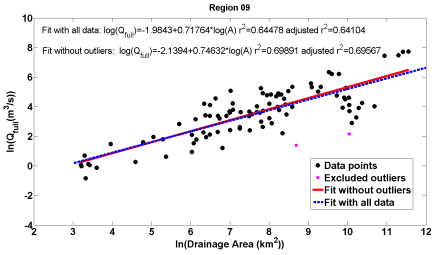

Region 07
Fit with all data: log(h_full)=0.23091+0.21461*log(q_full) r²=0.44331 adjusted r²=0.44205
Fit without outliers: log(h_full)=0.16327+0.23434*log(q_full) r²=0.5738 adjusted r²=0.57279
Data points
Excluded outliers
Fit without outliers
Fit with all data
Bankfull Depth(m)
Bankfull Discharge (m³/s)

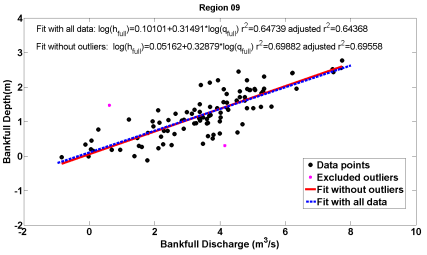

Region 07
One section: log(Q_full)=-0.8964+0.75243*log(A) r²=0.7161 adjusted r²=0.7154
Three sections: log(Q_full)=-1.2226+0.81293*log(A)
+0.012671*(log(A)-log(100)) (A>100)
-0.23834*(log(A)-log(2000)) (A>2000) r²=0.7215 adjusted r²=0.7196
ln(Q_full(m³/s))
ln(Drainage Area (km²))

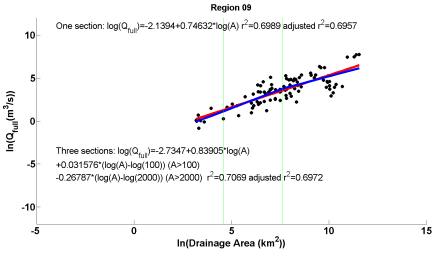

Region 08
Fit with all data: log(Q_full)=0.4916+0.63462*log(A) r²=0.60657 adjusted r²=0.60376
Fit without outliers: log(Q_full)=0.51375+0.64091*log(A) r²=0.66455 adjusted r²=0.6621
Data points
Excluded outliers
Fit without outliers
Fit with all data
ln(Q_full(m³/s))
ln(Drainage Area (km²))

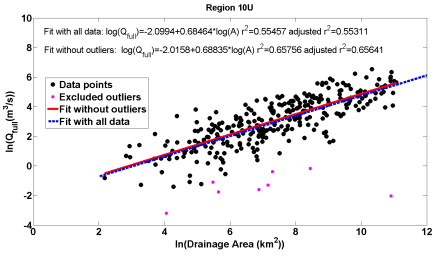

Region 08
Fit with all data: log(h_full)=0.62632+0.17577*log(q_full) r²=0.33623 adjusted r²=0.33149
Fit without outliers: log(h_full)=0.67569+0.17405*log(q_full) r²=0.4478 adjusted r²=0.44364
Data points
Excluded outliers
Fit without outliers
Fit with all data
Bankfull Depth(m)
Bankfull Discharge (m³/s)

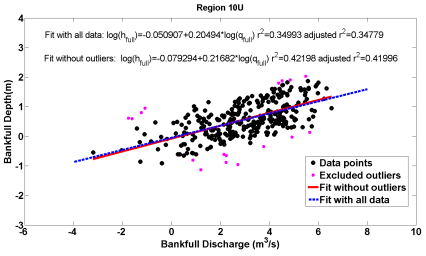

Region 08
One section: log(Q_full)=0.51375+0.64091*log(A) r²=0.6645 adjusted r²=0.6621
Three sections: log(Q_full)=-1.1188+1.0808*log(A)
-0.63254*(log(A)-log(100)) (A>100)
+0.24422*(log(A)-log(2000)) (A>2000) r²=0.6948 adjusted r²=0.6881
ln(Q_full(m³/s))
ln(Drainage Area (km²))

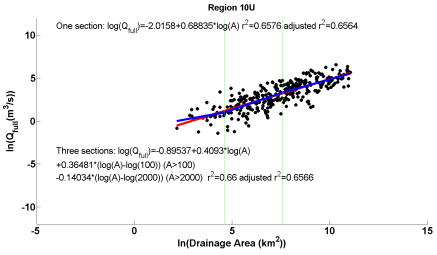

Region 09
Fit with all data: log(Q_full)=-1.9843+0.71764*log(A) r²=0.64478 adjusted r²=0.64104
Fit without outliers: log(Q_full)=-2.1394+0.74632*log(A) r²=0.69891 adjusted r²=0.69567
Data points
Excluded outliers
Fit without outliers
Fit with all data
ln(Q_full(m³/s))
ln(Drainage Area (km²))

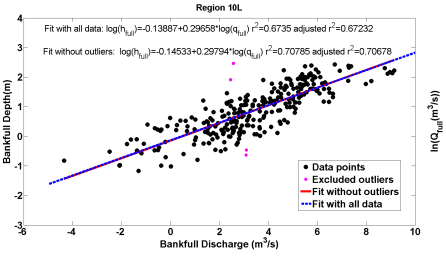

Region 09
Fit with all data: log(h_full)=0.10101+0.31491*log(q_full) r²=0.64739 adjusted r²=0.64368
Fit without outliers: log(h_full)=0.05162+0.32879*log(q_full) r²=0.69882 adjusted r²=0.69558
Data points
Excluded outliers
Fit without outliers
Fit with all data
Bankfull Depth(m)
Bankfull Discharge (m³/s)

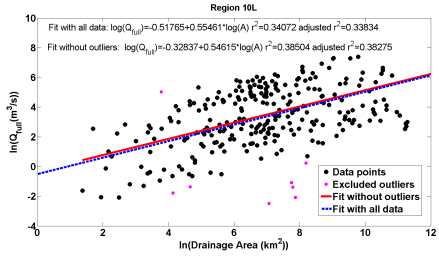

Region 09
One section: log(Q_full)=-2.1394+0.74632*log(A) r²=0.6989 adjusted r²=0.6957
Three sections: log(Q_full)=-2.7347+0.83905*log(A)
+0.031576*(log(A)-log(100)) (A>100)
-0.26787*(log(A)-log(2000)) (A>2000) r²=0.7069 adjusted r²=0.6972
ln(Q_full(m³/s))
ln(Drainage Area (km²))

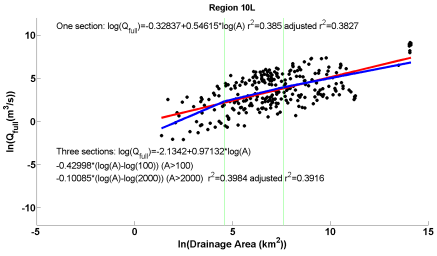

Region 10U
Fit with all data: log(Q_full)=-2.0994+0.68464*log(A) r²=0.55457 adjusted r²=0.55311
Fit without outliers: log(Q_full)=-2.0158+0.68835*log(A) r²=0.65756 adjusted r²=0.65641
Data points
Excluded outliers
Fit without outliers
Fit with all data
ln(Q_full(m³/s))
ln(Drainage Area (km²))

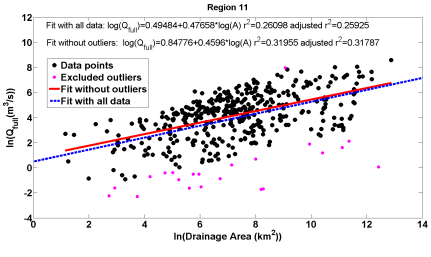

Region 10U
Fit with all data: log(h_full)=-0.050907+0.20494*log(q_full) r²=0.34993 adjusted r²=0.34779
Fit without outliers: log(h_full)=-0.079294+0.21682*log(q_full) r²=0.42198 adjusted r²=0.41996
Data points
Excluded outliers
Fit without outliers
Fit with all data
Bankfull Depth(m)
Bankfull Discharge (m³/s)

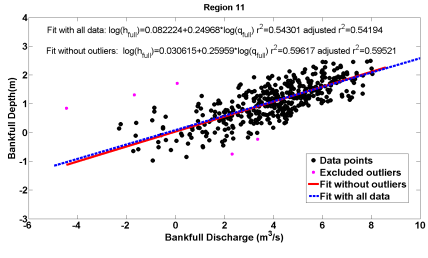

Region 10U
One section: log(Q_full)=-2.0158+0.68835*log(A) r²=0.6576 adjusted r²=0.6564
Three sections: log(Q_full)=-0.89537+0.4093*log(A)
+0.36481*(log(A)-log(100)) (A>100)
-0.14034*(log(A)-log(2000)) (A>2000) r²=0.66 adjusted r²=0.6566
ln(Q_full(m³/s))
ln(Drainage Area (km²))

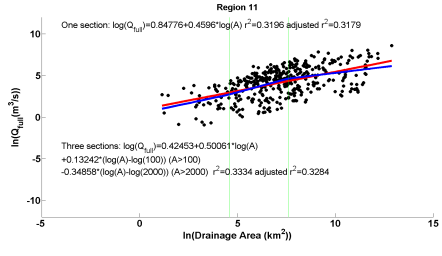

Region 10L
Fit with all data: log(h_full)=-0.13887+0.29658*log(q_full) r²=0.6735 adjusted r²=0.67232
Fit without outliers: log(h_full)=-0.14533+0.29794*log(q_full) r²=0.70785 adjusted r²=0.70678
Data points
Excluded outliers
Fit without outliers
Fit with all data
Bankfull Depth(m)
Bankfull Discharge (m³/s)

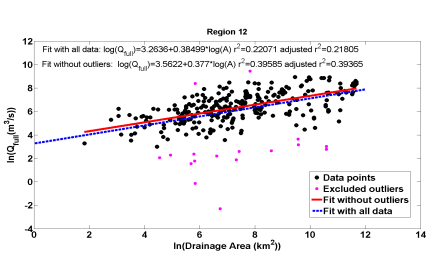

Region 10L
Fit with all data: log(Q_full)=-0.51765+0.55461*log(A) r²=0.34072 adjusted r²=0.33834
Fit without outliers: log(Q_full)=-0.32837+0.54615*log(A) r²=0.38504 adjusted r²=0.38275
Data points
Excluded outliers
Fit without outliers
Fit with all data
ln(Q_full(m³/s))
ln(Drainage Area (km²))

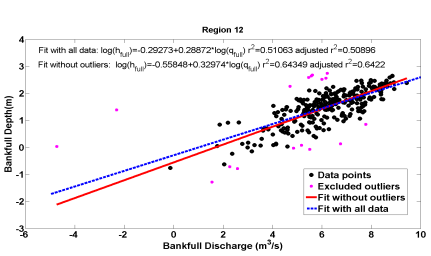

Region 10L
One section: log(Q_full)=-0.32837+0.54615*log(A) r²=0.385 adjusted r²=0.3827
Three sections: log(Q_full)=-2.1342+0.97132*log(A)
-0.42998*(log(A)-log(100)) (A>100)
-0.10085*(log(A)-log(2000)) (A>2000) r²=0.3984 adjusted r²=0.3916
ln(Q_full(m³/s))
ln(Drainage Area (km²))

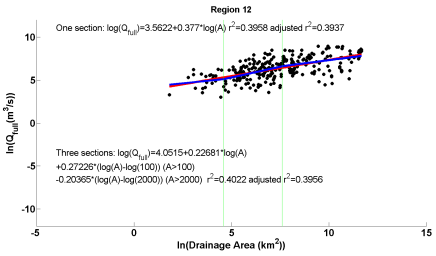

Region 11
Fit with all data: log(Q_full)=0.49484+0.47658*log(A) r²=0.26098 adjusted r²=0.25925
Fit without outliers: log(Q_full)=0.84776+0.4596*log(A) r²=0.31955 adjusted r²=0.31787
Data points
Excluded outliers
Fit without outliers
Fit with all data
ln(Q_full(m³/s))
ln(Drainage Area (km²))

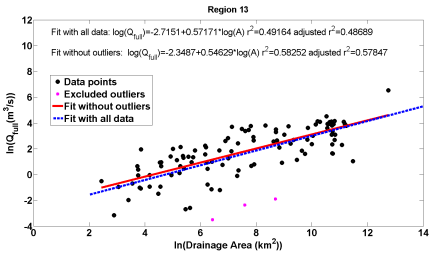

Region 11
Fit with all data: log(h_full)=0.082224+0.24968*log(q_full) r²=0.54301 adjusted r²=0.54194
Fit without outliers: log(h_full)=0.030615+0.25959*log(q_full) r²=0.59617 adjusted r²=0.59521
Data points
Excluded outliers
Fit without outliers
Fit with all data
Bankfull Depth(m)
Bankfull Discharge (m³/s)

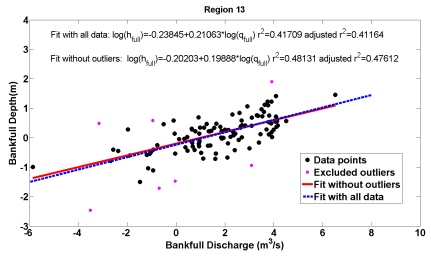

Region 11
One section: log(Q_full)=0.84776+0.4596*log(A) r²=0.3196 adjusted r²=0.3179
Three sections: log(Q_full)=0.42453+0.50061*log(A)
+0.13242*(log(A)-log(100)) (A>100)
-0.34858*(log(A)-log(2000)) (A>2000) r²=0.3334 adjusted r²=0.3284
ln(Q_full(m³/s))
ln(Drainage Area (km²))

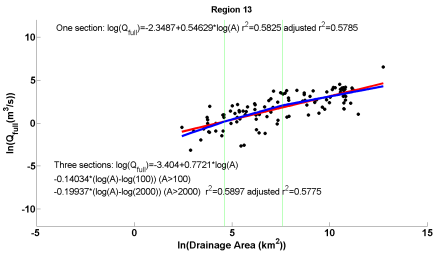

Region 12
Fit with all data: log(Q_full)=3.2636+0.38499*log(A) r²=0.22071 adjusted r²=0.21805
Fit without outliers: log(Q_full)=3.5622+0.377*log(A) r²=0.39585 adjusted r²=0.39365
Data points
Excluded outliers
Fit without outliers
Fit with all data
ln(Q_full(m³/s))
ln(Drainage Area (km²))

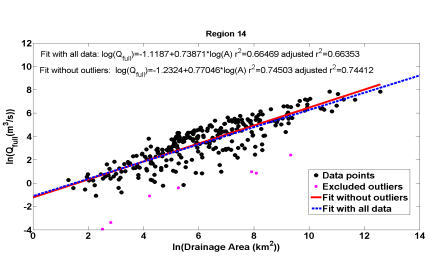

Region 12
Fit with all data: log(h_full)=-0.29273+0.28872*log(q_full) r²=0.51063 adjusted r²=0.50896
Fit without outliers: log(h_full)=-0.55848+0.32974*log(q_full) r²=0.64349 adjusted r²=0.6422
Data points
Excluded outliers
Fit without outliers
Fit with all data
Bankfull Depth(m)
Bankfull Discharge (m³/s)

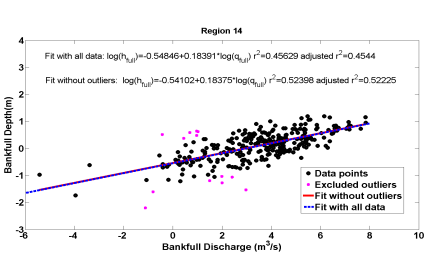

Region 12
One section: log(Q_full)=3.5622+0.377*log(A) r²=0.3958 adjusted r²=0.3937
Three sections: log(Q_full)=4.0515+0.22681*log(A)
+0.27226*(log(A)-log(100)) (A>100)
-0.20365*(log(A)-log(2000)) (A>2000) r²=0.4022 adjusted r²=0.3956
ln(Q_full(m³/s))
ln(Drainage Area (km²))

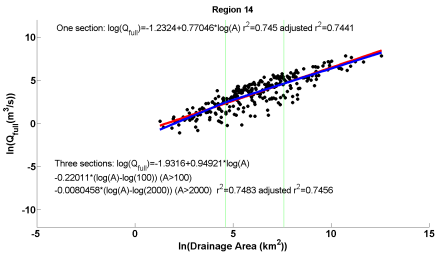

Region 13
Fit with all data: log(Q_full)=-2.7151+0.57171*log(A) r²=0.49164 adjusted r²=0.48689
Fit without outliers: log(Q_full)=-2.3487+0.54629*log(A) r²=0.58252 adjusted r²=0.57847
Data points
Excluded outliers
Fit without outliers
Fit with all data
ln(Q_full(m³/s))
ln(Drainage Area (km²))

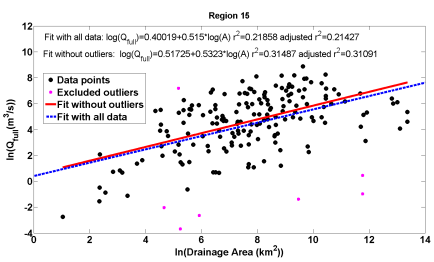

Region 13
Fit with all data: log(h_full)=-0.23845+0.21063*log(q_full) r²=0.41709 adjusted r²=0.41164
Fit without outliers: log(h_full)=-0.20203+0.19888*log(q_full) r²=0.48131 adjusted r²=0.47612
Data points
Excluded outliers
Fit without outliers
Fit with all data
Bankfull Depth(m)
Bankfull Discharge (m³/s)

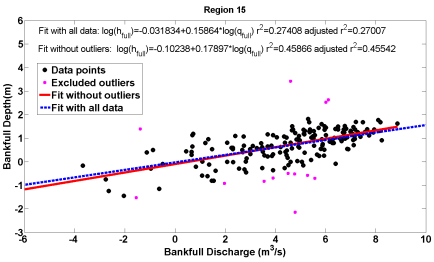

Region 13
One section: log(Q_full)=-2.3487+0.54629*log(A) r²=0.5825 adjusted r²=0.5785
Three sections: log(Q_full)=-3.404+0.7721*log(A)
-0.14034*(log(A)-log(100)) (A>100)
-0.19937*(log(A)-log(2000)) (A>2000) r²=0.5897 adjusted r²=0.5775
ln(Q_full(m³/s))
ln(Drainage Area (km²))

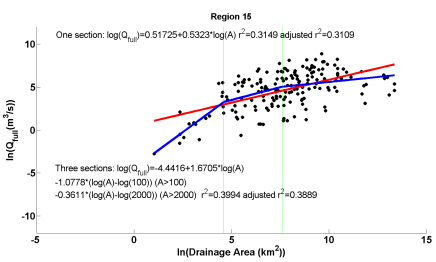

Region 14
Fit with all data: log(Q_full)=-1.1187+0.73871*log(A) r²=0.66469 adjusted r²=0.66353
Fit without outliers: log(Q_full)=-1.2324+0.77046*log(A) r²=0.74503 adjusted r²=0.74412
Data points
Excluded outliers
Fit without outliers
Fit with all data
ln(Q_full(m³/s))
ln(Drainage Area (km²))

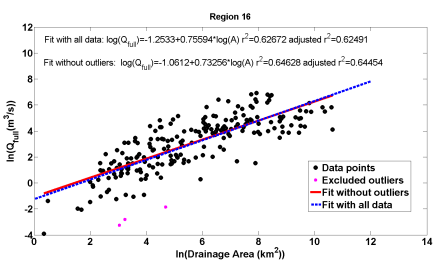

Region 14
Fit with all data: log(h_full)=-0.54846+0.18391*log(q_full) r²=0.45629 adjusted r²=0.4544
Fit without outliers: log(h_full)=-0.54102+0.18375*log(q_full) r²=0.52398 adjusted r²=0.52225
Data points
Excluded outliers
Fit without outliers
Fit with all data
Bankfull Depth(m)
Bankfull Discharge (m³/s)

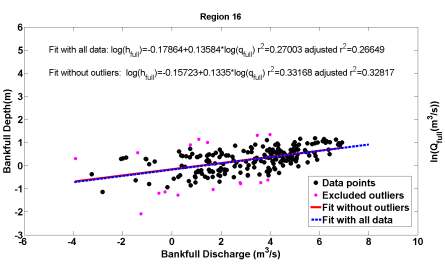

Region 14
One section: log(Q_full)=-1.2324+0.77046*log(A) r²=0.745 adjusted r²=0.7441
Three sections: log(Q_full)=-1.9316+0.94921*log(A)
-0.22011*(log(A)-log(100)) (A>100)
-0.0080458*(log(A)-log(2000)) (A>2000) r²=0.7483 adjusted r²=0.7456
ln(Q_full(m³/s))
ln(Drainage Area (km²))

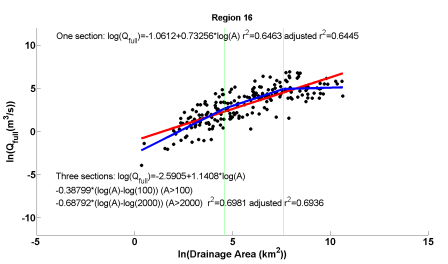

Region 15
Fit with all data: log(Q_full)=0.40019+0.515*log(A) r²=0.21858 adjusted r²=0.21427
Fit without outliers: log(Q_full)=0.51725+0.5323*log(A) r²=0.31487 adjusted r²=0.31091
Data points
Excluded outliers
Fit without outliers
Fit with all data
ln(Q_full(m³/s))
ln(Drainage Area (km²))

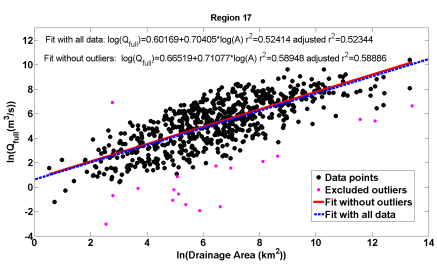

Region 15
Fit with all data: log(h_full)=-0.031834+0.15864*log(q_full) r²=0.27408 adjusted r²=0.27007
Fit without outliers: log(h_full)=-0.10238+0.17897*log(q_full) r²=0.45866 adjusted r²=0.45542
Data points
Excluded outliers
Fit without outliers
Fit with all data
Bankfull Depth(m)
Bankfull Discharge (m³/s)

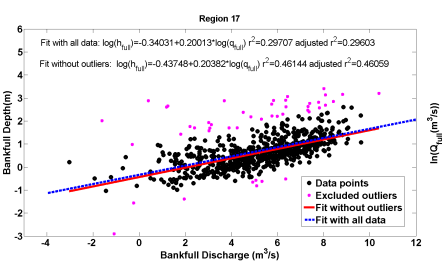

Region 15
One section: log(Q_full)=0.51725+0.5323*log(A) r²=0.3149 adjusted r²=0.3109
Three sections: log(Q_full)=-4.4416+1.6705*log(A)
-1.0778*(log(A)-log(100)) (A>100)
-0.3611*(log(A)-log(2000)) (A>2000) r²=0.3994 adjusted r²=0.3889
ln(Q_full(m³/s))
ln(Drainage Area (km²))

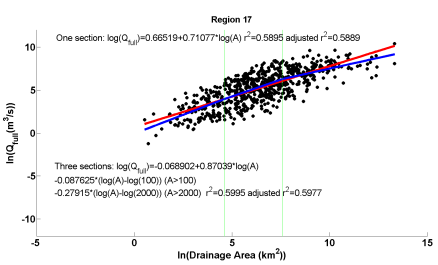

Region 16
Fit with all data: log(Q_full)=-1.2533+0.75594*log(A) r²=0.62672 adjusted r²=0.62491
Fit without outliers: log(Q_full)=-1.0612+0.73256*log(A) r²=0.64628 adjusted r²=0.64454
Data points
Excluded outliers
Fit without outliers
Fit with all data
ln(Q_full(m³/s))
ln(Drainage Area (km²))


Region 16
Fit with all data: log(h_full)=-0.17864+0.13584*log(q_full) r²=0.27003 adjusted r²=0.26649
Fit without outliers: log(h_full)=-0.15723+0.1335*log(q_full) r²=0.33168 adjusted r²=0.32817
Data points
Excluded outliers
Fit without outliers
Fit with all data
Bankfull Depth(m)
Bankfull Discharge (m³/s)


Region 16
One section: log(Q_full)=-1.0612+0.73256*log(A) r²=0.6463 adjusted r²=0.6445
Three sections: log(Q_full)=-2.5905+1.1408*log(A)
-0.38799*(log(A)-log(100)) (A>100)
-0.68792*(log(A)-log(2000)) (A>2000) r²=0.6981 adjusted r²=0.6936
ln(Q_full(m³/s))
ln(Drainage Area (km²))


Region 17
Fit with all data: log(Q_full)=0.60169+0.70405*log(A) r²=0.52414 adjusted r²=0.52344
Fit without outliers: log(Q_full)=0.66519+0.71077*log(A) r²=0.58948 adjusted r²=0.58886
Data points
Excluded outliers
Fit without outliers
Fit with all data
ln(Q_full(m³/s))
ln(Drainage Area (km²))


Region 17
Fit with all data: log(h_full)=-0.34031+0.20013*log(q_full) r²=0.29707 adjusted r²=0.29603
Fit without outliers: log(h_full)=-0.43748+0.20382*log(q_full) r²=0.46144 adjusted r²=0.46059
Data points
Excluded outliers
Fit without outliers
Fit with all data
Bankfull Depth(m)
Bankfull Discharge (m³/s)


Region 17
One section: log(Q_full)=0.66519+0.71077*log(A) r²=0.5895 adjusted r²=0.5889
Three sections: log(Q_full)=-0.068902+0.87039*log(A)
-0.087625*(log(A)-log(100)) (A>100)
-0.27915*(log(A)-log(2000)) (A>2000) r²=0.5995 adjusted r²=0.5977
ln(Q_full(m³/s))
ln(Drainage Area (km²))

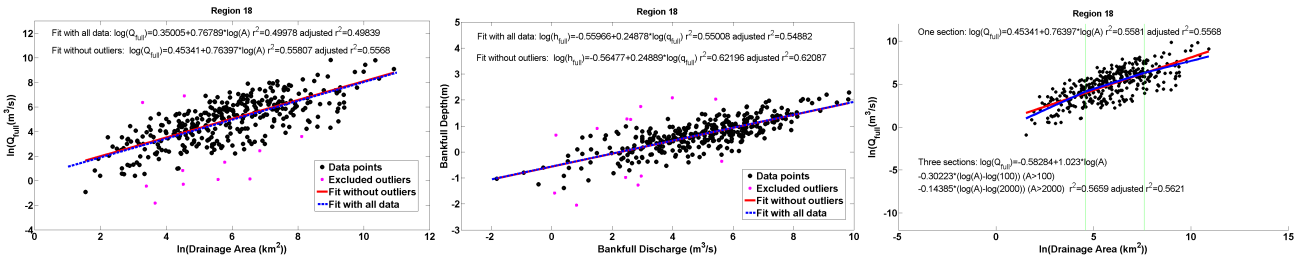


Figure 4.1 Fitted empirical power law relationships between bankfull discharge (Q_{full}) and drainage area (A), and between bankfull discharge (Q_{full}) and bankfull depth (h_{full}) at log scale for each HUC2 water resource region with USGS field measurements between 01/01/1990 to 03/31/2010 with outlier analysis

4.3 Impact of Drainage basin size

In the both Table 3.1 and Table 4.1, the empirical power relationships are derived for each water resources region. As one may expect, one uniform relationship can smooth out the within-basin variability of the behaviors of river reaches with different sizes. The smoothing effect can be more obvious over regions with a skewed distribution of river sizes, in which the power relationship coefficient will be dominated and mainly controlled by the small (or main) river branches, neglecting the bigger main (or smaller) river reaches. Therefore, to further test the impact of river sizes on the power relationship between bankfull discharge and area, within each water resource region, the gauging stations are divided into three sizes based on the drainage area. For each group, a separate power relationship is derived separately. The mathematical representation of the three-section relationship is as

$$Log(Q_{full}) = m_0 + m_1 * \log(A) + m_2(\log(A) - \log(A_1))(A > A_1) + m_3(\log(A) - \log(A_2))(A > A_2) \quad (4.1)$$

where m_0, m_1, m_2, *and* m_3 are coefficients, A_1 and A_2 are two threshold values for drainage area. Here we assume A_1 = 100km^2, and A_2=2000km^2 as the division to represent the small-sized river, mid-sized river, and larger sized river.

The right column in Figure 4.1 lists out all three-section relationship (blue line) compared with one uniform relationships (red line) for each water resource region. It is clear that for most of the regions, though correlation coefficient (R^2) increases for all the regions, the difference between the two types of power relationships (uniform and three-sections based on river sizes) is minimum. The correlation coefficient (R^2) increases most in region 08, 15, and 16. Region 08 is Lower Mississippi Region, and most of the gauging stations are along mid-sized and large-sized rivers. Upstream small river branches may have quite different behaviors compared to the large-sized rivers as Lower Mississippi in terms of the change of bankfull discharge and drainage area. Therefore, dividing the power relationship into three sections can separate different behaviors based on the river size, and increase the correlation coefficient from 0.66 to 0.69. Similarly, for region 15 (Lower Colorado Region) and region 16 (Great Plain Region), rivers with different drainage sizes also shows more diverse behaviors, which might be affected by different regulation rules at different locations. Thus separating the relationships into three sections also increases the correlation coefficients from 0.31 to 0.4, and from 0.64 to 0.69, respectively.

4.4 Impact of anthropogenic effect

The power relationship defined in the hydraulic geometry is mainly based on the behaviors of natural rivers. On the other hand, anthropogenic effect can strongly modify the river flows and thus streamflow variability [*Graf*, 1999; *Fitzhugh and Vogel*, 2011]. Especially over regions with heavy water management, those empirical power relationships might change significantly compared to natural river systems. Thus, to test the impact of the anthropogenic effect on the derived power relationship, we further divided the gauging stations into "natural gauges" and "managed gauges" for each water resources region. The Hydro Climate Data Network (HCDN) streamflow dataset (http://pubs.usgs.gov/wri/wri934076/) is developed to study the fluctuation of

surface water conditions under climate change over the U.S. This dataset specifically choose gauge stations record that relatively free of human impact and water management. Therefore, in this section, we assume all the gauges included in the HCDN dataset as the HDCN "Natural" gauges, with the rest of gauges as Non-HCDN "Managed" stations within each water resource region. Two separate power relationships are derived using the HCDN and Non-HCDN gauging stations respectively.

Figure 4.2a and Figure 4.2b shows the comparison of the HCDN and Non-HCDN relationship over Regions 10L, 10U, 14, 15, and 18. Those regions are Upper and Lower Missouri Regions, Lower Colorado Regions, and California Regions, where water management is relatively heavy compare to the other water resources regions [*Graf*, 1999]. For example, there are 4 largest dams over the U.S. located in regions 10L. As expected, all the correlation coefficients of the HCDN sites are higher than that of the relationship derived from Non-HDCN sites. For example, over the Lower Colorado region, (Region 15), the R^2 for two power relationships are 0.5759 and 0.7247 over HCDN sites, where the corresponding R^2 are 0.2913 and 0.3881 over non-HCDN sites. The scatter plots between bankfull discharge and drainage area, and between bankfull discharge and bankfull depth over the above corresponding regions also show that over the Non-HCDN gauging stations there is much more variability and the date points are much more spreaded-out relative to the fitted lines compared to that of HCDN sites. Though the number of HCDN ("natural") sites is smaller than that of non-HCDN ("managed") sites, the difference of the goodness of fit demonstrates the impact of the human interference of the behaviors of natural river system, suggesting the potential importance of derived the empirical relationship considering the human interference of behaviors of river system.

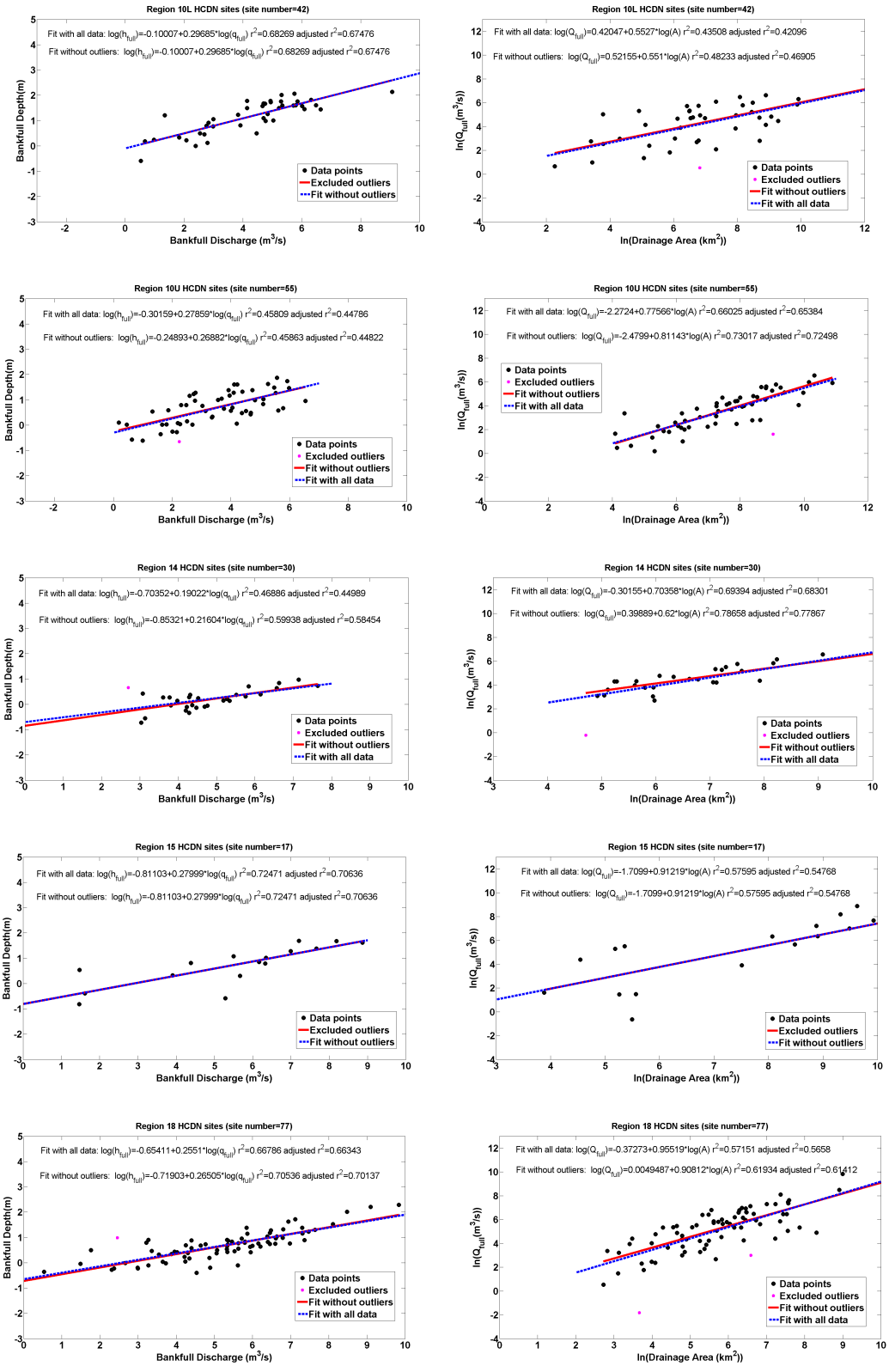


Figure 4.2 Fitted empirical power law relationships between bankfull discharge (Q_{full}) and drainage area (A), and between bankfull discharge (Q_{full}) and bankfull depth (h_{full}) at log scale for HUC2 water resource region 10U, 10L, 14, 15, and 18, with USGS field measurements between 01/01/1990 to 03/31/2010, over HCDN gauging stations.

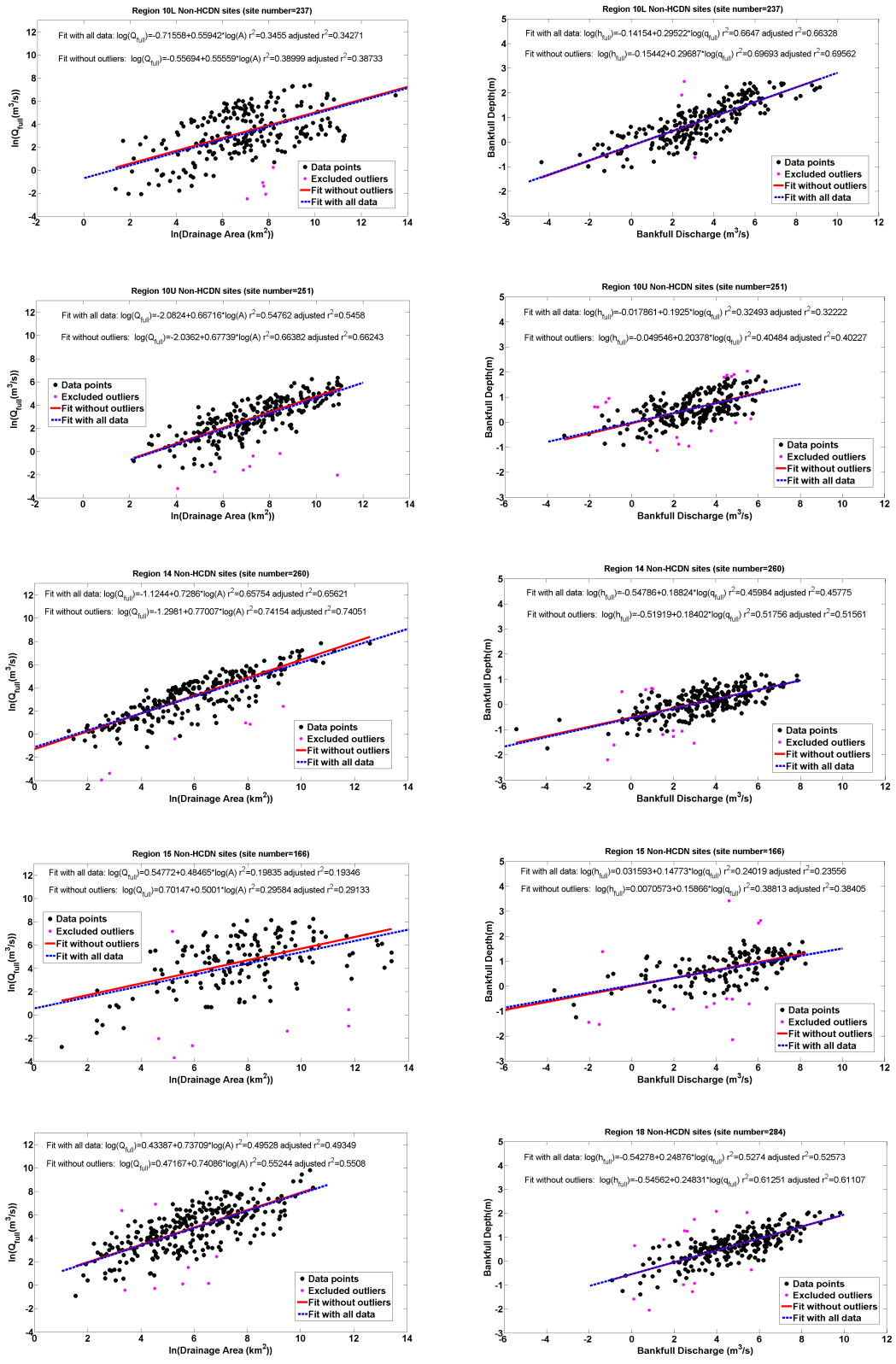


Figure 4.3 Fitted empirical power law relationships between bankfull discharge (Q_{full}) and drainage area (A), and between bankfull discharge (Q_{full}) and bankfull depth (h_{full}) at log scale for HUC2 water resource region 10U, 10L, 14, 15, and 18, with USGS field measurements between 01/01/1990 to 03/31/2010, over non-HCDN gauging stations.

5. Future work and Summary

In this study, we proposed to build a continental-scale, catchment-based land surface hydrologic modeling framework based on CHARMS. A complete set of empirical power relationships is derived and explored to extract an estimation of river-cross section profiles including bankfull discharge, bankfull depth, and bankfull width. This set of relationship is used to separate the river flow into floodplain and main river channel and to estimate the river depth and corresponding floodplain inundation extent. As a first step toward building an assimilation-ready continental-scale catchment-based land surface modeling framework with an explicit representation, the goal of this work is to facilitate the incorporation of the measurements from SWOT for hydrological and climate applications and improve the simulation and understanding surface water dynamics. Also, as a first step, there are still challenges and technical difficulties in the process as mentioned in Section 3.6. This Chapter briefly describes parts of future work that can potentially further improve the results of this study and next steps.

5.1 Adding hillslope river transport component

In Section 3.3.2, lumped runoff is added at the downstream end of each sub reach. The lumped runoff is calculated as the product of the drainage area and the sum of surface and subsurface runoff. The simplified version is used in the early study considering the computation cost. However, the lumped runoff omitted the water transport process from hillslope to reaches (Figure 5.1), which can largely affect the timing of the simulated hydrograph by ignoring the travel time from hillslope transport. The timing effect can be more apparent if the distance from hillslope is large. Kinematic wave approximation has been proven to be a powerful tool to simulate the hillslope river transport by different studies [*Li et al.*, 1975] . In the future work, both linear and non-linear solution of the kinematic water approximation as described by *Li et*

al., [1975] can be incorporated into CHARMS to consider different travel time for surface and subsurface runoff transport time joining river reach from hillslope.

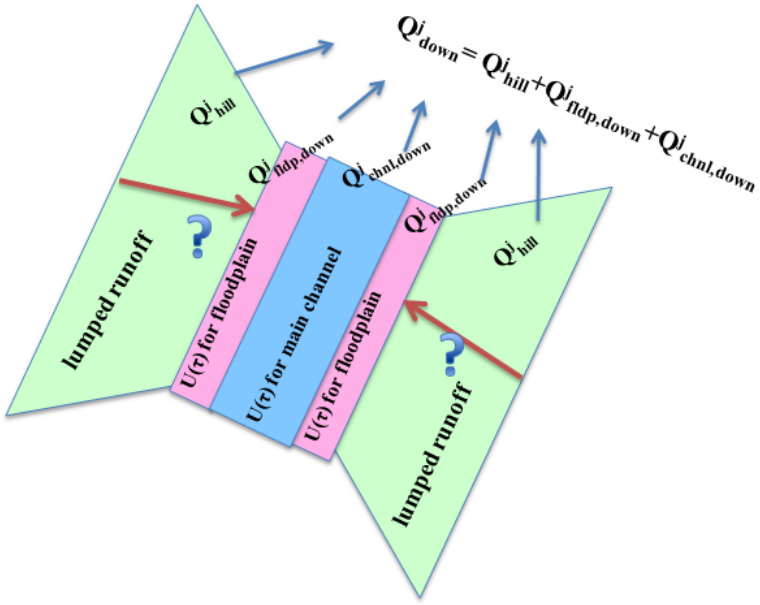


Figure 5.1 Schematic plot of lumped runoff process with hillslope-to-channel transport missing

5.1.1 Linear and non-linear kinematic wave approximation for water routing

The transport of runoff can be described by both continuity and momentum equations. For the momentum equations, kinematic wave approximation assumes that water surface slope is equal to the bed slope.

$$\frac{\partial Q}{\partial x} + \frac{\partial A}{\partial t} = q_l \quad \textit{Continuity Equation} \qquad (5.1)$$

$$S_0 = S_f \quad \textit{Kinematic Wave Assumption} \qquad (5.2)$$

The following description is largely drawn from [*Li et al.*, 1975]. The finite difference forms of Eq.(5.1) is

$$\frac{Q^{n+1}_{j+1} - Q^{n+1}_{j}}{\Delta x} + \frac{A^{n+1}_{j+1} - A^{n}_{j+1}}{\Delta t} = \frac{q^{n+1}_{l,j+1} - q^{n}_{l,j+1}}{2} \qquad (5.3)$$

where j is the space index, n is the time index. Δx is the space increment, and Δt is the time increment. The unknowns in Eq.(5.3) are Q_{j+1}^{n+1} and A_{j+1}^{n+1}. Based on the power relationship between Q and A,

$$Q = \alpha A^{\beta} \qquad (5.4)$$

Eq.(5.3) can be rewritten as,

$$\frac{\Delta t}{\Delta x} Q_{i+1}^{n+1} + \alpha (Q_{j+1}^{n+1})^{\beta} = \frac{\Delta t}{\Delta x} Q_{j}^{n+1} \alpha (Q_{j+1}^{n})^{\beta} + \Delta t \left(\frac{q_{l,j+1}^{n+1} - q_{l,j+1}^{n}}{2} \right) \qquad (5.5)$$

Using Ω representing the right side the of known quantities, and with $r = Q_{j+1}^{n+1}$, $\theta = \frac{\Delta t}{\Delta x}$, Eq.(5.5) can be rewritten as,

$$f(r) = \theta r + \alpha r^{\beta} = \Omega \qquad (5.6)$$

Therefore, solving for Q_{j+1}^{n+1} is to solve for r. *Li et al.*, [1975] provides both the linear and non-linear solutions for Eq. (5.6).

5.1.1.1 Linear Solution for Eq. (5.6)

Linear scheme shown as Eq. (5.7) provides the best initial solution for the nonlinear scheme.

$$r^{0} = Q_{j+1}^{n+1} = [\theta Q_{j}^{n+1} + \alpha\beta Q_{j+1}^{n} (\frac{Q_{j+1}^{n} + Q_{j}^{n+1}}{2})^{\beta-1} + \Delta t (\frac{q_{l,j+1}^{n+1} + q_{l,j+1}^{n}}{2})] \cdot \left[\theta + \alpha\beta (\frac{Q_{j+1}^{n} + Q_{j}^{n+1}}{2})^{\beta-1} \right]^{-1} \qquad (5.7)$$

If $\beta = 1$, this linear solution/first guess drops to

$$r^{0} = \Omega / (\theta + \alpha) \qquad (5.8)$$

5.1.1.2 Non-linear Solution for Eq. (5.6)

In non-linear scheme, r is solved iteratively based on Taylor series expansion of the function of f(r) (dropping third order and other higher terms).

$$f(r) \cong f(r^k) + (r - r^k) f'(r^k) + \tfrac{1}{2} (r - r^k)^2 f''(r^k) \qquad (5.9)$$

The solution of the iteration is to force $f(r^{k+1})$ close to the value of Ω

$$\Omega = f(r^k) + (r^{k+1} - r^k) f'(r^k) + \tfrac{1}{2} (r^{k+1} - r^k)^2 f''(r^k) \qquad (5.10)$$

Then, the iterative solution of Eq. (5.9) is

$$r^{k+1} = r^k - \frac{f'(r^k)}{f''(r^k)} \pm \left[\left(\frac{f'(r^k)}{f''(r^k)} \right)^2 - \frac{2(f(r^k) - \Omega)}{f''(r^k)} \right]^{\frac{1}{2}} \qquad (5.11)$$

where

$$\begin{aligned} f(r^k) &= \theta r^k + \alpha (r^k)^\beta \\ f'(r^k) &= \theta + \alpha\beta (r^k)^{\beta-1} \\ f''(r^k) &= \alpha\beta(\beta - 1)(r^k)^{\beta-2} \end{aligned} \qquad (5.12)$$

Starting with the initial linear guess provided by Eq. (5.7), the above iteration process in Eq. (5.11) continues until it satisfies the termination criterion (when $f(r^{k+1})$ is close enough to Ω).

$$\left| f(r^{k+1}) - \Omega \right| \leq \varepsilon \qquad (5.13)$$

where ε is the pre-assigned error tolerance. There can be two solutions shown in Eq.(5.11), the rule of thumb is to choose the solution generating a smaller value of $\left| f(r^{k+1}) - \Omega \right|$.

Early studies [*Beighley et al.*, 2009] suggest using linear solution for subsurface runoff routing with $\beta = 1$; while iterative non-linear solution is used to determine the surface flow routed from hillslope to main channel.

At each time step (n+1), surface and subsurface runoff (lateral flow) are routed separately from hillslope to main channel, generating Q_{j+1}^{n+1}. Therefore, Q_j^{n+1} represents the routed flow from immediate upstream channel segment at current time step; Q_{j+1}^{n}represents the routed flow at

current river reach from last time step. Similarly, $q_{l,j+1}^{n+1}$ refers to the lateral flow (either surface or subsurface runoff to be routed) coming into current channel at current step, and $q_{l,j+1}^{n}$ represents the lateral flow at current reach from last time step. Both α and β are pre-assigned differently for surface and subsurface runoff routing.

5.2 Separating natural and regulated gauging stations based on streamflow variability and flow duration curve

Section 4.4 provides a method of separating managed and un-managed gauge stations and to build empirical relationship over these two regions respectively. However, the separation of regulated and natural gauging stations is limited by the HCDN stations over the continental U.S. Therefore, for future global implementation, a more generic way is necessary to identify the regulated gauging stations from natural gauges. Flow Duration Curve (FDC) has been proven to be a useful and common way to identify the degree of alternation of streamflow regime [*Vogel and Fennessey*, 1994]. Readers are referred to *Vogel and Fennessey*, [1994, 1995] for a detailed review of FDC history.

Flow duration curve represents the percentage of time/probability of a particular value exceeded by streamflow of a given river basin, and the relationship between the magnitude and frequency of daily/monthly/annual streamflow over a given period of time [*Vogel and Fennessey*, 1994]. Therefore, FDC is able to provide a comprehensive and simple view of the variability of the historical streamflow record. Starting from a hydrograph, each value of streamflow discharge Q has a corresponding exceedance probability p, where p is defined as the complement of the cumulative probability $F_Q(q)$

$$p = 1 - P\{Q \le q\}$$
$$p = 1 - F_Q(q) \qquad (5.13)$$

Thus, FDC is a plot between the pth quantile or percentile of daily streamflow versus its exceedance probability (Figure 5.2).

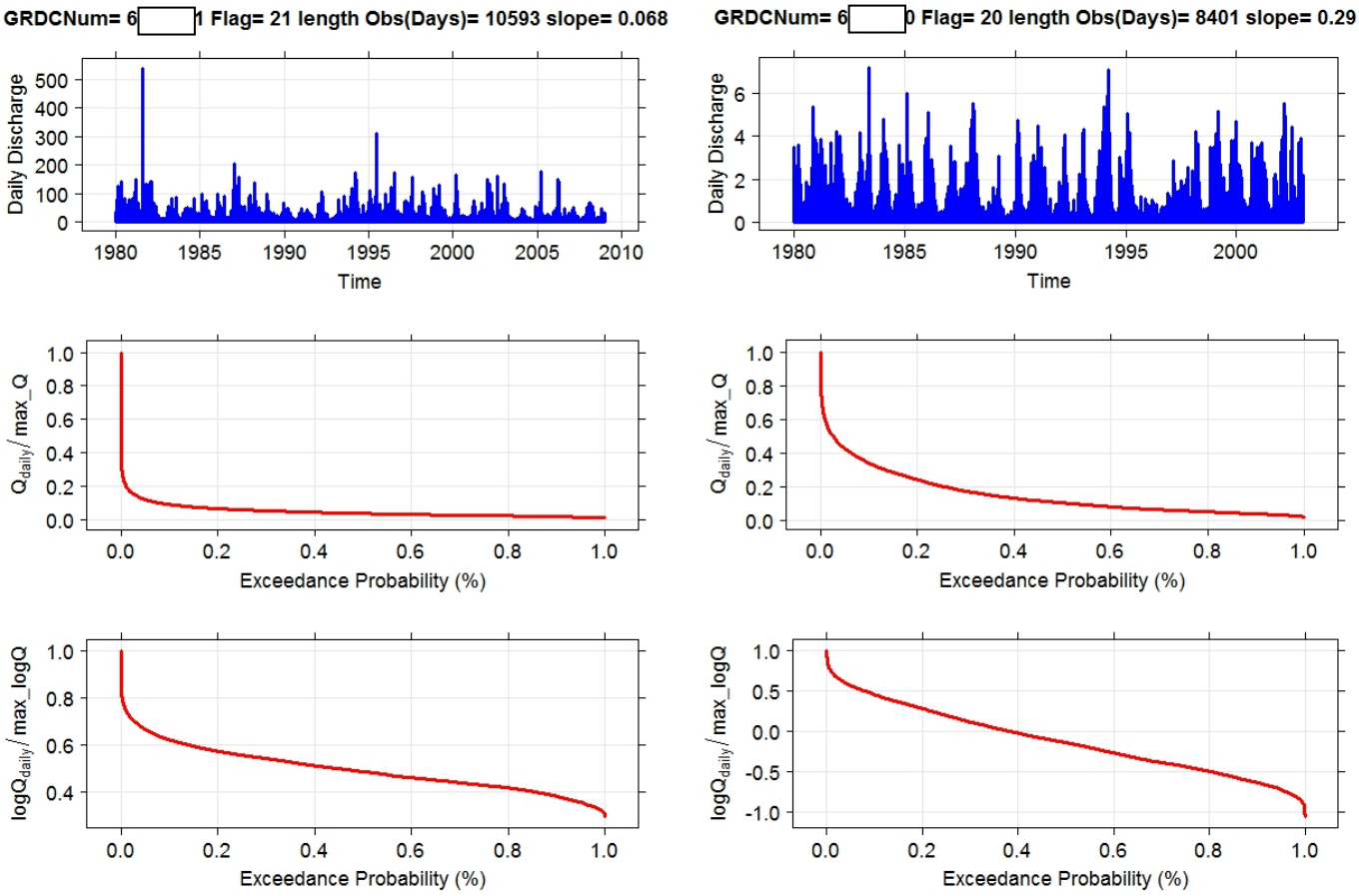


Figure 5.2 Hydrographs and flow duration curves (both normalized and log-normalized scale) over natural (right) and regulated (left) gauge stations.

Theoretically, streamflow observations from natural gauging stations have more variability compared to regulated gauges. For a natural gauging station without anthropogenic interference, it shows more variability with both high flow and low flow evenly distributed, and the variability of the observations will be more spread out through out the length of the record. Therefore, the slope of the linear section between 25% to 75% exceedance probability of the FDC curve over natural gauging stations will be steeper (Figure 5.2a). In Contrast, over regulated gauging stations, high flow and low flows are controlled through anthropogenic effect. There is in general much less percentage of chances to have extreme flows. Thus, the high flow and corresponding variability for regulated flows happens at a very small possibility, with all the rest of flows remain stable at the majority of time. Therefore, the flow duration curve of the regulated gauges should have a more sharp "elbow-like" shape, and the slope of the linear section between 25% to 75% exceedance probability should be much flatter, with a smaller variation percentage compared to the total difference between Qmin and Qmax (Figure 5.2b). Therefore, with the flow duration curve derived from streamflow observations, regulated gauging stations can be separated from natural gauging stations through cluster classify analysis (Figure 5.3). This separation can be used both for deriving empirical relationships separately for both natural and manage regions, and for model calibration for future global-scale CHARMS model framework implementation.

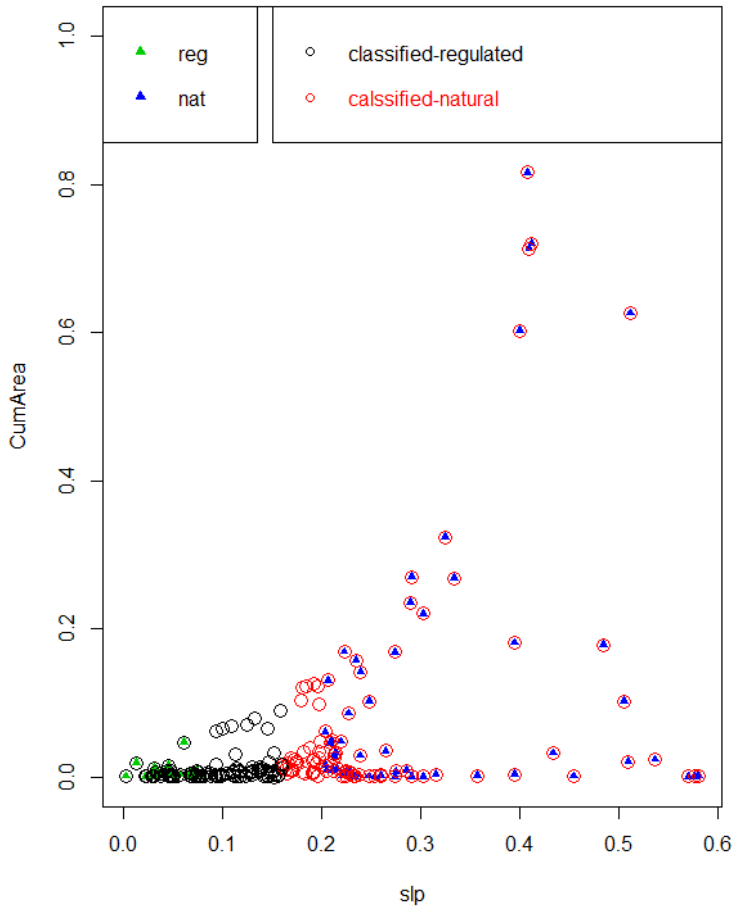


Figure 5.3 Cluster classification of regulated gauges and natural gauging stations based on slope of flow duration curves using Support Vector Machine (SVM). Green and blue triangles are the training datasets as pre-defined regulated and natural gauges, black and red circle are the classified regulated and natural gauges using SVM with the prior training information.

5.3 Future Global Application Feasibility

Here we proposed and built a continental-scale template for the implementation of the Catchment-based Hydrological And Routing Modeling System (CHARMS) that includes an explicit representation of river networks to estimate river discharge, river depth and the corresponding inundation extent. The long-term objective of this framework is toward building a global-scale catchment-based land surface model system with capabilities for SWOT assimilation, as well as for a range of studies in climate, hydrology and water management.

Efforts by different studies in recent years have made this long-term objective possible and approachable. For example, HydroSHEDS [*Lehner et al.*, 2008] has provided global available 3arc second (~90m) river network. *Andreadis et al.*, [2013] provided a global dataset for bankfull depth and bankfull width with one uniform empirical relationship applied over the HydroSHEDS river network (3.4(e, f).). Recent released Global Land and Data Assimilation System (GLDAS) version 2 [*Rui and Beaudoing*, 2013] will also provide a global dataset for meteorological forcing. With the input datasets mentioned above fed into the continental-scale CHARMS framework, river discharge, river depth, and corresponding floodplain inundation extent can be estimated globally. Ultimately, an assimilation-ready global-scale catchment-based hydrological and river routing model framework will facilitate the incorporation of SWOT mission and to enable significant improvement in predictive understanding of surface water dynamics.

References

Alsdorf, D. E., and D. P. Lettenmaier (2003), Tracking Fresh Water from Space, *Science*, *301*(5639), 1491–1494. [online] Available from: http://www.sciencemag.org/content/301/5639/1491.short

Alsdorf, D. E., E. Rodríguez, and D. P. Lettenmaier (2007), Measuring surface water from space, *Reviews of Geophysics*, *45*(2), doi:10.1029/2006RG000197. [online] Available from: http://dx.doi.org/10.1029/2006RG000197

Andreadis, K. M., E. A. Clark, D. P. Lettenmaier, and D. E. Alsdorf (2007), Prospects for river discharge and depth estimation through assimilation of swath-altimetry into a raster-based hydrodynamics model, *Geophysical Research Letters*, *34*(10), doi:10.1029/2007GL029721. [online] Available from: http://dx.doi.org/10.1029/2007GL029721

Andreadis, K. M., G. J.-P. Schumann, and T. Pavelsky (2013), A simple global river bankfull width and depth database, *Water Resources Research*, *49*(10), 7164–7168, doi:10.1002/wrcr.20440. [online] Available from: http://dx.doi.org/10.1002/wrcr.20440

Asante, K. O. (2000), Approaches to continental scale river flow routing, Ph.D. Dissertation, University of Texas at Austin.

Asante, K. O., G. A. Artan, S. Pervez, C. Bandaragoda, and J. P. Verdin (2008), Technical Manual for the Geospatial Stream Flow Model (GeoSFM): US Geological Survey Open-File Report 2007-1441, *US Geological Survey, Reston*.

Ashmore, P., and E. Sauks (2006), Prediction of discharge from water surface width in a braided river with implications for at-a-station hydraulic geometry, *Water Resources Research*, *42*(3), doi:10.1029/2005WR003993. [online] Available from: http://dx.doi.org/10.1029/2005WR003993

Bates, P. D., and A. P. J. De Roo (2000), A simple raster-based model for flood inundation simulation, *Journal of Hydrology*, *236*(1–2), 54–77, doi:10.1016/S0022-1694(00)00278-X. [online] Available from: http://www.sciencedirect.com/science/article/pii/S002216940000278X

Beighley, R. E., and V. Gummadi (2011), Developing channel and floodplain dimensions with limited data: a case study in the Amazon Basin, *Earth Surface Processes and Landforms*, *36*(8), 1059–1071, doi:10.1002/esp.2132. [online] Available from: http://dx.doi.org/10.1002/esp.2132

Beighley, R. E., K. G. Eggert, T. Dunne, Y. He, V. Gummadi, and K. L. C. H. Verdin (2009), Simulating hydrologic and hydraulic processes throughout the Amazon River Basin, *Hydrological Processes*, *23*, 1221–1235 ST – Simulating hydrologic and hydrauli, doi:10.1002/hyp.7252.

Beven, K. J., and M. J. Kirkby (1979), A physically based, variable contributing area model of basin hydrology/Un modèle à base physique de zone d'appel variable de l'hydrologie du bassin versant, *Hydrological Sciences Journal*, *24*(1), 43–69.

Biancamaria, S., M. Durand, K. M. Andreadis, P. D. Bates, A. Boone, N. M. Mognard, E. Rodríguez, D. E. Alsdorf, D. P. Lettenmaier, and E. A. Clark (2011), Assimilation of virtual wide swath altimetry to improve Arctic river modeling, *Remote Sensing of Environment*, *115*(2), 373–381, doi:10.1016/j.rse.2010.09.008. [online] Available from: http://www.sciencedirect.com/science/article/pii/S0034425710002816

Birkett, C. M., L. A. K. Mertes, T. Dunne, M. H. Costa, and M. J. Jasinski (2002), Surface water dynamics in the Amazon Basin: Application of satellite radar altimetry, *Journal of Geophysical Research: Atmospheres*, *107*(D20), doi:10.1029/2001JD000609. [online] Available from: http://dx.doi.org/10.1029/2001JD000609

Bjerklie, D. M. (2007), Estimating the bankfull velocity and discharge for rivers using remotely sensed river morphology information, *Journal of Hydrology*, *341*(3–4), 144–155, doi:10.1016/j.jhydrol.2007.04.011. [online] Available from: http://www.sciencedirect.com/science/article/pii/S002216940700220X

Bjerklie, D. M., S. Lawrence Dingman, C. J. Vorosmarty, C. H. Bolster, and R. G. Congalton (2003), Evaluating the potential for measuring river discharge from space, *Journal of Hydrology*, *278*(1–4), 17–38, doi:10.1016/S0022-1694(03)00129-X. [online] Available from: http://www.sciencedirect.com/science/article/pii/S002216940300129X

Bjerklie, D. M., S. L. Dingman, and C. H. Bolster (2005a), Comparison of constitutive flow resistance equations based on the Manning and Chezy equations applied to natural rivers, *Water Resources Research*, *41*, doi:10.1029/2004WR003776.

Bjerklie, D. M., D. Moller, L. C. Smith, and S. L. Dingman (2005b), Estimating discharge in rivers using remotely sensed hydraulic information, *Journal of Hydrology*, *309*(1–4), 191–209, doi:10.1016/j.jhydrol.2004.11.022. [online] Available from: http://www.sciencedirect.com/science/article/pii/S0022169404005724

Branstetter, M. L. (2001), Development of a parallel river transport algorithm and applications to climate studies, Ph.D. Dissertation, University of Texas at Austin.

Branstetter, M. L., and J. S. Famiglietti (1999), Testing the sensitivity of GCM-simulated runoff to climate model resolution using a parallel river transport algorithm.

Cai, X., Z.-L. Yang, C. H. David, G.-Y. Niu, and M. Rodell (2013), Hydrological evaluation of the Noah-MP land surface model for the Mississippi River Basin, *Journal of Geophysical Research: Atmospheres*, doi:10.1002/2013JD020792. [online] Available from: http://dx.doi.org/10.1002/2013JD020792

Chandanpurkar, H. A., J. T. Reager, J. S. Famiglietti, D. P. Chambers, and T. H. Syed (2014), Increasing global freshwater discharge from nearly two decades of ocean satellite observations, Under Review, *Geophysical Research Letters*.

Coe, M. T. (1998), A linked global model of terrestrial hydrologic processes: Simulation of modern rivers, lakes, and wetlands, *Journal of Geophysical Research: Atmospheres*, *103*(D8), 8885–8899, doi:10.1029/98JD00347. [online] Available from: http://dx.doi.org/10.1029/98JD00347

Coe, M. T. (2002), Long-term simulations of discharge and floods in the Amazon Basin, *Journal of Geophysical Research*, *107*, 1–17, doi:10.1029/2001JD000740.

Coe, M. T., and C. M. Birkett (2004), Calculation of river discharge and prediction of lake height from satellite radar altimetry: Example for the Lake Chad basin, *Water Resources Research*, *40*(10), doi:10.1029/2003WR002543. [online] Available from: http://dx.doi.org/10.1029/2003WR002543

National Research Concil, (2007), *Earth Science and Applications From Space: National Imperatives for the Next Decade and Beyond*, p.p. 418, Washington, D.C.

David, C. H., F. Habets, D. R. Maidment, and Z.-L. Yang (2011a), RAPID applied to the SIM-France model, *Hydrological Processes*, *25*, 3412–3425, doi:10.1002/hyp.8070.

David, C. H., D. R. Maidment, G.-Y. Niu, Z.-L. Yang, F. Habets, and V. Eijkhout (2011b), River Network Routing on the NHDPlus Dataset, *Journal of Hydrometeorology*, *12*(5), 913–934, doi:10.1175/2011JHM1345.1. [online] Available from: http://dx.doi.org/10.1175/2011JHM1345.1

David, C. H., Z. L. Yang, and S. Hong (2013), Regional-scale river flow modeling using off-the-shelf runoff products, thousands of mapped rivers and hundreds of stream flow gauges, *Environmental Modelling and Software*, *42*, 116–132, doi:10.1016/j.envsoft.2012.12.011.

Decharme, B., H. Douville, C. Prigent, F. Papa, and F. Aires (2008), A new river flooding scheme for global climate applications: Off-line evaluation over South America, *Journal of Geophysical Research*, *113*, 1–11, doi:10.1029/2007JD009376.

Decharme, B., R. Alkama, F. Papa, S. Faroux, H. Douville, and C. Prigent (2012), Global off-line evaluation of the ISBA-TRIP flood model, *Climate Dynamics*, *38*(7-8), 1389–1412, doi:10.1007/s00382-011-1054-9. [online] Available from: http://dx.doi.org/10.1007/s00382-011-1054-9

Dodov, B., and E. Foufoula-Georgiou (2004), Generalized hydraulic geometry: Derivation based on a multiscaling formalism, *Water Resources Research*, *40*(6), doi:10.1029/2003WR002082. [online] Available from: http://dx.doi.org/10.1029/2003WR002082

Döll, P., F. Kaspar, and B. Lehner (2003), A global hydrological model for deriving water availability indicators: model tuning and validation, *Journal of Hydrology*, *270*(1–2), 105–134, doi:10.1016/S0022-1694(02)00283-4. [online] Available from: http://www.sciencedirect.com/science/article/pii/S0022169402002834

Douglas, A. (2009), Social, Political, and Institutional Setting: Water Management Problems of the Rio Grande, *Journal of Water Resources Planning and Management*, *135*(6), 493–501. [online] Available from: http://ascelibrary.org/doi/abs/10.1061/(ASCE)0733-9496(2009)135:6(493)

Dunne, T., and L. B. Leopold (1978), Water in Environmental Planning, p. 617, W.H. Freeman Company, San Francisco.

Durand, M., K. M. Andreadis, D. E. Alsdorf, D. P. Lettenmaier, D. Moller, and M. Wilson (2008), Estimation of bathymetric depth and slope from data assimilation of swath altimetry into a hydrodynamic model, *Geophysical Research Letters*, *35*(20), doi:10.1029/2008GL034150. [online] Available from: http://dx.doi.org/10.1029/2008GL034150

Durand, M., E. Rodriguez, D. E. Alsdorf, and M. Trigg (2010), Estimating River Depth From Remote Sensing Swath Interferometry Measurements of River Height, Slope, and Width, *Selected Topics in Applied Earth Observations and Remote Sensing, IEEE Journal of*, *3*(1), 20–31, doi:10.1109/JSTARS.2009.2033453.

Entekhabi, D., and P. S. Eagleson (1989), Land Surface Hydrology Parameterization for Atmospheric General Circulation models Including Subgrid Scale Spatial Variability, *Journal of Climate*, *2*(8), 816–831, doi:10.1175/1520-0442(1989)002<0816:LSHPFA>2.0.CO;2. [online] Available from: http://dx.doi.org/10.1175/1520-0442(1989)002<0816:LSHPFA>2.0.CO

Famiglietti, J. S. (2004), Remote Sensing of Terrestrial Water Storage, Soil Moisture and Surface Waters, in *The State of the Planet: Frontiers and Challenges in Geophysics*, pp. 197–207, American Geophysical Union. [online] Available from: http://dx.doi.org/10.1029/150GM16

Famiglietti, J. S., and E. F. Wood (1994), Multiscale modeling of spatially variable water and energy balance processes, *Water Resources Research*, *30*(11), 3061–3078, doi:10.1029/94WR01498. [online] Available from: http://dx.doi.org/10.1029/94WR01498

Famiglietti, J. S., L. Murdoch, V. Lakshmi, and R. P. Hooper (2009), Towards a Framework for Community Modeling in Hydrologic Science.

Faustini, J. M., P. R. Kaufmann, and A. T. Herlihy (2009), Downstream variation in bankfull width of wadeable streams across the conterminous United States, *Geomorphology*, *108*(3–4), 292–311, doi:10.1016/j.geomorph.2009.02.005. [online] Available from: http://www.sciencedirect.com/science/article/pii/S0169555X09000762

Fitzhugh, T. W., and R. M. Vogel (2011), The impact of dams on flood flows in the United States, *River Research and Applications*, *27*, 1192–1215, doi:10.1002/rra.1417.

Frappart, F., F. Seyler, J.-M. Martinez, J. G. León, and A. Cazenave (2005), Floodplain water storage in the Negro River basin estimated from microwave remote sensing of inundation area and water levels, *Remote Sensing of Environment*, *99*(4), 387–399, doi:10.1016/j.rse.2005.08.016. [online] Available from: http://www.sciencedirect.com/science/article/pii/S0034425705002762

Garbrecht, J. (1990), Analytical representation of cross-section hydraulic properties, *Journal of Hydrology*, *119*(1-4), 43–56, doi:10.1016/0022-1694(90)90033-T.

Gauckler, P. (1867), Etudes Théoriques et Pratiques sur l'Ecoulement et le Mouvement des Eaux, vol. 64, pp. 818–822, Comptes Rendus de l'Académie des Sciences, Paris, France.

St. George, S., D. M. Meko, and E. R. Cook (2010), The seasonality of precipitation signals embedded within the North American Drought Atlas, *The Holocene*, *20*(6), 983–988. [online] Available from: http://hol.sagepub.com/content/20/6/983.abstract

Gleason, K. (2008), *2008 Midwestern U.S. Floods*, Asheville, NC.

Goteti, G., J. S. Famiglietti, and K. Asante (2008), A Catchment-Based Hydrologic and Routing Modeling System with explicit river channels, *Journal of Geophysical Research: Atmospheres*, *113*(D14), doi:10.1029/2007JD009691. [online] Available from: http://dx.doi.org/10.1029/2007JD009691

Graf, W. L. (1999), Dam nation: A geographic census of American dams and their large-scale hydrologic impacts, *Water Resources Research*, *35*, 1305, doi:10.1029/1999WR900016.

Horizon Systems Corporation (2010), *NHDPlus User Guide*. [online] Available from: ftp://ftp.horizon-systems.com/NHDPlus/NHDPlusV1/documentation/NHDPLUSV1_UserGuide.pdf

Huntington, T. G. (2006), Evidence for intensification of the global water cycle: Review and synthesis, *Journal of Hydrology*, *319*(1–4), 83–95, doi:10.1016/j.jhydrol.2005.07.003. [online] Available from: http://www.sciencedirect.com/science/article/pii/S0022169405003215

Jowett, I. G. (1998), Hydraulic geometry of New Zealand rivers and its use as a preliminary method of habitat assessment, *Regulated Rivers: Research & Management*, *14*(5), 451–466, doi:10.1002/(SICI)1099-1646(1998090)14:5<451::AID-RRR512>3.0.CO;2-1. [online] Available from: http://dx.doi.org/10.1002/(SICI)1099-1646(1998090)14:5<451::AID-RRR512>3.0.CO

Kite G.W., A. Dalton, and K. Dion (1994), Simulation of streamflow in a macroscale watershed using general circulation model data, *Water Resources Research*, *30*, 1547–1559.

Knighton, A. D. (1974), Variation in Width-Discharge Relation and Some Implications for Hydraulic Geometry, *Geological Society of America Bulletin*, *85*(7), 1069–1076. [online] Available from: http://gsabulletin.gsapubs.org/content/85/7/1069.abstract

Knighton, A. D. (1975), Variations in at-a-station hydraulic geometry, *American Journal of Science*, *275*(2), 186–218. [online] Available from: http://www.ajsonline.org/content/275/2/186.short

Koster, R. D., M. J. Suarez, A. Ducharne, M. Stieglitz, and P. Kumar (2000), A catchment-based approach to modeling land surface processes in a general circulation model: 1. Model structure, *Journal of Geophysical Research: Atmospheres*, *105*(D20), 24809–24822, doi:10.1029/2000JD900327. [online] Available from: http://dx.doi.org/10.1029/2000JD900327

Kouraev, A. V, E. A. Zakharova, O. Samain, N. M. Mognard, and A. Cazenave (2004), Ob' river discharge from TOPEX/Poseidon satellite altimetry (1992–2002), *Remote Sensing of Environment*, *93*(1–2), 238–245, doi:10.1016/j.rse.2004.07.007. [online] Available from: http://www.sciencedirect.com/science/article/pii/S0034425704002184

Kumar, S., and V. Merwade (2011), Evaluation of NARR and CLM3.5 outputs for surface water and energy budgets in the Mississippi River Basin, *Journal of Geophysical Research*, *116*, D08115, doi:10.1029/2010jd014909.

Lee, K. T., and C.-H. Chang (2005), Incorporating subsurface-flow mechanism into geomorphology-based IUH modeling, *Journal of Hydrology*, *311*(1), 91–105.

LeFavour, G., and D. Alsdorf (2005), Water slope and discharge in the Amazon River estimated using the shuttle radar topography mission digital elevation model, *Geophysical Research Letters*, *32*(17), doi:10.1029/2005GL023836. [online] Available from: http://dx.doi.org/10.1029/2005GL023836

Lehner, B., K. Verdin, and A. Jarvis (2008), New Global Hydrography Derived From Spaceborne Elevation Data, *Eos, Transactions American Geophysical Union*, *89*, 93, doi:10.1029/2008EO100001.

Leon, J. G., S. Calmant, F. Seyler, M.-P. Bonnet, M. Cauhopé, F. Frappart, N. Filizola, and P. Fraizy (2006), Rating curves and estimation of average water depth at the upper Negro River based on satellite altimeter data and modeled discharges, *The ICWRER - Symposium in Dresden, Germany*, *328*(3–4), 481–496, doi:10.1016/j.jhydrol.2005.12.006. [online] Available from: http://www.sciencedirect.com/science/article/pii/S0022169406000163

Leopold, L. B., and T. Maddock (1953), The hydraulic geometry of stream channels and some physiographic implications, *Geological Survey professional paper*, (252).

Leopold, L. B., M. G. Wolman, and J. P. Miller (1964), Fluvial processes in geomorphology, p. 251, W.H. Freeman and Company, San Francisco.

Lettenmaier, D. P., and J. S. Famiglietti (2006), Hydrology: Water from on high, *Nature*, *444*(7119), 562–563, doi:10.1038/444562a. [online] Available from: http://dx.doi.org/10.1038/444562a

Li, H., M. Huang, M. S. Wigmosta, Y. Ke, A. M. Coleman, L. R. Leung, A. Wang, and D. M. Ricciuto (2011), Evaluating runoff simulations from the Community Land Model 4.0 using observations from flux towers and a mountainous watershed, *Journal of Geophysical Research: Atmospheres*, *116*(D24), doi:10.1029/2011JD016276. [online] Available from: http://dx.doi.org/10.1029/2011JD016276

Li, R.-M., D. B. Simons, and M. A. Stevens (1975), Nonlinear kinematic wave approximation for water routing, *Water Resources Research*, *11*(2), 245–252, doi:10.1029/WR011i002p00245. [online] Available from: http://dx.doi.org/10.1029/WR011i002p00245

Liston, G. E., Y. C. Sud, and E. F. Wood (1994), Evaluating GCM land surface hydrology parameterizations by computing river discharges using a runoff routing model: Application to the Mississippi basin, *Journal of Applied Meteorology*, *33*(3), 394–405.

Lohmann, D., R. NOLTE-HOLUBE, and E. Raschke (1996), A large-scale horizontal routing model to be coupled to land surface parametrization schemes, *Tellus A*, *48*(5), 708–721.

Maidment, D. R. (2002), *Arc Hydro: GIS for Water Resources*, ESRI Press. [online] Available from: http://books.google.com/books?id=-ZllngEACAAJ

MANABE, S. (1969), CLIMATE AND THE OCEAN CIRCULATION1, *Monthly Weather Review*, *97*(11), 739–774, doi:10.1175/1520-0493(1969)097<0739:CATOC>2.3.CO;2. [online] Available from: http://dx.doi.org/10.1175/1520-0493(1969)097<0739:CATOC>2.3.CO

Manning, R. (1891), On the flow of water in open channels and pipes, vol. 20, pp. 161–207, Transactions of the Institution of Civil Engineers of Ireland.

Mersel, M. K., L. C. Smith, K. M. Andreadis, and M. T. Durand (2013), Estimation of river depth from remotely sensed hydraulic relationships, *Water Resources Research*, *49*(6), 3165–3179, doi:10.1002/wrcr.20176. [online] Available from: http://dx.doi.org/10.1002/wrcr.20176

Miller, J. R., G. L. Russell, and G. Caliri (1994), Continental-Scale River Flow in Climate Models, *Journal of Climate*, *7*(6), 914–928, doi:10.1175/1520-0442(1994)007<0914:CSRFIC>2.0.CO;2. [online] Available from: http://dx.doi.org/10.1175/1520-0442(1994)007<0914:CSRFIC>2.0.CO

Milly, P. C. D. (2005), *Trends in the water budget of the Mississippi River basin, 1949-1997 from the National Streamflow Information Program.*, U.S. Dept. of the Interior, U.S.

Geological Survey, Reston, Va. [online] Available from: http://purl.access.gpo.gov/GPO/LPS93945

Milly, P. C. D., and K. A. Dunne (2001), Trends in evaporation and surface cooling in the Mississippi River Basin, *Geophysical Research Letters*, *28*(7), 1219–1222, doi:10.1029/2000GL012321. [online] Available from: http://dx.doi.org/10.1029/2000GL012321

Mo, K. C. (2010), Interdecadal Modulation of the Impact of ENSO on Precipitation and Temperature over the United States, *Journal of Climate*, *23*(13), 3639–3656, doi:10.1175/2010JCLI3553.1. [online] Available from: http://dx.doi.org/10.1175/2010JCLI3553.1

Naden, P. S. (1993), A routing model for continental-scale hydrology, *IAHS PUBLICATION*, 67.

Nilsson, C., C. A. Reidy, M. Dynesius, and C. Revenga (2005), Fragmentation and Flow Regulation of the World's Large River Systems, *Science*, *308*(5720), 405–408. [online] Available from: http://www.sciencemag.org/content/308/5720/405.abstract

Niu, G.-Y., and Z.-L. Yang (2003), The versatile integrator of surface atmospheric processes: Part 2: evaluation of three topography-based runoff schemes, *Project for Intercomparison of Land-surface Parameterization Schemes, Phase 2(e)*, *38*(1–2), 191–208, doi:10.1016/S0921-8181(03)00029-8. [online] Available from: http://www.sciencedirect.com/science/article/pii/S0921818103000298

Niu, G.-Y., Z.-L. Yang, R. E. Dickinson, and L. E. Gulden (2005), A simple TOPMODEL-based runoff parameterization (SIMTOP) for use in global climate models, *Journal of Geophysical Research: Atmospheres*, *110*(D21), doi:10.1029/2005JD006111. [online] Available from: http://dx.doi.org/10.1029/2005JD006111

Niu, G.-Y., Z.-L. Yang, R. E. Dickinson, L. E. Gulden, and H. Su (2007), Development of a simple groundwater model for use in climate models and evaluation with Gravity Recovery and Climate Experiment data, *Journal of Geophysical Research: Atmospheres*, *112*(D7), doi:10.1029/2006JD007522. [online] Available from: http://dx.doi.org/10.1029/2006JD007522

NRC (2008), *Integrating Multiscale Observations of U.S. Waters*, The National Academies Press. [online] Available from: http://www.nap.edu/openbook.php?record_id=12060

Ohmura, A., and M. Wild (2002), Is the Hydrological Cycle Accelerating?, *Science*, *298*(5597), 1345–1346. [online] Available from: http://www.sciencemag.org/content/298/5597/1345.short

Oki, T., and S. Kanae (2006), Global Hydrological Cycles and World Water Resources, *Science*, *313*(5790), 1068–1072. [online] Available from: http://www.sciencemag.org/content/313/5790/1068.abstract

Oki, T., T. Nishimura, and P. Dirmeyer (1999), Assessment of annual runoff from land surface models using Total Runoff Integrating Pathways (TRIP), *J. Meteorol. Soc. Jpn*, *77*, 235–255.

Oleson, K. W., G.-Y. Niu, Z.-L. Yang, D. M. Lawrence, P. E. Thornton, P. J. Lawrence, R. Stockli, R. E. Dickinson, G. B. Bonan, and S. Levis (2007), *CLM3.5 Documentation*. [online] Available from: http://www.cgd.ucar.edu/tss/clm/distribution/clm3.5/CLM3_5_documentation.pdf

Oleson, K. W. et al. (2008), Improvements to the Community Land Model and their impact on the hydrological cycle, *Journal of Geophysical Research: Biogeosciences*, *113*(G1), doi:10.1029/2007JG000563. [online] Available from: http://dx.doi.org/10.1029/2007JG000563

Olivera, F., J. Famiglietti, and K. Asante (2000), Global-scale flow routing using a source-to-sink algorithm, *Water Resources Research*, *36*(8), 2197–2207, doi:10.1029/2000WR900113. [online] Available from: http://dx.doi.org/10.1029/2000WR900113

Papa, F., C. Prigent, F. Aires, C. Jimenez, W. B. Rossow, and E. Matthews (2010), Interannual variability of surface water extent at the global scale, 1993–2004, *Journal of Geophysical Research*, *115*, doi:10.1029/2009JD012674.

Park, C. C. (1977), World-wide variations in hydraulic geometry exponents of stream channels: An analysis and some observations, *Journal of Hydrology*, *33*(1–2), 133–146, doi:10.1016/0022-1694(77)90103-2. [online] Available from: http://www.sciencedirect.com/science/article/pii/0022169477901032

Pavelsky, T. M., and L. C. Smith (2008), RivWidth: A Software Tool for the Calculation of River Widths From Remotely Sensed Imagery, *Geoscience and Remote Sensing Letters, IEEE*, *5*(1), 70–73, doi:10.1109/LGRS.2007.908305.

Portmann, R. W., S. Solomon, and G. C. Hegerl (2009), Spatial and seasonal patterns in climate change, temperatures, and precipitation across the United States, *Proceedings of the National Academy of Sciences*, *106*(18), 7324–7329. [online] Available from: http://www.pnas.org/content/106/18/7324.abstract

Prigent, C., F. Papa, F. Aires, W. B. Rossow, and E. Matthews (2007), Global inundation dynamics inferred from multiple satellite observations, 1993–2000, *Journal of Geophysical Research*, *112*, doi:10.1029/2006JD007847.

Reichle, R. H., and R. D. Koster (2005), Global assimilation of satellite surface soil moisture retrievals into the NASA Catchment land surface model, *Geophysical Research Letters*, *32*(2), doi:10.1029/2004GL021700. [online] Available from: http://dx.doi.org/10.1029/2004GL021700

Rhodes, D. D. (1977), The b-f-m diagram; graphical representation and interpretation of at-a-station hydraulic geometry, *American Journal of Science*, *277*(1), 73–96. [online] Available from: http://www.ajsonline.org/content/277/1/73.short

Richards, K. S. (1976), Complex width-discharge relations in natural river sections, *Geological Society of America Bulletin*, *87*(2), 199–206. [online] Available from: http://gsabulletin.gsapubs.org/content/87/2/199.abstract

Richey, J. E., J. M. Melack, A. K. Aufdenkampe, V. M. Ballester, and L. L. Hess (2002), Outgassing from Amazonian rivers and wetlands as a large tropical source of atmospheric CO2, *Nature*, *416*(6881), 617–620, doi:10.1038/416617a. [online] Available from: http://dx.doi.org/10.1038/416617a

Rodell, M. et al. (2004), The Global Land Data Assimilation System, *Bulletin of the American Meteorological Society*, *85*, 381–394, doi:10.1175/BAMS-85-3-381.

Rui, H., and H. Beaudoing (2013), README Document for Global Land and Data Assimilation Sytem Version 2 (GLDAS-2) Products

Seaber, P. R., F. P. Kapinos, and G. L. Knapp (1987), *Hydrologic Unit Maps: US Geological Survey Water Supply Paper 2294*, US Geological Survey.

Sellers, P. J., M. D. Heiser, and F. G. Hall (1992), Relations between surface conductance and spectral vegetation indices at intermediate (100 m2 to 15 km2) length scales, *Journal of Geophysical Research: Atmospheres*, *97*(D17), 19033–19059, doi:10.1029/92JD01096. [online] Available from: http://dx.doi.org/10.1029/92JD01096

Sivapalan, M., K. Beven, and E. F. Wood (1987), On hydrologic similarity: 2. A scaled model of storm runoff production, *Water Resources Research*, *23*(12), 2266–2278, doi:10.1029/WR023i012p02266. [online] Available from: http://dx.doi.org/10.1029/WR023i012p02266

Smith, L. C., and T. M. Pavelsky (2008), Estimation of river discharge, propagation speed, and hydraulic geometry from space: Lena River, Siberia, *Water Resources Research*, *44*(3), doi:10.1029/2007WR006133. [online] Available from: http://dx.doi.org/10.1029/2007WR006133

Smith, L. C., B. L. Isacks, A. L. Bloom, and A. B. Murray (1996), Estimation of Discharge From Three Braided Rivers Using Synthetic Aperture Radar Satellite Imagery: Potential Application to Ungaged Basins, *Water Resources Research*, *32*(7), 2021–2034, doi:10.1029/96WR00752. [online] Available from: http://dx.doi.org/10.1029/96WR00752

Stewardson, M. (2005), Hydraulic geometry of stream reaches, *Journal of Hydrology*, *306*(1–4), 97–111, doi:10.1016/j.jhydrol.2004.09.004. [online] Available from: http://www.sciencedirect.com/science/article/pii/S0022169404004226

Stieglitz, M., D. Rind, J. Famiglietti, and C. Rosenzweig (1997), An Efficient Approach to Modeling the Topographic Control of Surface Hydrology for Regional and Global Climate Modeling, *Journal of Climate*, *10*(1), 118–137, doi:10.1175/1520-0442(1997)010<0118:AEATMT>2.0.CO;2. [online] Available from: http://dx.doi.org/10.1175/1520-0442(1997)010<0118:AEATMT>2.0.CO

Strahler, A. N. (1957), Quantitative analysis of watershed geomorphology, *Transactions of the American geophysical Union*, *38*(6), 913–920.

Syed, T. H., J. S. Famiglietti, D. P. Chambers, J. K. Willis, and K. Hilburn (2010), Satellite-based global-ocean mass balance estimates of interannual variability and emerging trends in continental freshwater discharge, *Proceedings of the National Academy of Sciences*. [online] Available from: http://www.pnas.org/content/early/2010/09/28/1003292107.abstract

Vogel, R. M., and N. M. Fennessey (1994), Flow-Duration Curves. I: New Interpretation and Confidence Intervals, *Journal of Water Resources Planning and Management*, *120*, 485–504, doi:10.1061/(ASCE)0733-9496(1994)120:4(485).

Vogel, R. M., and N. M. Fennessey (1995), Flow duration curves II: a review of applications in water resources planning, *Journal of the American Water Resources Association*, *31*, 1029–1039, doi:10.1111/j.1752-1688.1995.tb03419.x.

Vörösmarty, C. J., B. Moore, A. L. Grace, M. P. Gildea, J. M. Melillo, B. J. Peterson, E. B. Rastetter, and P. A. Steudler (1989), Continental scale models of water balance and fluvial transport: An application to South America, *Global Biogeochemical Cycles*, *3*(3), 241–265, doi:10.1029/GB003i003p00241. [online] Available from: http://dx.doi.org/10.1029/GB003i003p00241

Ward, F., and M. Pulido-Velazquez (2012), Economic Costs of Sustaining Water Supplies: Findings from the Rio Grande, *Water Resources Management*, *26*(10), 2883–2909, doi:10.1007/s11269-012-0055-8. [online] Available from: http://dx.doi.org/10.1007/s11269-012-0055-8

Wilson, M., P. Bates, D. Alsdorf, B. Forsberg, M. Horritt, J. Melack, F. Frappart, and J. Famiglietti (2007), Modeling large-scale inundation of Amazonian seasonally flooded wetlands, *Geophysical Research Letters*, *34*(15), doi:10.1029/2007GL030156. [online] Available from: http://dx.doi.org/10.1029/2007GL030156

Xia, Y. et al. (2012), Continental-scale water and energy flux analysis and validation for North American Land Data Assimilation System project phase 2 (NLDAS-2): 2. Validation of model-simulated streamflow, *Journal of Geophysical Research: Atmospheres*, *117*(D3), doi:10.1029/2011JD016051. [online] Available from: http://dx.doi.org/10.1029/2011JD016051

Yamazaki, D., S. Kanae, H. Kim, and T. Oki (2011), A physically based description of floodplain inundation dynamics in a global river routing model, *Water Resources Research*, *47*, doi:10.1029/2010WR009726.

Zaitchik, B. F., M. Rodell, and F. Olivera (2010), Evaluation of the Global Land Data Assimilation System using global river discharge data and a source-to-sink routing scheme, *Water Resources Research*, *46*(6), doi:10.1029/2009WR007811. [online] Available from: http://dx.doi.org/10.1029/2009WR007811